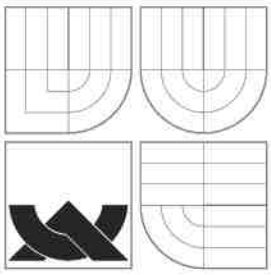

BRNO UNIVERSITY OF TECHNOLOGY
VYSOKÉ UČENÍ TECHNICKÉ V BRNĚ

FACULTY OF INFORMATION TECHNOLOGY
DEPARTMENT OF COMPUTER GRAPHICS AND MULTIMEDIA

FAKULTA INFORMAČNÍCH TECHNOLOGIÍ
ÚSTAV POČÍTAČOVÉ GRAFIKY A MULTIMÉDIÍ

PROTOTYPING OF A DIGITAL FLIGHT CONTROL SYSTEM

PROTOTYPOVÁNÍ DIGITALNÍHO SYSTÉMU ŘÍZENÍ LETU

HABILITATION THESIS
HABILITAČNÍ PRÁCE

AUTHOR
AUTOR PRÁCE

Ing. PETER CHUDÝ, Ph.D. MBA

BRNO 2016

Project TA01010678 "Smart Autopilot" has been supported by the Technology Agency of the Czech Republic

Summary

The limitations of early analog electronics and mechanical systems were overcome by reliable computer platforms and safe digital data processing technologies integrated within an innovative digital flight control system for light aircraft. The required level of redundancy and physical dimensions of a fully digital fly-by-wire installation are acceptable for large aircraft, but represent a cost prohibitive solution with a substantial weight penalty considering the operational concept of sport and leisure flying. A digital automatic flight control system for light aircraft presented in this thesis was designed and developed upon utilizing an industry accepted single line system approach for flight controls and digital avionics. Redundancy considerations were resolved through a parallel integration of the electromechanical actuators to the primary mechanical control system. This approach found support in the digital flight control system's use case scenario, assuming the support of visual flight rules operations only and including a manual override capability (as such logic has been applied in successfully marketed light aircraft autopilot designs). The control system's flight envelope protection zone was by design restricted to a typical touring/cross-country flying profile.

Keywords

Flight control system, control laws, digital control, linear control, nonlinear control, avionics, hardware-in-the-loop, software-in-the-loop, rapid prototyping, light aircraft, elastic aircraft, equations of motion.

Citation

P. Chudý: Prototyping of a Digital Flight Control System, Habilitation thesis, Brno: BUT FIT, 2016

Shrnutí

Omezení prvotní analogové elektroniky a mechanických systémů bylo překonáno spolehlivými počítačovými platformami a bezpečnými technologiemi pro zpracování dat integrovanými do inovativního digitálního systému řízení letu pro lehká letadla. Požadovaná úroveň zálohování a fyzické rozměry plné instalace digitálního systému fly-by-wire jsou akceptovatelné pro velká letadla, ale s přihlédnutím k provoznímu konceptu sportovního a rekreačního létání představují příliš nákladné řešení s výrazným hmotnostním nárůstem. Digitální automatický systém řízení letu pro lehká letadla představený v této práci byl navržen a vyvinut na základě průmyslově akceptovaných přístupů v řízení letu a návrhu digitálních avionických systémů. Zálohování bylo zohledněno paralelní integrací elektromechanických aktuátorů do primárního mechanického okruhu řízení. Tento přístup našel oporu v navrženém provozním scénáři digitálního systému řízení letu, který předpokládá podporu provozu při letu za viditelnosti a zahrnuje možnost manuálního překonání automatického řízení. Využívá tedy podobnou logiku, která byla aplikována na komerčně úspěšné systémy autopilota pro lehká letadla. Ochranná zóna letové obálky systému řízení letu byla cíleně omezena na profily letu typické pro turistické létání.

Klíčová slova

Systém řízení letu, zákony řízení, lineární řízení, nelineární řízení, digitální řízení, avionika, hardware-in-the-loop, software-in-the-loop, rapid prototyping, lehké letadlo, elastické letadlo, pohybové rovnice.

Citace

P. Chudý: Prototypování Digitalního Systému Řízení Letu, Habilitační práce: Brno, VUT v Brně FIT, 2016

Contents

INTENTIONALLY LEFT BLANK

Abbreviations

Symbol	Description
3D	3 Dimensional
A/P	Autopilot
ADC	Air Data Computer
AFCS	Automatic Flight Control System
AGL	Above Ground Level
AHRS	Attitude and Heading Reference System
AIAA	American Institute of Aeronautics and Astronautics
ASTM	American Society for Testing and Materials
ATC	Air Traffic Control
BAT	Battery
BIT	Built–in Test
CAD	Computer Aided Design
CAN	Controller Area Network
CEST	Central European Summer Time
CFD	Computational Fluid Dynamics
CHT	Cylinder Head Temperature
DAQ	Data Acquisition Unit
DASC	Digital Avionics Systems Conference
DNP	Digital Navigation Platform
EGT	Exhaust Gas Temperature
EMA	Electromechanical Actuator
EUROCAE	The European Organisation for Civil Aviation Equipment
FCS	Flight Control System
FF	Fuel Flow
FP	Fuel Pressure
FPL	Flight Plan
GPS	Global Positioning System
IEEE	Institute of Electrical and Electronics Engineering
MFD	Multifunction Display
MIMO	Multiple–Input Multiple–Output
MIRA	Motor Industry Research Association
MISRA	Motor Industry Software Reliability Association
MP	Manifold Pressure
NDI	Nonlinear Dynamic Inversion
PFD	Primary Flight Display
PMU	Propulsion Monitoring Unit

RMS	Root Mean Square
RPM	Revolutions per Minute
RTCA	Radio Technical Commission for Aeronautics
SAE	Society of Automotive Engineers
SISO	Single Input Single Output
TECS	Total Energy Control System
THCS	Total Heading Control System
USAF	United States Air Force
UTC	Universal Time Coordinated
VFR	Visual Flight Rules
WGS84	World Geodetic System 1984
WPT	Waypoint

Greek Symbols

Symbol	**Description**
$\Delta\beta$	Incremental Sideslip Angle
ϕ	Roll Angle
θ	Pitch Angle

Latin Symbols

Symbol	**Description**
a_y	Lateral Acceleration at the Aircraft Center of Gravity
ALT	Pressure Altitude
HDG	Heading Angle
IAS	Indicated Airspeed
Lat	Geodetic Latitude in WGS84
Lon	Geodetic Longitude in WGS84
n_z	Load Factor at the Aircraft Center of Gravity
p	Roll Rate
QNH	Atmospheric Pressure at Mean Sea Level
VS	Vertical Speed

1 Introduction

A successful design starts from a product utilization perspective. Prototyping a digital flight control system begins with the definition of its contributing role to the overall aircraft design concept.

Different approaches meet different design expectations. The philosophy of stability augmentation elements is in the suppression of unfavorable inherent stability characteristics originating from the aircraft designer's structural and aerodynamic preferences and performance driven goals. Their successful implementation provides the crew and passengers with improved comfort and performance. A widespread on-board automation concept is the autopilot. Its primary function is the reduction of pilot workload through the stabilization of flight relevant quantities. In a combination with the flight management system, the autopilot provides to pilots a workload relief solution in aerial navigation and precision trajectory tracking. Reliability driven mechanical/electromechanical system complexity and associated weight penalty, along with advances in electronics and software engineering, brought the aircraft flight control community to consider, design and implement fly-by-wire controls. These systems integrate previously isolated flight control and automation elements into a unifying framework, but introduce new challenges due to pilot's closed-loop interaction with the control system. The selection of the flight control system specification has an impact on the overall system architecture, extent of modeling and simulation, software and hardware considerations including concerns of operational reliability, physical system redundancy, human machine interface design, system integration, validation, verification and testing. On top of that, depending on the class of applicable aircraft, the flight control system design has to comply with valid legislation framework installed by respective regulatory agencies. All such constraints must be considered when designing a pilot centered flight control system.

The flight control system design process benefits from modeling and simulation techniques, introduced to describe aircraft/systems dynamics and performance characteristics. An industry accepted framework utilizes two global approaches in modeling and simulation. The first approach is based on the point mass approximation of rigid body dynamics described by a set of nonlinear equations of motion; whereas, the latter approach accounts for the structural elasticity effects due to fluid structure interaction phenomena. The former modeling technique uses a set of differential equations to describe the translational, rotational, attitude and position quantities. The equations of motion in translation and rotation include the effects of aerodynamic, mass and propulsion induced forces and moments. And, it is these respective forces and moments that introduce uncertainties into the modeling process. The need to estimate aerodynamic characteristics of wings and bodies dates back to the origins of manned flight. The aviation pioneers introduced estimation of aerodynamic characteristics in wind tunnels based on the similarity/scale concept. Their approach finds its relevance even today, when high performance computer clusters capable of parallel Computational Fluid Dynamics (CFD) processing are increasingly gaining in relevance. Computational aerodynamics utilizes a variety of methods depending on the modeled physics and aircraft design maturity level. At a conceptual stage, panel methods have been successfully used due to their favorable computational cost and modeling agility. However, these methods usually predict conservative force and moment estimates as most of the available implementations use potential field theory. The finite volume method based CFD tools offer higher fidelity computation on complex 3D geometries as compared to panel methods. A finite volume method implementation may use Reynolds Averaged Navier-Stokes equations, supplemented with a variety of applicable turbulence models. However, the computational expense to run high fidelity CFD aerodynamic analysis is higher even by today's standards.

A conceptual design level requires decisions to be made that predefine the course of future development without the availability of high fidelity data to support the case. A proven alternative to computational aerodynamics is the utilization of United States Air Force (USAF) Datcom. This method estimates respective aerodynamic, stability and control derivatives based on similarity criteria derived from experimental data. The fallback of the method is the lack of tools to predict behavior of unconventional aircraft configurations.

Aerodynamic computational analyses verified against wind tunnel measured data represent an important element of modern flight control design. Once the designed aircraft takes flight, new source of information becomes available for a high fidelity estimation of aerodynamic, stability and control characteristics. At this stage, test data acquired at flight envelope target points become available to the aircraft flight parameter estimation process. This however does not come cheap. The aircraft/subject of parameter estimation needs to be instrumented with laboratory grade measurement and data logging equipment. The onboard sensor network requires calibration before and verification after each experimental flight. The instrumentation is a necessary but not sufficient assumption in the testing process. A balanced flight test program including identification maneuvers in longitudinal and lateral–directional motion will provide information of the flight envelope test point coverage. Each of the identification maneuvers must be flown repeatedly, to acquire sufficient amount of data for the identification and subsequent validation procedures. Two basic options for execution of the flight test maneuvers are at hand: the first accounts for a manual maneuver execution, and the latter one relies on the automation. To achieve test execution repeatability in the manual test mode, a graphical user interface has been developed and implemented by the Brno University of Technology to indicate to the pilot a desired flight test trajectory. In order to reduce the level of complexity in identification, flight tests under no wind and no turbulence conditions are preferred over flying through gust fields and modeling its effects by wind/gust induced velocity and attitude rate increments. Several numerical optimization methods can be considered in the parameter estimation process. Among the most popular are the Equation Error and Output Error approaches. One of the main driving points in identification is the kinematic consistency verification followed by the flight trajectory reconstruction. But to reach this point, a sufficiently dense set of measured flight data must be available. For aerodynamic, stability and control characteristic identification, this would usually require recording the data at a sample rate of $100\,Hz$. Recorded data also need to be properly time synchronized.

Another important aspect having a direct influence on the quality of the identified data and quality of flight simulation is the proper estimation of moments of inertia and instantaneous location of center of gravity. These quantities can be conveniently estimated for smaller objects using known experimental techniques, but their quantification for the entire aircraft can become a challenge. Due to this, the mass and inertia characteristics are treated as uncertain quantities. To avoid expensive and lengthy physical experiments, the moments of inertia for respective mass configurations can be advantageously computed from the investigated aircraft 3D Computer Aided Design (CAD) model. A virtual modeling approach may also be used for definition of changes in fuel level of respective fuel tanks and their effects on global inertia characteristics. A unique chapter in the modeling and simulation process represents the modeling of the propulsion system. Description complexity may, in the best case, be overcome by using engine manufacturer provided data.

Aircraft designs with large wingspan and lightweight composite structure challenge the simulation and modeling community with structural elasticity effects causing redistribution of loads due to elastic deformations and simultaneously influencing aircraft stability and control characteristics. Estimation of the elastic effects on the aircraft flight dynamics is predominantly executed in the frequency domain with results being transformed to time domain for more intuitive evaluation. The equations of motion for elastic aircraft contain eigen modes

and eigen frequencies which can be conveniently estimated using computation–based tools or a modal analysis experiment. Both estimation approaches have their own implementation details that must be considered. The computational approach uses modal analysis theory implemented within the finite element method environment. This approach, when properly utilized, provides accurate results already from the virtual prototyping stage. The second estimation method, based on ground vibration testing, requires the existence of a full-scale prototype, sensitive testing and recoding infrastructure and experience in test execution and evaluation. Once the mode frequencies and shapes are known, aeroelastic modeling can proceed. Elastic bodies exposed to fluid flow are often subject to oscillatory motion, which introduces unsteady aerodynamic phenomena leading to an increase in aerodynamic loads causing higher structural stresses. The effects of structural elasticity on aircraft stability and control characteristics gain importance with the increase in aircraft size, flight performance and lightweight structures.

The solution of the equations of motion, whether for rigid body point mass dynamics approximation or elastic structures, represents the computational basics in the overall simulation framework. The leading objective of simulation technologies is to provide solutions with adequate fidelity for research and development and positive training transfer when utilized in training organizations. In case of flight simulators, this objective often leads to solutions that contain technological sophistication influenced by human factor driven imperfections.

The man–machine interaction phenomena are in many cases of the same level of importance as the hard science phenomena introduced through modeling, simulation, control, software and hardware design. A poorly designed interface may devaluate otherwise brilliant technology; whereas, a unique combination of intuitive elements may introduce new operational concepts rendering the man–machine interaction a positive experience. The latter is a preferred option as it typically blends technological advances with design innovation. As responsible visual display design accounts for the human operator's limited ability to process multiple parallel data management tasks, an innovative utilization of advances in computer graphics and hardware may serve to present differently composed redundant state information on a single visual display; thus, improving the user's situational awareness. A well designed visual interface can stimulate user confidence by displaying data the user can correlate to images acquired through a simultaneous independent observation of the outside world. The flight control automation belongs to the mission critical application group, with operational reliability and redundancy playing a vital role in the system's overall design. Reliability driven considerations related to an automation system's enabling and disconnect elements introduce user interface design requirements. Their utilization within the automation framework must follow rational operational concepts avoiding hazardous transition states.

The flight control system prototyping should be guided by a complex development plan. Such a plan should specify the design approach proposed along with clarification of the technologies and processes to be utilized to meet the software and hardware design milestones within the project's time and budget constraints. The development plan structure should include performance, safety, reliability and maintainability verification strategies supplemented by the plans for piloted simulations as well as ground and flight testing.

Linear-based control laws are currently those that are mostly employed when dealing with automatic flight control problems. A flight control system based on these approaches (e.g. Eigenstructure Assignment or Linear Quadratic Regulator) often assumes the availability of a mathematical model of the aircraft. This model is typically subjected to an approximation through its linearization at a trim point of interest. This specific model is then used in the controller design considering its functional and performance specifications. Commonly known control applications contain the stability augmentation systems composed of simple Single Input Single Output (SISO) designs found in yaw dampers, pitch dampers and

sideslip minimization controllers. Another category of controllers may be used to command aircraft flight trajectory through Heading Angle, Pressure Altitude or Vertical Speed control. These more complex controllers operate with MIMO strategies. From the flight control system design perspective, it is useful to separate the controller structure into cascaded levels known as the inner loop, outer loop and the navigation loop. The inner loop takes the control of angular rates, while the outer loop controls the aircraft attitude or aerodynamic angles since the Heading Angle, Pressure Altitude and Vertical Speed are addressed by the navigation loop. Linear–based control technique utilization provides advantages in availability of tools for system stability analysis, automatic flight control synthesis and the possibility of certification. However, the drawback of this technique is in limited validity of the controller settings outside the trim point location, resulting into the need to adjust controller gains with respect to the current aircraft state. This approach is known as gain scheduling. An alternative to the classical linear-based control strategies is the nonlinear flight control. A state-of-the-art control approach offering favorable design features is the Nonlinear Dynamic Inversion (NDI). This approach embraces the entire state space of the controlled aircraft without the need for gain scheduling. However, NDI's associated implementation costs include the need for accurate aircraft models, its incapability of dealing with non-minimum phase systems and especially its lack of robustness. Another actively researched alternative includes the use of nonlinear adaptive flight control algorithms, which utilize online system identification techniques based on onboard sensor data. This approach reduces aircraft model fidelity requirements in the controller development phase. A reconfigurable system is capable of handling configuration changes influencing aircraft weight, moments of inertia or aerodynamic characteristics.

Allocation of the digital flight control system's respective software and hardware functionalities is recommended to be guided by an industry standard such as [22], in the optics of which the main requirements specification processes originating from the conceptual system development address the functional and safety requirements along with related requirements validation, implementation verification, configuration management and process assurance activities. A responsible digital flight control system's item development process contains: a definition of the system's general functional requirements, a system–level function allocation and architecture design, and a specification of the hardware and software item requirements that are the prerequisites to a full system implementation. Airborne systems and equipment are known for their high safety standards. The reliability aspects of a digital flight control system account for the execution of hazard and safety assessment as recommended by [23]. The assessment results provide the system designers with important inputs that directly influence the system's overall architecture.

It is recommended that software design activities are guided by recognized standards such as [17]–[19], which provide considerations on software planning, development and verification. The software development activities include the definition of high and low-level requirements, software architecture and, finally, the composition of the actual source code. Considering the specified verification strategy, the developed software should be at the integrated target level robustly compliant to the defined high-level requirements. An important aspect in airborne system software development is the concept of maintained traceability between requirements, architecture, implementation and testing. Given the considerable importance underlying critical system software development beyond the aerospace industry itself, guidelines originally developed for reliable critical system automotive software applications have found acceptance within the avionics industry. It is recommended that airborne hardware design processes consider guidelines introduced in [15], [20], [24]. These design guidelines recommend defining the high and low-level requirements, the architecture and its prototyping. However, unlike the case with software design, an early rapid prototyping of hardware development boards is favored in order to investigate the functional characteristics and operational dependencies of respective hardware blocks. Clearing the software integration phase

on a development board allows for the item's hardware prototype design. Once available, the prototype hardware can be subjected to tests under defined environmental conditions. The final design step, prior to a system level testing, calls for the integration of the respective software application onto the dedicated hardware platform.

Testing requirements form a natural part of the flight control system's development process. The scope and focus of testing includes ground–based laboratory hardware and software tests followed by digital control system in–flight testing. Clear delineation of the methods and infrastructure used to demonstrate compliance with the design requirements should be made available beforehand. The defined software system specification compliance must be evaluated throughout the system's multiple development levels with the initial performance demonstrations executed within the comfort zone of a laboratory level verification. The system's acceptance level testing includes the software execution on the target hardware platform. An important field of interest is digital interface testing with the communication protocol's messages content and traffic verification. Best practice standards that meticulously capture and track compliance with the respective design specifications can lead to piloted simulations for hardware functional evaluations. Research flight simulators utilized for piloted trials should be able to support item design testing at its various level of maturity. The safety of flight testing is executed prior to piloted maiden flight for both safety reasons as well as to document and confirm compliance with specified performance and system integrity requirements. A critical testing aspect is the evaluation of electromagnetic interference effects. Actual flight testing is to be executed according to approved flight test program protocols set to investigate the flight control system's performance at various points of the operational flight envelope. Reliability driven issues are to be monitored and recorded into the flight test program's log book for further processing.

The following chapters introduce steps taken in prototyping a digital flight control system for light aircraft. Chapter 2 provides an overview of actions taken in system design, development and testing, with different control strategies implemented and evaluated within the prototyping framework. Chapter 3 introduces the designed Automatic Flight Control System (AFCS), its system architecture, developed hardware units, modes of operation and operational evaluation. The presented test results include a brief evaluation of the system's user interface, operational trials and performance evaluation in smooth air and atmospheric turbulence. The final chapter includes concluding remarks on the light aircraft digital flight control system design process.

INTENTIONALLY LEFT BLANK

2 Digital flight control system design

The complexity of operating and navigating a high-performance light aircraft, and the dangers posed by weather, mechanical problems, and inevitable pilot carelessness pave a logical frame for a pilot workload reduction system. A key role in facilitating the system's design is attributed to accurate simulations. Two flight simulators dedicated to flight control system research and development are introduced in Section 2.1 [14]. The functionality of these devices has been extended over the last years by improvements made to their real-time simulation environments, software and hardware compatibility, visual displays and digital cockpit's user interface design. Both simulators support the integration of commercial or open-source flight dynamics models, or utilization of custom aircraft models run within the simulators' real-time framework. The open and modular architecture of the simulators allows for a rapid prototyping of digital flight control systems including their user interfaces.

A preliminary design of an intuitive flight display motivated by advances in state-of-the-art, commercially available, products and conceptual research ideas is introduced in Section 2.2 [6]. Different aspects have been evaluated in order to propose a flight display layout that would reduce pilot workload and improve situational awareness. The aim was neither to create a futuristic design beyond the support of current legislation, nor a design that would require major retraining. Instead, the intention was to intuitively display flight relevant data without the bias imposed by secondary information. This led to an integrated display solution featuring basic flight data visualization along with selected customized propulsion, navigation and communication instruments, usually displayed on a separate Multifunction Display (MFD). The display size and information structure do not support a full implementation of all information usually found on an instrument panel, as clarity and readability issues limit the scope of implemented features and elements on a flight control system's user interface.

The flight control laws for light aircraft are introduced in Section 2.3 [8]. Whereas poorly coordinated SISO control laws reduce the controller performance if not properly managed by the pilot or autopilot, the Total Energy Control System (TECS) and Total Heading Control System (THCS) represent an elegant way of controlling longitudinal and lateral-directional aircraft motion. The TECS is based on energy distribution logic, compared to the THCS that uses lateral-directional criteria for aircraft control. The advantages of the TECS over classical control law designs proved to be excellent performance, moderate complexity of the resulting controller structure, and support provided by proven analytical tools compatible with airworthiness certification procedures.

Desired fight controller performance over the specified operational flight envelope calls for a sophisticated control system tuning tool based on numerical optimization techniques. The evolution driven optimization approaches achieved recognition in aerospace disciplines when successfully used in the design of high performance airfoils, efficient high lift systems and unconventional aircraft configurations. The multi-criteria nature of the controller design process supports the rationality of utilizing a robust evolution–based optimization technique.

Section 2.4 [11] discusses an evolution driven controller design approach that has been applied to a rigid-body light sport aircraft model. The model comprises inertial, aerodynamic and flight dynamics related elements and a controller architecture based on classical control theory. The evolution driven concept plays a significant role in the optimization of the proposed controller structure by providing tuned controller parameters that meet the designed fitness function criteria imposed through the optimization problem formulation. The proposed fitness function combines significant controller stability evaluation conditions into a single abstraction. The use of a robust optimization framework based on the genetic algorithms has allowed the suggested form of multi-criteria optimization definition.

In order to demonstrate further benefits of employing evolution-based optimization approaches during the design of aeroservoelastic aircraft controllers, a realistic nonlinear simulation model comprising both structural and rigid-body dynamics as well as unsteady aero and control surface dynamics has been implemented in Section 2.5 [13]. The controller design process integrates not only an evolution driven optimization technique but, also, makes use of modern control design approaches such as the Nonlinear Dynamic Inversion (NDI). The utilization of the NDI allowed creating a state-of-the-art baseline control system implementation capable of handling complexities introduced through the elastic modes of an aeroservoelastic aircraft model. The suitability of an evolutionary optimization has been successfully tested on a set of examples that provided rigid body aircraft dynamics as well as elastic structural modes. Time-domain simulation results have shown the compliance of the tuned controller performance to its anticipated behavior.

Section 2.6 [9] describes the general idea, design, and implementation of a safety enhanced digital control system applicable to General Aviation aircraft. The proposed flight control framework is intended to simplify piloting, reduce pilot workload, and allow low-end general aviation aircraft to operate safely under deteriorating meteorological conditions. It represents control technology that transforms a simplistic control surface command into a sophisticated motion control process. This capability is a next step in the technology's evolution that might ultimately lead to trajectory-based free-flight aircraft operations. Implemented flight control laws are designed using classical control theory with measured variables fed back through the controllers that contain proportional, integral and derivative gains tuned to achieve desired stability and performance characteristics. The digital control technology does not eliminate the human pilot from the control loop; instead, the technology conforms the pilot's role to more of a flying platform manager.

Prototyping and simulation of an innovative assisting flight control system for light aircraft is described in Section 2.7 [21]. The presented concept introduces a virtual co-pilot, enabling cockpit workload reduction and a redirection of pilot's focus to careful navigation and communication with the air traffic control. This approach utilizes hidden and unused resources of modern digital Automatic Flight Control Systems while respecting the limitations imposed through the weight and cost sensitivities of the light aircraft market. The introduced flight control strategy integrates the mechanical and digital flight control system into a synergic platform, combining the high reliability of mechanical controls with the computation and actuation power introduced through a single line digital flight control system. Classical control theory has been used for the flight control laws design. Its implementation also includes flight envelope protection features. A prototype of the flight control system has been subjected to validation trials during series of hardware-in-the-loop simulations.

Software and hardware-in-the-loop simulations are indisputably perceived as an integral part of the flight control system's design and development process. Section 2.8 [12] introduces a prototyping framework employed for the development of a light aircraft digital flight control system. This framework accounts for simulations performed at two different ground-testing levels. The first level consists of a laboratory grade testing phase, whereas the later accounts for the full complexity of a digital flight control system's aircraft installation. A series of simulated flights were performed within the prototyping framework, with the mission profiles selected to demonstrate the digital controllers' stability and the ability to execute complex flight trajectories. System elements whose evaluation has been of primary interest were the flight control computer, visual displays, touch controlled user interfaces, a set of digitally controlled electromechanical actuators and the onboard avionics network itself. Individual units were connected within the simulation network using the Controller Area Network (CAN) and CANaerospace communication protocol. Simulations aimed at the evaluation of the automatic flight modes under different operational scenarios confirmed compliance to

selected performance objectives. Software and hardware-in-the-loop simulations provided a deep insight into the flight control system's performance prior to its maiden flight.

Transitioning from mechanical to digital flight control systems is an evolutionary and qualitative improvement from designing simple systems to designing systems that are safe and highly economical across a range of different light aircraft platforms. A digital Automatic Flight Control System (Autopilot – A/P) has been developed using the prototyping framework introduced in Section 2.8 [12]. Its units have been subjected to simulations in the light aircraft flight simulator laboratory SimStar; and, such units were also tested under conditions of full implementation onboard an Evektor SportStar aircraft. An important aspect of the flight control system development process was the performance evaluation of the designed technology in real operating conditions. A series of flight evaluations provide an incremental form of testing, spanning from ground testing up to full automatic flights. The aim of the system inflight testing was both a quantifiable evaluation of the flight control parameters and, also, an investigation of the onboard automation's user interface's operational intuitiveness.

INTENTIONALLY LEFT BLANK

AIAA Modeling and Simulation Technologies Conference
2 - 5 August 2010, Toronto, Ontario Canada

AIAA 2010-8097

Affordable Light Aircraft Flight Simulators

Peter Chudy[1] and Pavel Zemcik[2]
Brno University of Technology, Brno, Czech Republic

Pawel Rzucidlo[3]
Rzeszow University of Technology, Rzeszow, Poland

Two designs of a low-cost flight simulator for research, development and training purposes are being presented in this paper. The first simulator has been designed and built at the Brno University of Technology, Faculty of Information Technologies. This simulator is based on a cockpit of a popular Evektor SportStar light sport aircraft. SportStar was the first Light Sport Aircraft to receive the Federal Aviation Administration airworthiness certificate. Due to Evektor's strong tradition in the design and manufacturing of light and general aviation aircraft, the SportStar represents a successful conceptual evolution that is increasingly gaining popularity among the flying public worldwide. In contrast to the original aircraft the simulator's cockpit is equipped with an experimental dual 12" touch screen flight data visualization system. The flight simulator designed at Rzeszow University of Technology, Department of Avionics and Control, is based on the cabin of the M-15 aircraft. The M-15 was a unique "crop duster" jet plane built in Poland at the beginning of the 1980's. One cabin of this aircraft type has been adopted for didactical and demonstration purposes in the 1990's. Functionality of this device has been extended in last years by adding a visualization system, real-time simulation environment and an electronic representation of flight instruments. Both simulators support two operational modes. The first mode uses a model of the flight dynamics delivered from an external, commercial or open-source software. The second mode supports custom aircraft models and an environment dynamics run in a selected real-time simulation. Open and modular architecture of simulators allows for a rapid prototyping of new cockpit layouts, the design of intuitive flight control systems and user interfaces for the light and ultra-light aircraft.

Nomenclature

α	=	*angle of attack [rad]*
b_1, b_2, b_3	=	*derivatives of hinge moments due to α, δ and δ_t*
c_{mac}	=	*mean aerodynamic chord [m]*
CAN	=	*controller area network*
CAS	=	*control augmentation system*
d_s	=	*control stick deflection [rad]*
d_{sfv}	=	*modified control signal*
DOF	=	*degree of freedom*
δ	=	*control surface deflection [rad]*
δ_t	=	*trimmer deflection [rad]*
$\Delta\delta/\Delta x$	=	*control stick transmission ratio*
E_T	=	*total energy [J]*
$\dot{E}$	=	*specific total energy rate*
EFCS	=	*environmentally friendly flight control system*
$f(d_s)$	=	*static component of shaping function*
FCS	=	*flight control system*

[1] PhD., Faculty of Information Technology, E-mail: chudyp@fit.vutbr.cz , AIAA Member.
[2] Associate professor, Faculty of Information Technology, E-mail: zemcik@fit.vutbr.cz .
[3] PhD., Department of Avionics and Control, E-mail: pawelrz@prz.edu.pl .

FF = *force feedback*
FSA = *flight simulator application*
g = *acceleration due to gravity [9,81 $m.s^{-2}$]*
GA = *general aviation*
γ = *flight path angle (vertical) [rad]*
h = *height [m]*
Iyy = *moment of inertia about the y axis [$kg.m^2$]*
K = *controller gain*
LSA = *light sport aircraft*
m = *mass [kg]*
PFD = *primary flight display*
q = *pitch rate [$rad.s^{-1}$]*
$RTRPE$ = *real-time rapid prototyping environment*
ρ = *air density [$kg.m^{-3}$]*
s = *Laplace operator*
S = *control surface area [m^2]*
SAS = *stability augmentation system*
T = *aircraft thrust [N]*
t = *time [s]*
θ = *pitch attitude angle [rad]*
ULL = *ultralight aircraft*
V = *aircraft forward speed [$m.s^{-1}$]*

I. Introduction

The light piston aircraft are becoming an increasingly popular option within the global personal transportation network. The progress in light and ultra-light aircraft technology led in recent years to a significant reduction of light aircrafts' ownership and operational costs. Flying thus became more accessible, offering a convenient alternative to the railway or car travel by utilizing a well developed network of local airports. Unfortunately for the light aircraft industry, the public opinion often questions the comfortableness and safety of the light aviation transport when compared to the commercial airliners or business jets. The principal issue behind the lack of the public acceptance hides in the single pilot operations of mostly amateur crews. The inexperienced pilots with a limited training are ill prepared for solving critical situations related to bad weather conditions or in-flight failures and emergencies.

A multi-modal fly-by-wire (light) flight control system with an intuitive user interface can significantly support and improve piloting process of a light aircraft and reduce the number of errors related to the "human factor" phenomenon. Unfortunately, commercial fly-by-x systems are overly complex and too expensive designs for a potential successful industrial application within the "small aviation". The main problem remains the guarantee of an overall sufficient fault-tolerance of the electronic and the electromechanical systems as a satisfactory system redundancy cannot be achieved without a multiplication of expensive components and devices.[3, 9, 11] In addition to the hardware redundancy a reliable flight control system requires utilization of a reliable and redundant control code and an implementation of (re)configurable flight control rules.[3, 8] Being aware of these difficulties, the authors have decided to create simulation environments which can support automatic flight control system and user interface designs aimed to simplify the piloting process of a light aircraft without introducing a control redundancy risk.

The transition from a flight control system's laboratory testing towards the airborne phase of the experiments should account for a pilot and hardware-in-the loop simulations on a suitably adapted ground based flight simulator. A modification of a state of the art professional flight simulator is a feasible, but at the same time a challenging task considering the number of difficulties related to the simulator's withdrawal from the training process, the loss of product certificate, potential violations of proprietary data protocols, different hardware standards, etc. A more flexible and accessible solution seemed to be a purposely built experimental simulation equipment. Therefore, two research simulators are being simultaneously developed at the Brno University of Technology (BUT) and Rzeszow University of Technology (RUT). Both unique solutions are designed for the purposes of an Advanced Light Aircraft (ALA) modeling and simulation.

II. SimStar experimental simulator

The SimStar is a light aircraft simulator stationed at the Faculty of Information Technology at the Brno University of Technology, Czech Republic. It is based on the cockpit section of the Evektor SportStar aircraft. Fig. 1.a and 1.b depict the SimStar with an opened canopy during a simulation break. Different from the original aircraft, the simulator's cockpit is equipped with an experimental dual 12" touch screen data visualization system, which can be seen in Fig. 2. The "smart/touch screen" technology allows for a rapid visualization of design changes and quick modifications to the flight display layout. This plays a critical role in the simulators overall conceptual design. An instrument panel of a state of the art light aircraft (GA, LSA, ULL) typically features a "glass-cockpit" unit with backup analog instruments, commonly referred to as the "steam gauges". These provide the crew with basic aircraft flight state information in case the electronics of the flight displays fails. In order to comply with the current perception of the flight deck safety, an airspeed indicator and an altimeter have been installed into SimStar's instrument panel, to support the crew with a classical reference of the flight data readout. One of the principal concerns during the instrument panel design phase was the enabling of a hardware environment with large digital screens that would have the potential to evolve into a standardized interface combining different, currently functionally isolated replaceable units (radio, GPS, round dial instruments). One of the PFD designs that accommodate the above mentioned principles can be seen in Fig. 2.

Figure 1.a Front view.

Figure 1.b Rear view.

Figure 2. Glass-cockpit's displays installation.

A. Cockpit configuration and flight controls

The basic principle upon which the PFD has been composed is the clarity and the readability of the depicted information. The flight display supports different modes of operation, ranging from a traditional visualization of the flight instruments, to enhanced synthetic vision concept with a tunnel in the sky flight path symbols. All of the advanced tools have been implemented with a single vision – to provide the pilot with a concept of visual aids that would result into a safer flying.

Since the visual stimulation does not represent the sole source of the flight state information, other perceptual channels needed to be included as well. A critical aspect in successful piloting of a light aircraft lies behind the unique perception of the haptic clues experienced by a pilot in flight. Therefore a cautious approach has been undertaken during the early stages of SimStar's conceptual design, to correctly include this requirement to the overall system's architecture. The currently installed FF system for the control stick and the rudder pedals provides the crew with a virtual link between the maneuvering state of the aircraft and the forces acting on its control system. A rudder pedal assembly allowing dual, side-by-side, rudder control that can be found in a light aircraft is shown in Fig. 2. In SimStar, the depicted system has been fitted with a loading mechanism that generates pedal forces due to the control surface deflection, based on the dependency between several flight variables extracted from the in-flight experimental measurements. A similar design approach has been applied to the simulation of the stick forces. Part of the future research is being directed towards the identification of smart visual cues that would supress the necessity of an active force feedback in pilot's inceptors for different fly-by-wire modes. Therefore, the loading mechanisms in SimStar can optionally be disengaged or modified to provide linear variation between the perceived loading and an adequate control surface deflection.

Figure 3. SimStar during a flight simulation.

Figure 4. Pilot's view from SimStar's cockpit.

B. Multimedia tools

In addition to the previously mentioned components, the SimStar has been equipped with devices supporting a voice activated communication between the crew or between the pilot and the SimStar's operator. It not only provides for more realism, but helps to identify and prevent possible emergencies. Simulator's principal multimedia platform features a planar 4m:3m projection screen and an audio system providing for enhanced authenticity during simulated flight operations. For convenience, the simulator currently resides on a stable platform with an optional alternation to a 6 DOF motion pad planned as a part of the future upgrades. A typical simulation run is presented in Fig. 3 and Fig. 4. The modular design of simulator's hardware and software architecture allows for a direct integration or sharing of simulated system's flight models. By applying extension blocks, the simulator can be subsequently used for hardware in the loop ground based simulations of an experimental avionics. The simulator's architecture features a data recording platform used to store the time histories of the simulated flights, which are a valuable source of information for a post-processing and debugging tasks.

C. Simulation of innovative flight control systems

It is industry's belief that a control system with a direct stabilized control of airspeed and flight path will be a major step in making personal air transport more accessible to broad public.[7] This opinion motivated the experimental implementation of a flight control concept known as the Total Energy/Heading Control System (TECS/THCS, Total-X). The total energy E_T of an aircraft in longitudinal motion can be defined as the sum of three energies: kinetic E_K, potential E_P and rotational E_R:

$$E_T = E_{Kinetic} + E_{Potential} + E_{Rotational} = mgh + \frac{mV^2}{2} + \frac{I_{yy}q^2}{2} \tag{1}$$

Value of E_R is nearly zero during steady or quasi steady flight states as climbing, cruise and approach, when the pitch rate approaches zero, $q \approx 0$. Considering light aviation class of non-aerobatic aircraft, rotational energy terms in Eq. (1) can be neglected. The difference (error) between commanded energy and actual flight state is defined as:

$$E_e = mg(h_{cmd} - h) + \frac{m(V_{cmd}^2 - V^2)}{2} \tag{2}$$

The principal motivation behind TECS strategy is to drive the energy error to zero with a minimal dissipation or build up of total energy. Differentiating E_e and making some detailed assumptions and manipulations, we can obtain formulas for energy rate error $\dot{E}_e$ and energy rate $\dot{D}_e$ distribution error Eqs. (3, 4).

$$\dot{E}_e = mg\left(\gamma_e + \frac{\dot{V}_e}{g}\right), \qquad \dot{D}_e = \gamma_e - \frac{\dot{V}_e}{g} \tag{3), (4)}$$

where,

$$\dot{V}_e = \dot{V}_{cmd} - \dot{V}, \qquad \gamma_e = \gamma_{cmd} - \gamma$$

In a steady level flight conditions is the aircraft drag compensated by an engine thrust T and the rate of an energy change can be produced directly by the change of the thrust $\Delta T_{cmd}=\dot{E}_e$. In TECS control laws, the amount of a total energy rate $\dot{E}_e$ is being influenced by inputs through different thrust settings Eq. (5), whereas the changes of pitch attitude lead to an energy redistribution Eq. (6) with the help of an elevator control θ_{cmd}. The TECS control strategy allows thrust and elevator control coordination in a decoupled response, causing the γ_{cmd} having a negligible influence on speed fluctuation and vice versa.

$$T_{cmd} = \left(K_{TP} + \frac{K_{TI}}{s}\right)\cdot \dot{E}_e, \qquad \theta_{cmd} = \left(K_{EP} + \frac{K_{EI}}{s}\right)\cdot \dot{D}_e \tag{5), (6)}$$

The core feedback integral K_{TI}, K_{EI} and proportional K_{TP}, K_{EP} gains are designed to yield identical dynamics for energy rate error and energy distribution rate error for either a flight path angle command or a longitudinal acceleration command. Proportional feedback gains operate with absolute values of the energy rate and the energy distribution rate. The TECS doesn't command elevator deflection directly, but generates a pitch attitude command, which is under the action of a pitch inner loop subsequently transformed to an elevator input. Similarly, a thrust scaling inner loop is transforming the thrust commanding signal into thrust lever setting.

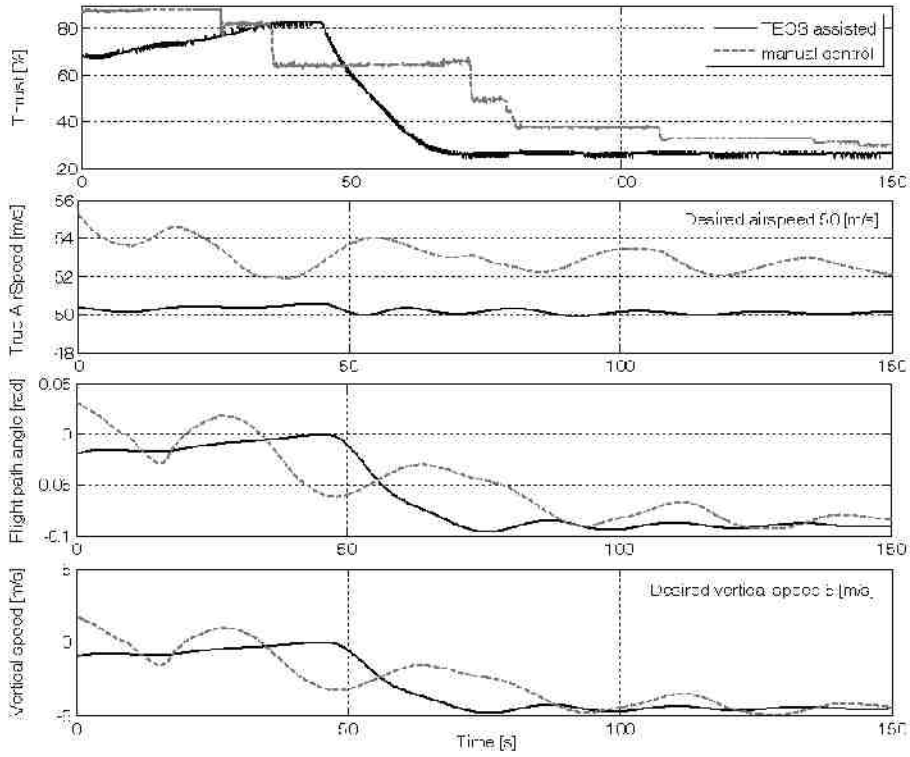

Figure 5. Simulations of fully manual and EFCS assisted approach task.

The concept behind the Total-X algorithms inspired the authors to work on an Environmentally Friendly Control System (EFCS), which can assist pilots of light aircraft during typical piloting and navigational tasks to minimize noise and fuel consumption.[2] Aircraft with standard avionics can be equipped with an additional set of sensors and a dedicated control panel as the EFCS can work as a flight assisting tool and an autopilot simultaneously. After the activation, the system initiates an electromechanical system which trims pilot's inceptors (pitch channel and thrust lever) to execute the flight plan in accordance with the energy conserving control and navigation algorithms. The pilot is enabled to manually control the aircraft during all phases of flight, while the EFCS prompts her/him to actively manage aircraft's total energy states and reduce noise. Simulations of the EFCS have been performed on XM-15 flight simulator featuring the mathematical models from the SimStar. A set of the flight parameters was recorded during a fully manual as well as during an EFCS assisted descend on the initial approach to EPRZ runway 09 (Rzeszów-Jasionka airport). The test cases have been performed for a moderate turbulence conditions. A comparison between the manual and an electronically assisted flight control indicates EFCS's capability to support the pilot to maintain precisely a constant airspeed and the desired flight trajectory. The manual flight regime exhibits a significant throttle activity during a descent to the approach, while EFCS assisted flight allows maintaining a constant engine setting at a reduced thrust (Fig. 5). Performed experiments showed the average thrust setting being close to about 10% higher in the manual mode than in the EFCS assisted control mode.[2]

III. Simulator based on M15 cabin

The next flight simulator, which was designed at the RUT, Faculty of Mechanical Engineering and Aeronautics, Department of Avionics and Control, is based on the cockpit section of an M-15 aircraft. The M-15 was originally a "crop duster" jet plane built in Poland at the beginning of 1980's. One cabin of this aircraft type has been adopted by the RUT in the 1990's for educational and demonstration purposes. The functionality of this device has been continuously improved during the last years by adding a digital visualization system, FF, RTRPE, an electronic instrument panel and a set of FSA.

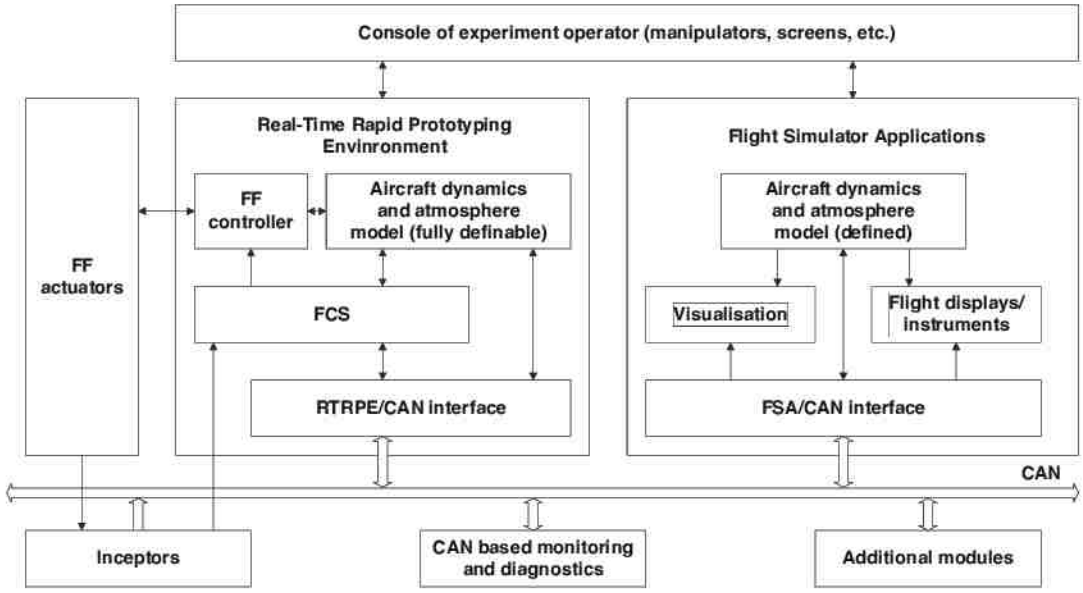

Figure 6. Structure of experimental simulator XM-15.

A. Simulator architecture

The main modules of the simulator shown in Fig. 6 are connected by a CAN data bus.[1] Application of the CAN network and CANaerospace standard communication protocol, described in Ref. 10, makes this solution compatible and open to some of the other on-board systems. The experimental simulator XM-15 enables hardware in the loop simulation of electromechanical actuators, control panels and inceptors equipped with CAN controllers.[9]

Particular modules and subsystems of the XM-15 flight simulator are grouped into the following areas of functionality:

- aircraft dynamics and atmosphere models,
- inceptors and FF system,
- flight control system,
- flight displays and visual system,
- monitoring and experiment management,
- additional modules (hardware in the loop).

The designed structure of the experimental simulator allows for a straightforward integration of the modeled, aircraft specific dynamics and atmospheric models with the RTRPE or to use defined, external models as a separate application. The XM-15 simulator is equipped with an in-build non-linear model of the PZL-110 Koliber's dynamics.[5] However, the implemented specialized software provides libraries of tens of different aircrafts models. A bi-directional accessibility of the external model parameters is realized through a TrueSight application which constitutes a software element of the FSA/CAN interface.

The flight deck of the XM-15 simulator is based on the original and suitably adapted equipment of the M-15 cockpit as seen in Fig. 7. The instrument panel with an analogue flight state and system status indicators has been replaced by a single 24'' screen LCD. This solution proved more flexible and allowed for a visualization of different types and configurations of classical analogue as well as digital indicators as seen in Fig. 8.

Figure 7. General view of XM-15 simulator.

Figure 8. Flight deck of the XM-15.

The XM-15 experimental platform offers monitoring and data acquisition on three particular levels. Selected parameters processed in RTRPE system can be observed, tuned and recorded at the time of the experiment from the operator's console (designed especially for unexperienced operators). The external data recording, monitoring and diagnostics is possible with the use of a CAN Monitor system.[6] The TrueSight application offers a simultaneous access to the internal parameters of the FSA as well as to the data transferred via the CAN data bus. Advanced users, especially programmers, have the option to define a detailed list of parameters which are recorded by the TrueSight only.

B. Flight control system

The XM-15 simulator features the original inceptors: control wheel, rudder and thrust lever. The mechanical system transmits movements of the inceptors to the block of potentiometers located at the back of cabin. Movements are measured with the use of A/D converters of the RTRPE, and send directly via CAN to a custom designed data acquisition unit. The force feedback controller takes into account the actual flight parameters, simulated wind effects and the inceptor's position to compute the desired force acting on the pilot's inceptors. Estimation of the forces acting on the controls is realized through the use of Eq. 7.

$$P_H = -(b_1 \cdot \alpha + b_2 \cdot \delta + b_3 \cdot \delta_t) \cdot \rho \cdot V^2 \cdot S \cdot \frac{c_{mac}}{2} \cdot \frac{\Delta\delta}{\Delta x} \tag{7}$$

The forces in the pitch and roll channels are realized physically by the FF actuators integrated to a set of springs and levers. The yaw channel is loaded proportionally to the rudder deflection.

The FCS module, depending on selected configuration, emulates the following control systems:
- mechanical control system based on levers, strands, pushers and springs,
- mechanical control system with hydraulic amplifiers,
- fly-by-wire system,
- autopilot (classical or Total-X mode),
- pilot assistant module (EFCS mode).

The fully mechanical control system is simulated with the use of the potentiometers connected to the strands and bars. Signals from the A/D converters are calibrated, corrected by the gain factor and send via CAN to the aircraft dynamic model as the actual control surfaces deflections and throttle settings. The control system with the hydraulic components includes additional software components for the simulation of the rate limiting elements with the backlash and hysteresis effect.

Simulation of the fly-by-wire is realized on three levels of control:
- normal,
- simplified,
- direct.

In the normal control, all the properties of a fly-by-wire are employed and a SAS is used. This mode provides the pilot with a superior and easy control of chosen flight parameters and has a great influence on the handling qualities. It improves the safety of flight and minimizes pilot's workload. A simplified mode uses a simple CAS and can be optionally engaged on demand for a more "manual flying". The direct control is designed for an emergency control only, the deflections of the control surfaces are directly related to the displacements of the inceptors.

In a mechanical control system, the deflection of a lever is proportional to a consequent control surface deflection. In a fly-by-wire control system, this is not the case at all. Pilots of the aircraft equipped with a fly-by-wire system should therefore be aware of this feature. The movement of the control lever directly influences the flight parameters (not the displacement of the aerodynamic surfaces).

A model of a fly-by-wire system simulated in XM-15 includes the dynamics of:
- shaping functions of control elements,
- control laws,
- actuators (rate limiting elements with backlash and hysteresis),
- measurement units and data buses (delays and quantization effect).

Signals from the controls are modified with the use of a shaping function presented in Eq. 8. This dependence allows for a static as well as for a dynamic modification of signals. Using a cubic function from Eq. 9 as a static component leads to small and precise corrections of the flight parameters without any limitations for maximal control surface deflections. On the other hand, the dynamic component in Eq. 8 reduces phase lag and minimizes the succeptibility of an aircraft to the pilot induced oscillations.

$$d_{sfv} = \min\left\{\begin{matrix} \left|f(d_s) + k_V \cdot \dot{d}_s\right| \\ 1 \end{matrix}\right\} \cdot \mathrm{sgn}\left(f(d_s) + k_V \cdot \dot{d}_s\right), \quad f(d_s) = \left(\frac{d_s}{d_{s_{max}}}\right)^2 \cdot \mathrm{sgn}(d_s) \qquad (8), (9)$$

Models of three control laws are implemented in a fly-by-wire structure of XM-15:
- stabilization of the angular rates,
- stabilization of the attitude,
- stabilization of the flight path and heading.

The XM-15 simulated control laws based on the classical algorithms as well as on the Total-X theory (stabilization of flight path and heading only).[4] A required control scheme can then be selected before the initiation of the experiment from the operator's console. The thrust lever sets the desired air speed for all algorithms. The flight simulator's environment also supports an integration of a real/hardware based autopilot solution as a part of

the hardware in the loop simulation cycle. A pilot assistant module enables an interactive support of the piloting process. After the activation, the system initiates a force feedback system which trims the particular inceptor to execute the flight plan with an energy conserving control and navigation algorithms.[2] The pilot is also enabled to manually control the aircraft during all phases of flight, while the FCS prompts her/him to actively manage aircraft's total energy states and reduce the acoustic emisions . The pilot assistant module has the potential to improve the piloting performance or prevent a potential loss of control in a case of panic or bad weather conditions. The idea of an interactive pilot assistant module is presented as block scheme in Fig. 9.

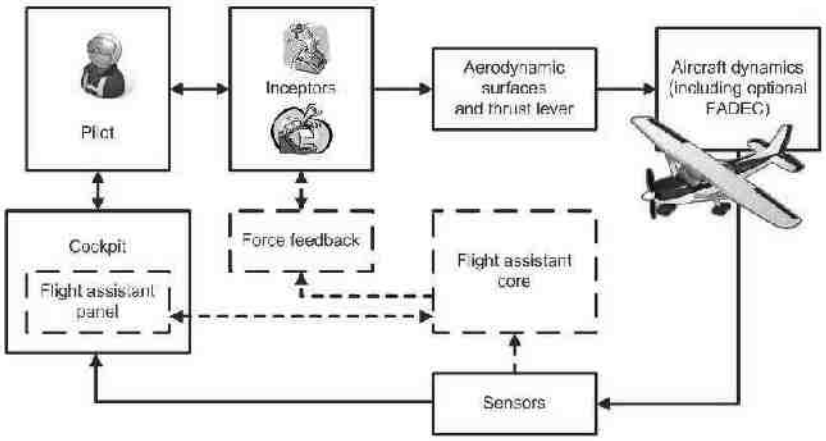

Figure 9. Block scheme of interactive pilot assistant module.

IV. Conclusion

To the current date, the design of the SimStar simulator is primarily targeted towards research and development on issues related to the intuitive pilot/aircraft interfaces design. Integrated flight displays with applied synthetic vision technology allow safety improvments of the single pilot operations, positively stimulating the social impact of the light aircraft travel. Small aircraft equipped with the intuitive flight displays, an electronic assistance module and autopilot have the potential to be safe, popular and affordable aids to the personal transportation systems. On the other hand, the complexity of the man-machine interactions and some of their unpredictable aspects require advanced pilot in the loop tests which can be realized on the high fidelity simulator of a specified aircraft type only.

Experimental flight simulator XM-15 was originally developed for the purposes of the fly-by-wire flight control system design. A real time, rapid prototyping environment integrated with the simulator allows for a design, prototyping and testing of the advanced control modes, including nontypical structures of the formulated models and algorithms. This feature promoted the implementation decision of the Total-X concept on the XM-15. The positive results of the real time experiments of the autopilot based on the Total-X boosted further research that led to the EFCS. The solution of the flight assisting tool was verified during the simulated flight tests which confirmed the suitability of a practical realization of a Total-X based system.

The genesis of the development of the flight simulators presented in this paper is different; however they complement each other in a convenient way. The fusion of the solutions designed at BUT and RUT accelerates the progress on both simulators. Practical tests of the identical concepts executed in parallel on two independently developed experimental flight simulators allow for a more rigorous testing of the verified systems.

Acknowledgments

This work has been supported by the "Security-Oriented Research in Information Technology" research project CEZ MŠMT, MSM 0021630528 and supported from Polish scientific founds within the framework of development project in years 2007-2010.

References

[1]CAN Specification Version 2.0, Robert Bosch GmbH, 1991.

[2]Chudy P., Pieniazek J., Rzucidlo P., "Flight Control System for Environmentally Friendly Light Aircraft," *Polish Journal of Environmental Studies*, Vol. 18, No. 4B, pp. 21-25, 2009.

[3]Chudy P., Rzucidlo P., Tomczyk A., "Safety enhanced digital flight control system," *Aircraft Engineering and Aerospace Technology*, Vol. 81, Issue 5, pp. 416-423, 2009.

[4]Chudy P., Rzucidlo P., "Controller Design for a Digital Flight Control System DFCS," *The 2nd International Multi-Conference on Engineering and Technological Innovation*, IMETI 2009, Orlando, Florida, 2009, 6 ps

[5]Cieciński, P., Pieniążek, J., "Aircraft Model for Purposes of Control Systems Synthesis," *Mechanics in Aviation IX Conference*, Warsaw, 2004.

[6]Kopecki G., Rzucidło P., "Problems of Monitoring in the Fly-by-Wire System for Small Aircraft," *AIAA Guidance, Navigation, and Control Conference and Exhibit*, AIAA, Keystone, Colorado, 2006, 8 ps.

[7]Lambregts, A. A., "Fundamentals of Fly-By-Wire Augmented Manual Control," *SAE 2005 AeroTech Congress & Exhibition*, Forth Worth, Texas, SAE 2005-01-3419, 2005.

[8]Rzucidlo P., Tomczyk A., "Prediction of Susceptibility of Small Aircraft to Pilot-Induced Oscillations," *SAE 2007 Transactions Journal of Aerospace*, Warrendale, Pensylwania, 2008, pp. 819-827.

[9]Rzucidlo P., "Laboratory and Preliminary In-Flight Tests of Electromechanical Actuators," *General Aviation Technology Conference & Exhibition*, Wichita, Kansas, SAE Paper 2006-01-2414, 2006, 10 ps.

[10]Stock M., "CAN Aerospace Interface specification for airborne CAN applications V 1.7," Revision 1.7, 2008, 58 ps

[11]Tomczyk A., "Facilitated Airplane – Project and Preliminary In-Flight Experiments," *Aerospace Science and Technology*, Elsevier, Vol. 8, No 6, 2004, pp. 469-477

AIAA Modeling and Simulation Technologies Conference
08 - 11 August 2011, Portland, Oregon

AIAA 2011-6348

Intuitive flight display for light aircraft.

Peter Chudy[1] and Karol Rydlo[2]
Brno University of Technology, Brno, Czech Republic

Responsible piloting requires constant mental effort to monitor the aircraft's systems, conduct flight data management and, in extreme cases, to develop and execute a correction plan within the constrains of limited time. This is in direct contradiction with human ability to successfully solve simultaneous data management tasks while under stress. Modern light aircraft are designed to support a wide community of pilots with different levels of piloting skills and personal preferences. The SimStar light aircraft flight simulator with its intuitive flight display was designed to improve situational awareness and to support pilot decision making processes. Initial testing of SimStar and its advanced flight display system was performed on the cockpit section of an Evektor SportStar, a popular light aircraft.

Nomenclature

ALT	=	Altitude
COM	=	Communication
DOF	=	Degrees of freedom
ENG	=	Engine data
FPA	=	Flight Path Angle
GA	=	General Aviation
GPS	=	Global Positioning System
GS	=	Ground Speed
h	=	Height
HDG	=	Heading
IAS	=	Indicated Airspeed
IFD	=	Intuitive Flight Display
KIAS	=	Knots – Indicated Airspeed
LAT	=	Latitude
LON	=	Longitude
LSA	=	Light Sport Aircraft
m	=	Mass
MAP	=	Moving Map Display
MFD	=	Multifunction Display
NAV	=	Navigation
OAT	=	Outside Air Temperature
P	=	Pressure
PFD	=	Primary Flight Display
PFPA	=	Potential Flight Path Angle
QNH	=	Barometric Pressure Adjusted to Sea Level
RPM	=	Revolutions per Minute
SVS	=	Synthetic Vision System
TRK	=	Track
ULL	=	Ultralight Aircraft
V	=	Airplane velocity
v	=	Speed along flight path
VSI	=	Vertical Speed Indicator

[1] PhD, Faculty of Information Technology, Email: chudyp@fit.vutbr.cz, AIAA Member.
[2] Research Assistant, Faculty of Information Technology, Email: krydlo@gmail.com.

I. Introduction

The appreciation of the value of time and living a low-stress lifestyle is increasingly gaining in importance. Individual air transport, motivated by the advantages of useful time, avoidance of exhausting terrestrial travel on crowded highways, along with the risks of terrorist attacks on transportation infrastructures, led to increased interest in General Aviation, Ultralight and Light Sport Aircraft flying. Introducing aircraft categories intended solely for private use and individual operations revitalized the light aviation market and opened it to a new class of users. However, operational experience confirms the dangers associated with inadequate piloting skills and insufficiencies in pilot training.

Piloting an aircraft is a demanding task requiring constant mental effort. However, safety improvements have been rather gradual thanks to trainers with exceptional stick and rudder skills passing these on to new pilots. What safety improvements have been introduced,have been technological innovations flowing from proven "good enough" solutions. State-of-the-art flight deck designs, for example, integrate flight guidance, aircraft systems, situational awareness control tools and display functions to a minimum number of interdependent electronic displays. Even scaled down versions of such technology include electronic displays, control of all primary airspeed, altitude and attitude instruments, along with all essential navigation and communication functions.[1]

II. Intuitive Flight Display

Advances in electronics, software design, accessibility of sophisticated testing tools and market availability of new products made the integrated flight displays suitable for installations in light aircraft. Flight displays, offering flexible presentation of flight instruments and system controls, became a preferred option among pilots and aircraft operators. Based on a recent survey, 90% of new-built light piston aircraft were equipped with "glass cockpits".[2] This quantitatively high number doesn't, however, account for a larger market of retrofit avionics designed to fit earlier production aircraft models. Saying "people will get used to anything" certainly has undisputable historical roots, but it doesn't allow for performance and safety improvements expected by today's users. The objective of intuitive display design was to create a flight display that features intuitive indicators allowing safe aircraft control and comfortable aerial navigation across a wide range of piloting skills: from the novice to the expert.

A. Why intuitive?

The state-of-the-art flight displays stimulated improvements in situational awareness through data integration and user centered visualization of flight surrounding events (weather image; traffic and terrain situation). The basic principle upon which the flight displays have traditionally been constructed is the clarity and readability of the presented content. This is of high importance as the correct interpretation of flight critical data reduces pilot workload and can dramtically improve overall piloting safety. The display integration of the instruments redefined the classical round dial appearance, but has failed to led to the next logical step of introducing intuitive indicators that would simplify the task of creating a mental model of the current flight state. Energy based indicators of currently isolated flight data, for example, have the potential to provide pilots with a tool that assists in optimizing a system's total energy distribution in flight and requiring less control effort.

Operational intuitiveness does not account for the display part only, however, but imposes requirements on the display control elements as well. Advances in touch screen user interface designs directly support clarity of operation and control by replacing buttons and encoders, allowing the user to approach the desired functionality directly by accessing/touching the icons on the display's screen.

B. Energy management concept

Since the evolution of heavier-then-air flight, the concept of flying has been traditionally tied to energy management principles. Gliders, among others, are a suitable candidate for explaining transformation processes between the kinetic and the potential components of the total energy. Assuming zero wind conditions, no convective air currents in the atmosphere and a constant weight of the system, the glider pilot uses the

Figure 1. Evektor SportStar - light sport aircraft.

elevator and the elevator trim to command the distribution of airspeed (kinetic energy) and altitude (potential energy) accordingly to the intended flight profile. If drag induced energy dissipation is not compensated for by an additional power input, the glider enters an unpowered descent. The most demanding piloting task, however, is the final approach and landing when the pilot needs to properly adjust the glider's flight path and airspeed to avoid optional deployment of speed breaks in order to enhance the dissipation of excessive energy on landing. Elevators are thus used to control the distribution between the kinetic and the potential energy. Flying powered aircraft offers more operational flexibility but, also, introduces additional complexity into the energy balance scenario. There are two longitudinal motion control strategies commonly used by the pilots: "throttle to speed and elevator to altitude" and the "throttle to altitude and elevator to speed".[3] Along with the glider analogy, the "throttle to altitude and elevator to speed" seems to be a more appropriate and preferred control technique for flying light aircraft.[4]

It is industry belief that an aircraft control system with a directly stabilized control of airspeed and flight path will be a major step in making personal air transport more accessible and safer to the broader public.[5] Considering the above mentioned concepts of energy related to safe piloting techniques, the task at hand becomes answering how to visualize control cues. Visualizing such cues would allow the pilot to easily make necessary coordinated adjustments to elevator and thrust lever, leading to appropriate airspeed and flight path angle targets. The convenient way to achieve this goal is through the concept of total energy E_T.[3-8] For longitudinal motion, best suiting the descent profile during approach and landing, the total energy of the system can be defined as the sum of energies: $E_{Kinetic}$ and $E_{Potential}$,

$$E_T = E_{Potential} + E_{Kinetic} = mgh + \frac{mV^2}{2} \tag{1}$$

By further manipulations of the energy balance equation from Eq. (1), and introducing a new quantity, the specific total energy Es, the specific total energy rate equation can be derived according to Ref 9. This introduces additional important quantities to describe the flight state of an aircraft, namely the FPA (γ) and the PFPA (γ_P).

$$\frac{\dot{E}_s}{gV} = \frac{\dot{v}}{g} + \gamma\,, \tag{2}$$

$$\gamma_P = \frac{\dot{v}}{g} + \gamma\,, \tag{3}$$

$$\gamma = \frac{\dot{h}}{V} \tag{4}$$

Both, FPA and PFPA have been used in Head-Up Displays to provide an effective thrust guidance cue.[9] By definition, the FPA is a quantity relative to air mass that does not necessarily match the pitch angle and can be described through a function of airspeed and vertical speed (Eq. (4)). PFPA is a hypothetical quantity, which when visualized provides the pilot with a optimal flight path angle margin. This margin is achievable if the actual excess energy needed to maintain desired altitude and airspeed is fully transformed into potential energy in a climb. In situations where the aircraft's total energy level drops, the PFPA represents a flight path angle of constant airspeed in continuous descent. In steady flight conditions, the deflection of elevator causes a change in $\dot{v}/g$ that is equal and opposite to the change in FPA. From Eq. (2) and Eq. (3), the changes in thrust setting influence the total energy of the system and lead to changes in γ_P (PFPA).

C. Software implementation

The intuitive flight display application, internally designated as the AW-PFD, has been written in C++ using the OpenGL and GLUT toolkit. The application is based on parallel data processing to benefit from available performance data and better utilization of hardware resources. GPX files are implemented as a standard format providing the information on displayed objects and airspace classes. Further advantage of using the GPX is its convenient portability to different GPS navigations platforms.

The main thread services the initiation of visualization, communication and objects loading, and provides the support for multithread operations. After the completion of the initialization phase, the main thread initiates individual service threads and subsequently manages the visualization and the input/output (I/O) operations only. The service threads encapsulate individual I/O operations with disk subsystem, network communication, and

application timers as well as their actual status. The network communication is provided by the AW NetCom module using the TCP/IP protocol. This allows for direct communication with the main server, or an individual communication with applications serving the hardware sensors or the simulation core with the AW NetComSrv module. Two pairs of threads (Near, Far) are used for asynchronous loading and data processing for the 3D terrain visualization in the SVS and the visualization of the moving map in the flight display's lower left corner. In addition, these threads are used to load and process objects (obstacles, airspace classes, significant points, runways, etc) presented on the flight display. The system timer controls the optimal utilization of resources by limiting the number of frames per second, providing more computational capacity to the remaining service threads. The last thread is used to initiate the internal simulation that is used for testing and presentation purposes with the server connection closed.

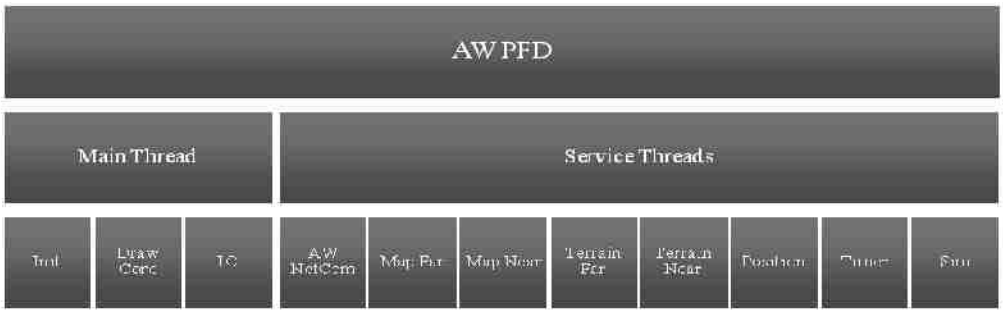

Figure 2. PFD's software implementation scheme.

The synthetic 3D terrain is divided into tiles of given sizes being asynchronously loaded and processed using service threads. The terrain processing service threads are utilized to correct potential errors, to avoid the occurrence of artifacts on the tile edges, and to load tile related objects.

D. Flight display elements

As typical GA/LSA/ULL pilots transition between different aircraft makes and models, industry guidelines have been implemented throughout the design phase in order to avoid an unnecessary increase in display diversity leading to a potential safety hazard due to user irritation. [1]

The airspeed indicator, shown in Fig. 3, has been presented as a tape indicator with a fixed position of the digital airspeed readout. There are different recommendations regarding the color of the tape indicators, ranging from transparent with contrast edges to colored strips with white airspeed digits.[1] Color coded speed ranges on the airspeed indicator use standard color classification where the white range represents aircraft operating speed range with flaps extended; the green strip indicates normal operating speed limits; and, the yellow airspeed range (ending with a red line) for never exceed speed which assists piloting while in rough or turbulent air.

The altimeter, introduced in Fig. 3, is subjected to number of the recommendations already declared for the airspeed indicator. The scale is based on 500 ft and 1000 ft altitude increment markers presented on a contrast background. An important feature is the indication of minimum selectable sector altitude accompanied with an aural warning. The vertical speed indicator can be based on the graphical design which is conveniently located on both sides (left or right) of the altimeter presenting the pilot with important altitude trend information. Displayed range depends on the aircraft's performance class but generally shouldn't span less then +/-2000 $ft.min^{-1}$.

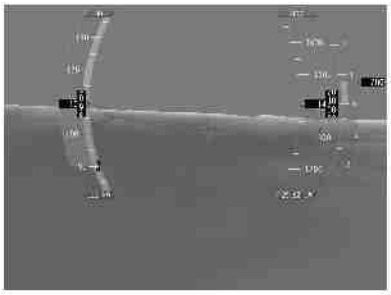

Figure 3. Airspeed indicator, altimeter and VSI.

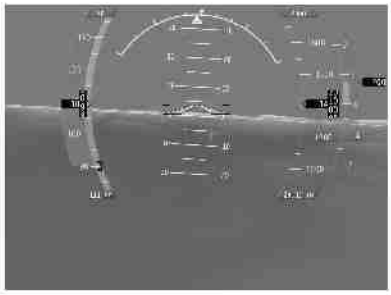

Figure 4. Artificial horizon on synthetic terrain.

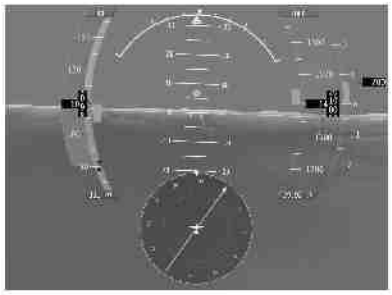

Figure 5. Integration of the heading indicator.

The artificial horizon uses standardized wedge shaped aircraft representation with horizontal marks on the sides, along with a linear representation of the horizon. Further features include position markers in case the whole display area is submerged into the artificial terrain or sky. Side marks on the round artificial horizon image indicate bank angles of 10, 20, 30, 45, 60 degrees. The heading indicator is visualized as a circular pattern in the lower central part of the display and allows manipulations with a selector bug. Visualized engine management indicators feature a set of basic quantities: propeller speed, engine manifold pressure (engine power), oil pressure and temperature, fuel pressure, remaining fuel quantity in fuel tanks, and immediate fuel flow indication.

Figure 6. Landing approach to LKTB.

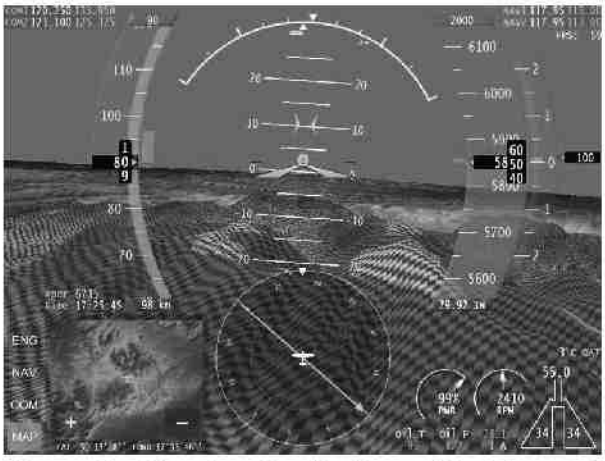

Figure 7. Terrain visualization with integrated moving map.

State-of-the-art flight displays feature differently detailed synthetic 3D terrain models with a wide scope of integrated safety features. The SVS uses aircraft position information, along with stored terrain data, to present the pilot with a situational overview in front of the aircraft. Flight displays with operational SVS also support visualization of airspace classes, graphic representation of obstacles along the flight path and runways ahead. Collision detection algorithms identify potential dangerous terrain for the pilot to avoid.

Tape indicators, similar to those used for displaying airspeed and altitude data, have been implemented into (energy) and on the inner edges (energy rate) of the airspeed and altitude indicators in order to provide the pilot with an interpretation of the accumulated amount of kinetic and potential energy and their rates. The size of the energy indicators has been subjected to scaling procedures.[9] The scaling factors for the FPA, PFPA were set to match the pitch scale of the artificial horizon. Figures 8 and 9 show the indicators implemented within the intuitive flight display design.

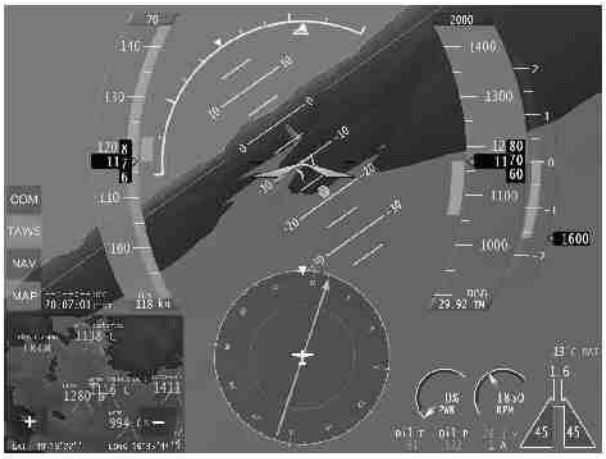

Figure 8. Potentially dangerous terrain and obstacles.

Figure 9. Energy management flight indicators.

The wide range of integrated visualization remains the principal concept for situational awareness improvements. Additionally, imbedded aural warnings have been shown to efficiently stimulate pilots' awareness in

critical cases such as low fuel level, prohibited configuration changes, collision avoidance, fire detection or airspeed approaching stall limit for given configurations.

III. Light aircraft flight simulator SimStar

The SimStar is a light aircraft flight simulator stationed at the Faculty of Information Technology, Brno University of Technology. It is based on the cockpit section of an Evektor SportStar aircraft. Figure 10 shows the SimStar with a closed canopy during a simulation break. Compared to the original aircraft, the simulator's cockpit is equipped with a dual 12" touch screen flight data visualization system, as seen in Fig. 11. The "smart screen" technology allows for rapid design changes and quick modifications of the display layout and plays a vital role in the simulator's overall conceptual design. A state-of-the-art light aircraft (LSA, ULL) instrument panel typically features a "glass-cockpit" unit with a host of backup analog instruments. In order to comply with current perceptions of flight deck safety, an airspeed indicator and an altimeter have been implemented into the instrument panel to support the crew with a classical reference for the flight data readout.

Figure 10. SimStar's cockpit section.

Figure 11. Instrument panel flight displays.

A. Architecture

Modules and subsystems of the SimStar are grouped into functional blocks shown in Fig. 12. The modular design of simulator's hardware and software architecture allows for a direct integration or sharing of different flight models through Matlab/Simulink or via a direct upload of XML files with the aircraft's dynamic model. The simulator is by default equipped with a non-linear 6 DOF aircraft dynamics model of the Evektor SportStar light aircraft. [11]

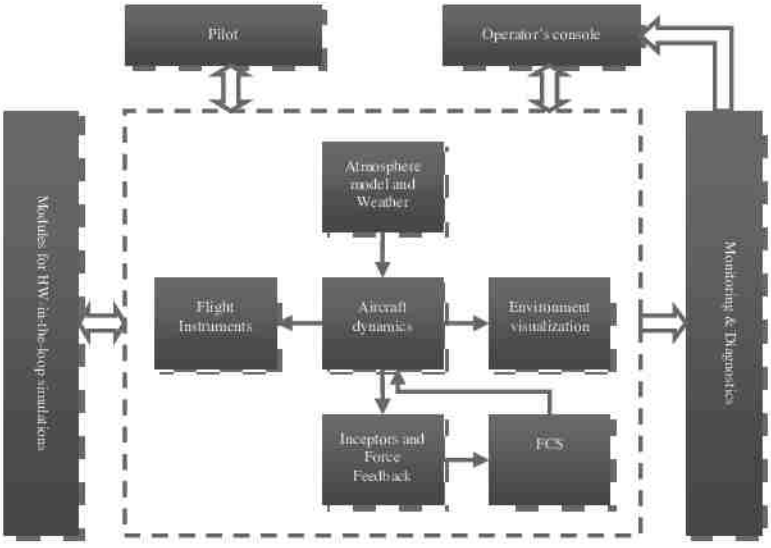

Figure 12. SimStar's architectural design with functional blocks.

The simulator's multimedia platform features a planar 4m/3m projection screen and an audio system providing enhanced authenticity during simulated flight operations. SimStar has been equipped with tools supporting voice activated communication between the pilots or between the pilot and the operator. It not only provides for more realism, but helps identify and prevent possible emergencies.

Figure 13. Initial design of SimStar's instrument panel.

A critical aspect of successfully piloting a light aircraft lies in the unique perception of haptic clues experienced by the pilot in flight. Therefore, a cautious approach has been selected during the early stages of SimStar's conceptual design to correctly include this requirement into the system's overall architecture. The currently installed force-feedback system for the control stick and the rudder pedals provides the crew with a virtual link between the maneuvering state of an aircraft and the forces acting on its control systems. The simulator's design philosophy retained the concept of using the original pilot inceptors, i.e., control stick, rudder pedals and thrust lever, where the control inceptors' deflections are transmitted via mechanical linkages to potentiometers. In order for the controller to compute the forces in the control stick, the force feedback controller accounts for the actual flight parameters, atmospheric conditions and the inceptors' position. Forces in the pitch and roll channels are introduced through the force feedback actuators. During simulations, the yaw channel is proportionally loaded to match the rudder deflection.

The integrated flight control system (FCS) block emulates control system configurations depending on aircraft models and makes. The FCS offers a classical mechanical control system with pushrods, levers, cables and springs, circuits with hydraulic systems, or a fly-by-wire system when using the available direct CAS (Control Augmentation Stabilization) and SAS (Stability Augmentation System) modes. By default, it features autopilot algorithms for longitudinal and lateral-directional modes, with classical or energy based control logic.[8,10] Due to the simulator's open architecture and its inbuilt hardware-in-the-loop capability, experimental avionics hardware can be integrated and tested within the SimStar as well. The simulator's architecture supports data recording capability primarily used to store the time histories of simulated flights. These histories are a valuable source of information for post-processing and subsequent debugging tasks. One of the principal objectives during the instrument panel design phase was to utilize a large digital screen display environment that would could evolve into a standardized interface combining different, currently functionally isolated, replaceable units (radio, GPS, round dial instruments) as seen in modern integrated avionics solutions. One of the Primary Flight Display (PFD) designs that accommodate the above mentioned principles can be seen in Fig. 13.

B. Integration into SimStar

SimStar's flight display integration was provided by the main communication server AW-COM-SRV that supports connection to different systems and their encapsulation during communication with the AW-PFD.

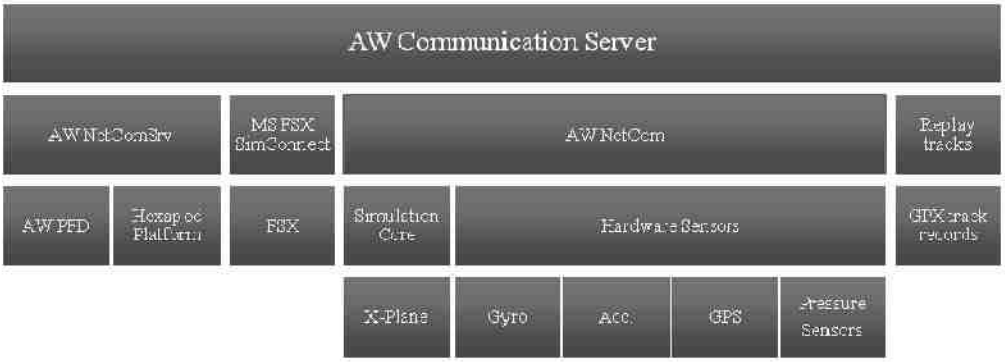

Figure 14. Server communication scheme for integration into SimStar.

Communication is based on a proprietary coded protocol running on TCP/IP. The server uses a server module to service client applications (PFD, Hexapod platform), client modules for the communication with different flight simulation systems (X-plane via AW-Xplane-plugin), or a client module for communications with sensor data applications. The server module and the client module are executed in parallel with only one client module running at a time. The selection of the client modules is accomplished through custom settings during the loading process.

As already mentioned, communication is based on the server module AW NetComSrv, which runs in data gathering applications, and the server module AW NetCom. The server module supports the clients independently and works in an asynchronous regime with the client receiving all data with a given guaranteed time marker. The client module works in an asynchronous regime as well and periodically attempts to reestablish server connection in case the source data becomes lost or unavailable. AW-COM-SRV allows replaying recorded flight data captured in the GPX format.

IV. Simulation and verification

Pilot-in-the-loop simulation of intuitive flight displays has been performed with three groups of users ranging from inexperienced novices, to intermediate ULL/LSA/PPL pilots, to experienced certified flight instructors (FI, CPL). Candidates were give instructions in terms of position and airspeed targets they were asked to acquire. The intention of the verification phase was not to conclude the experiments with a lengthy statistically correct outcomes of the designed display implementation suitability; instead, it was intended to evaluate the intuitiveness of the presented features and to issue recommendations for the design improvements on an expert basis.

Figure 15. Groups for Pilot-in-the-loop evaluations in SimStar simulator.

As expected, novice candidates had initial difficulties with accomplishing the predefined tasks, which included 3D maneuvers in both vertical and horizontal planes, and flying VFR patterns at LKTB (Brno Turany International Airport, Czech Republic). After brief familiarization training under the supervision of a skilled instructor, and practicing awareness distribution during maneuvering, the inexperienced candidates were able to maneuver the aircraft correctly into the required position and speed profile (also while being supervised by an instructor). This group, initially overwhelmed by the display's information content richness, tended to use the display as a primary reference during the entire simulation without employing the VFR specific "looking out and remembering the scenery" technique. This observation confirmed the integration capability of the display. Relevant flight indicators were presented in a SVS environment that helped the users to mentally correlate the current flight state to the outside terrain. The flight display with its integrated energy states and path indicators assisted in explaining and correcting candidates' maneuvering habits. Adding total energy through operating the thrust lever was conveniently indicated by the growing energy rate indicators and motion of the PFPA symbol. While selecting the airspeed and altitude targets is an indisputably well accepted concept for automatic flight control modesm it introduces extra work when flying the aircraft manually.

The ULL/PPL holders, with a total flight time between 100 – 200 hours, flying different aircraft models primarily equipped with classical instrument panel, enjoyed the added functionality of the energy and flight path indicators integrated into the SVS environment. However, it was found that the SVS can cause irritation in near terrain flight when the terrain data do not exactly match the real environment as seen from the cockpit. Energy management indicators, with properly defined target values used to define the energy

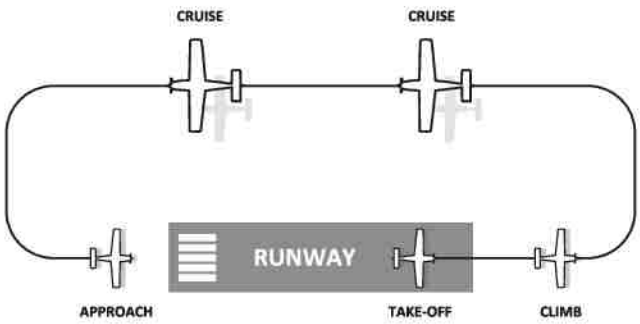

Figure 16. Simulated pattern at Turany Airport.

differences between the desired and the actual states, supported the aircraft control technique "throttle to altitude and elevator to speed". The FPA and PFPA indicators on a synthetic terrain background, along with the energy trend tapes, helped create intuitive terrain awareness solutions. The mental image extracted from the collision avoidance indicators resulted in the expected collision avoidance reactions, with the PFPA and FPA positions also suggesting the amount of energy needed to clear/avoid obstacles. The pilots were not provided with direct avoidance maneuver cues, but were given the status information that increased their situational awareness. Since this group has had sufficient flying experience, the energy management and flight path indicators were perceived useful in precision piloting tasks as, for example, during landing approach maneuvering.

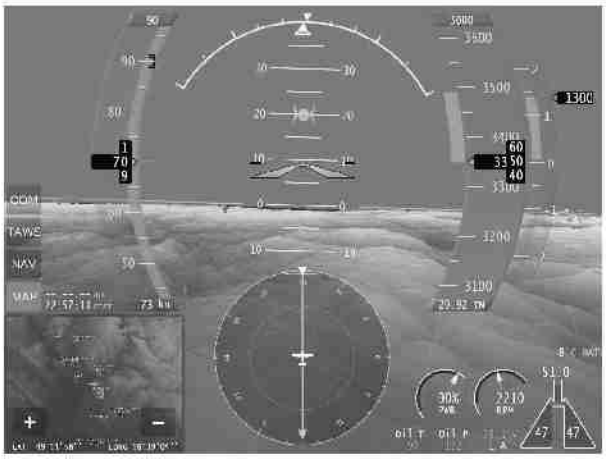

Figure 17. Excess energy used to change altitude.

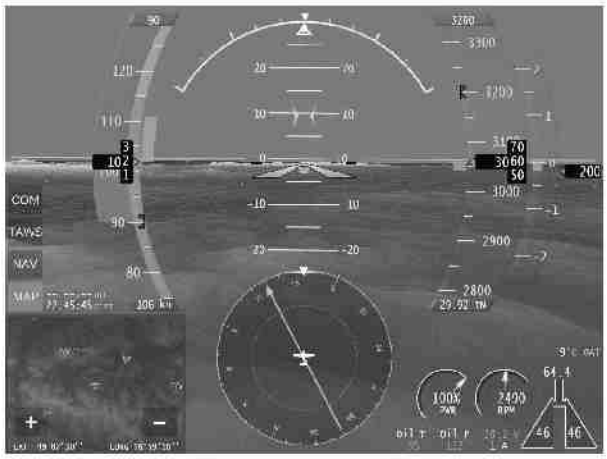

Figure 18. Excess energy used for acceleration.

The experienced pilots who took part in the display design evaluation stressed the importance of situational awareness. They also suggested moving the terrain awareness features to a HUD instead of requiring a VFR pilot to redistribute focus between the instrument panel and the view from the cockpit, especially during precision flying. Compared to heavier aircraft classes, the light/sport aircraft have a lower degree of inertia that makes them more susceptible to turbulences and unintended control inputs. Displaying flight relevant information within the ergonomic field of view thus reduces the amount of distracting factors, and unnecessary redistribution of pilot's attention and positively influences overall flight safety.

V. Conclusion

This paper describes an intuitive flight display designed to improve light aircraft flight safety. The design has been studied and preliminary evaluated in the SimStar laboratory. The aim of the work was the design of an intuitive primary flight display with an inbuilt terrain visualization capability that shows offending obstacles and alerts the pilot to avoid hazardous/restricted areas.

The preliminary design of the intuitive flight display was motivated by the advances in state of the art, commercially available, products and conceptual research ideas. Different aspects of the concepts have been evaluated in order to design a flight display layout that would reduce pilot workload and improve situational awareness. The aim was not to create an overly futuristic solution that would not find rational support in current legislation, or which would suggest major retraining issues. Instead, the intention was to display flight relevant data without the possible bias imposed by unnecessary secondary information. This led to an integrated display solution featuring basic flight data visualization along with engine and NAV/COM instruments, usually displayed separately on a MFD. Logically, the display size and information structure does not support a full implementation of all information usually found on a MFD, as clarity and readability issues limited the scope of implemented features and elements.

Experimental, ground based SimStar simulations proved the suitability of the designed intuitive flight display for light aircraft cockpit installation. The final hardware implementation will be flight tested on board of Evektor SportStar microlight aircraft.

Acknowledgments

This work has been supported by the research project CEZ MSMT, MSM 0021630528 "Security-Oriented Research in Information Technology" and Technology Agency of the Czech Republic research project "Smart Autopilot", TACR TA01010678.

References

[1]Recommended Practices and Guidelines for an Integrated Cockpit/Flightdeck In A 14 CFR PART 23 Certified Airplane; The GAMA-Class Integrated Cockpit / Flightdeck, *General Aviation Manufacturers Association*, Washington, DC, 2005, URL: http://www.gama.aero/files/gama_publication_12_p23cockpit_april_2005_pdf_498cadb978.pdf [cited 29 June 2011].

[2]Introduction of Glass Cockpit Avionics into Light Aircraft, Safety Study NTSB/SS-10/01, *National Transportation Safety Board*, Washington, DC, 2010, URL: www.ntsb.gov/doclib/safetystudies/SS1001.pdf [cited 29 June 2011].

[3]Amelink, M. H. J., Mulder, M., van Paassen, M. M., Flach, J., "Theoretical Foundations for a Total Energy-Based Perspective Flight-Path Display," *The International Journal of Aviation Psychology*, Vol 15, No 3, 2005, pp.205–231.

[4]Lambregts, A. A., "Fundamentals of Fly-By-Wire Augmented Manual Control," *SAE 2005 AeroTech Congress & Exhibition*, SAE 2005-01-3419, Forth Worth, Texas, 2005.

[5]Lambregts, A. A., "Integrated System Design for Flight and Propulsion Control using Total Energy Principles," *AIAA Aircraft Design, System and Technology Meeting*, AIAA-83-2561, Fort Worth, Texas, 1983.

[6]Chudy, P., Pieniazek, J., Rzucidlo, P., "Flight Control System for Environmentally Friendly Light Aircraft," *Polish Journal of Environmental Studies*, Vol. 18, No. 4B, 2009, pp. 21-25.

[7]Chudy, P., Rzucidlo, P., Tomczyk, A., "Safety enhanced digital flight control system," *Aircraft Engineering and Aerospace Technology*, Vol. 81, Issue 5, 2009, pp. 416-423.

[8]Chudy, P., Rzucidlo, P., "TECS/THCS Based Flight Control System for General Aviation,". Meeting Papers on Disc, Vol. 14, No. 9, AIAA, Renton, 2009.

[9]Lambregts, A.A., Rademaker, R.M. and Theunissen, E., "A New Ecological Primary Flight Display Concept,"*Proceedings of the 27th Digital Avionics Systems Conference*, 2008.

[10]*FAR Part 91 General Operating and Flight Rules § 91.205 Subpart C-Equipment, Instrument, and Certificate Requirements*, URL: http://rgl.faa.gov/Regulatory_and_Guidance_Library/rgFar.nsf/FARSBySectLookup/91.205 [cited 29 June 2011].

[11]Chudy, P., Rzucidlo, P., Zemcik, P., "Affordable Light Aircraft Flight Simulators," Meeting Papers on Disc, Vol. 15, No. 9, AIAA, Renton, 2010.

[12]Bilek, J.,"Energy management primary flight display," *Proceedings of the 16th conference Student EEICT 2010, vol. 3*, Brno, 2010, pp. 47-49

[13]Tadema, J., Theunissen, E., Lambregts, T., "Exploring the potential of energy and terrain awareness information in a synthetic vision display for UAV control," *Volume 7328 (1)*, SPIE, 2009.

AIAA Modeling and Simulation Technologies Conference
10 - 13 August 2009, Chicago, Illinois

AIAA 2009-5689

TECS/THCS based flight control system for general aviation

Peter Chudy[1]
Brno University of Technology, Brno, Czech Republic

and

Pawel Rzucidlo[2]
Rzeszow University of Technology, Rzeszow, Poland

This paper discusses the implementation of TECS and THCS based flight controller for a low-end general aviation application. TECS is based on energy distribution logic, whereas THCS uses lateral/directional criteria for aircraft control. TECS/THCS control system was subjected to simulations. The advantage of the TECS over classical control law designs proved to be in excellent performance and moderate complexity of the resulting controller structure. TECS/THCS's expected ability to support proven analytical tools compatible with the airworthiness certification procedure makes it an ideal candidate for implementation on board of a General Aviation aircraft.

Nomenclature

A, B, C, D	=	airplane dynamics in state-space form
x, y, u, r	=	airplane states, outputs, inputs and references
β	=	sideslip angle [rad]
D	=	aircraft drag [N]
$\delta_e, \delta_a, \delta_r$	=	control surface deflection [rad]
δ_{th}	=	throttle setting [%]
E_T	=	total energy [J]
$\dot{E}$	=	specific total energy rate
Φ	=	roll angle [rad]
g	=	acceleration due to gravity [9,81 $m.s^{-2}$]
γ	=	flight path angle (vertical) [rad]
h	=	height [m]
K	=	feedback gain matrix
L	=	aircraft lift [N]
$\dot{L}$	=	specific energy distribution rate
m	=	mass [kg]
q	=	pitch rate [$rad.s^{-1}$]
s	=	Laplace operator
T	=	aircraft thrust [N]
t	=	time [s]
θ	=	pitch attitude angle [rad]
u	=	body axis forward speed [$m.s^{-1}$]
V	=	aircraft forward speed [$m.s^{-1}$]
w	=	body axis downward speed [$m.s^{-1}$]
z	=	earth axis downward disp. [m]
ψ	=	heading [rad]
0	=	zero matrix

[1] PhD., Faculty of Information Technology, E-mail: chudyp@fit.vutbr.cz
[2] PhD., Department of Avionics and Control, E-mail: PawelRz@prz.edu.pl, AIAA Member.

I. Introduction

The complexity of operating and navigating an airplane, magnified by the dangers posed by weather, mechanical problems, and inevitable pilot carelessness advocate the rationality of a pilot workload reducing system. As General Aviation aircraft are mostly flown by a single pilot, their operational concept would benefit from an intelligent flight control system assisting in aircraft's safe operation.

Logical implications of a functionally isolated, "purpose driven", classical design philosophy resulted in suboptimal performance of separate trajectory and speed control single input singe output (SISO) control laws. Traditional design approach for conventional aircraft configurations assumes the flight path being controlled solely by means of elevator, whereas speed control is maintained by throttle.[1, 2, 3] However, elevator and thrust command responses of conventional configuration are coupled phenomena, logically requiring a coordinate control action.[4] SISO speed control law doesn't consider flight path angle as a parameter for estimating desired thrust, whereas the classical autopilot's control logic operates without the knowledge of aircraft's steady state performance. Serious safety implication has the current SISO autopilot/autothrottle system's lack of capability to provide integral flight envelope protection and prevent control coupling problems, requiring the pilot to continually monitor automatic system's performance. Inconsistencies in operation and limitations of control modes make it difficult to effectively manage an onboard automation based on SISO control logic.[5]

It is industry's belief that a control system with a direct stabilized control of airspeed and flight path will be a major step in reducing pilot workload.[6, 7] This opinion motivated the authors to experimental implementation of a flight control strategies known as the Total Energy Control System (TECS) and Total Heading Control System (THCS). The former concept mimics an intuitive human piloting for longitudinal aircraft motion by commanding the flight path angle and speed simultaneously. The coupling of V and γ is elegantly resolved in TECS core in a way that eliminates a functional disharmony between thrust and flight path control loops. TECS and THCS were reportedly successfully implemented in a UAV program called Condor.[6]

This paper is organized as follows. The next two sections introduce TECS and THCS control strategy, in lieu with basic description of their control logic. The section thereafter introduces linear model of experimental flying platform for a number of configurations used in controller tuning. Controller designs based on TECS and THCS strategies are initially evaluated in off-line simulation regime and subsequently implemented into purposely built simulator described in section V and VI. The final section features concluding remarks on design and testing of the controllers.

II. TECS for longitudinal aircraft control

TECS was derived from a point mass approximation of the aircraft dynamics. Its control logic uses energy states of the system based on premises of trajectory control being a point mass kinematic problem sufficiently described by time history of trajectory acceleration.[8] Hence the aircraft dynamics could be rewritten using energy states as following

$$E_T = E_{kinetic} + E_{potential}, \tag{1}$$

Aircraft thrust change alters proportionally the aircraft flight path angle γ and acceleration along flight trajectory. In TECS, the amount of total energy rate is being influenced by inputs through different thrust settings[8] Eq. (2) whereas the changes of pitch attitude lead to energy redistribution[8] Eq. (3) with the elevator control assuming the role of a conservative energy distributor.[5, 6] Subscript e refers to error in control variable.

$$T_{cmd} = \left(K_{TP} + \frac{K_{TI}}{s} \right) \cdot \dot{E}_e \tag{2}$$

$$\theta_{cmd} = \left(K_{EP} + \frac{K_{EI}}{s} \right) \cdot \dot{L}_e \tag{3}$$

The TECS control strategy allows thrust and elevator control coordination in a decoupled response, causing the flight path angle command having a negligible influence on speed fluctuation and vice versa. The core feedback

integral K_{TI}, K_{EI} and proportional K_{TP}, K_{EP} gains are designed to yield identical dynamics for energy rate error $\dot{E}_e$ and energy distribution rate error $\dot{L}_e$ for either a flight path angle command or a longitudinal acceleration command.[8]

$$\dot{E}_e = \frac{\dot{V}_e}{g} + \gamma_e \,,\; \dot{L}_e = \frac{\dot{V}_e}{g} - \gamma_e \qquad (4), (5)$$

$$\gamma_e = \gamma_{cmd} - \gamma \,,\; \dot{V}_e = \dot{V}_{cmd} - \dot{V} \qquad (6), (7)$$

As seen in Fig. 1, proportional feedback gains operate with absolute values of energy rate $\dot{E}$ and energy distribution rate $\dot{L}$. The classic TECS core shown in Fig. 1 does not command elevator deflection directly, but generates a pitch attitude command, which is under the action of a pitch inner loop subsequently transformed to an elevator input. Similarly, a thrust scaling inner loop transforming thrust commanding signal into thrust lever setting is being included in the control scheme.

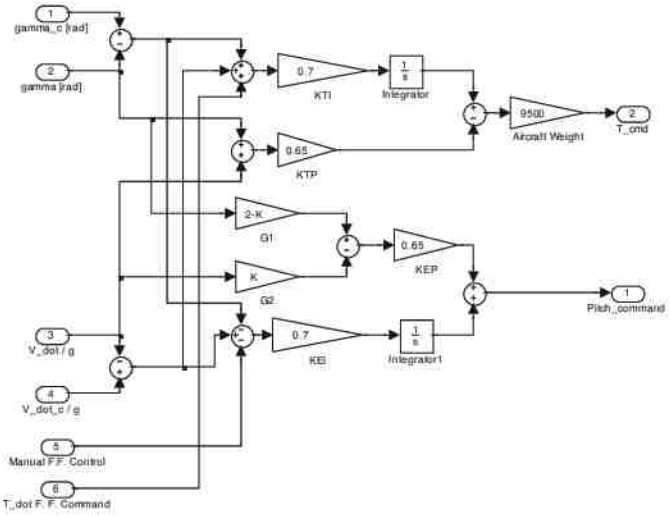

Figure 1. General structure of longitudinal control of aircraft motion based on TECS.

For the case of a decoupled longitudinal motion, the TECS core algorithm influences system's phugoid dynamics. In order for the system to stabilize fast short period aircraft dynamics, an inner-loop design from Fig. 2 is being implemented. TECS core algorithm requires feedback of $\dot{E}_e$ and $\dot{L}_e$, which are a linear combination of the aircraft states x and control inputs u. $\dot{E}_e$ and $\dot{L}_e$ need to be identical, otherwise energy is added or subtracted from the variable that is commanded to be held constant.[9]

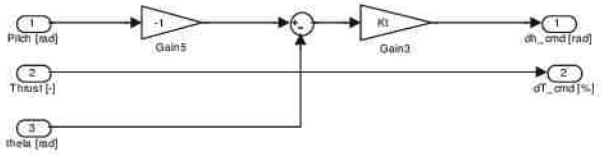

Figure 2. Aircraft dependent design.

TECS has been successfully implemented on a NASA B737 technology demonstration airplane, followed by application onboard of Condor UAV project.[6] More recently published results describe successfully simulated TECS based designs for medium size transport aircraft type.[7,9]

III. THCS for lateral-directional aircraft control

THCS eliminates the traditionally separated Yaw Damper, Turn Coordination and Thrust Asymmetry Compensation functions as these are functionally integrated as part of the THCS algorithm.[6, 10] The control strategy introduces roll control loop and yaw control loop as shown in Fig. 3, with yaw error ψ_e and sideslip error β_e being determined during flight based on following relationship

$$\psi_e = \psi_{cmd} - \psi \ , \ \beta_e = \beta_{cmd} - \beta \tag{8), (9}$$

Similarly to TECS, the THCS core does not command aileron deflection directly, but generates a roll attitude command (Eq. 10), which by means of a roll inner loop subsequently transforms Φ_{cmd} to an aileron input δ_{acmd}. For the yaw control loop, rudder command δ_{rcmd} is being developed from yaw rate command, which is, as shown in Eq.11, a difference between yaw rate error $\dot{\psi}_e$ and sideslip rate error $\dot{\beta}_e$. Under normal operational conditions, sideslip command β_{cmd} will equal zero. The integral gains K_{RI} and K_{YI} should be equal.[10]

$$\dot{\psi}_{cmd} = \left(\underbrace{\left(\psi_e K_{\psi_0} \frac{g}{V_T} - \dot{\psi} \right)}_{\dot{\psi}_e} - \underbrace{\left(\beta_e K_{\beta_0} \frac{g}{V_T} - \dot{\beta} \right)}_{\dot{\beta}_e} \right) \frac{K_{YI}}{s} \tag{10}$$

$$\phi_{cmd} = \left(\underbrace{\left(\beta_e K_{\beta_0} \frac{g}{V_T} - \dot{\beta} \right)}_{\dot{\beta}_e} + \underbrace{\left(\psi_e K_{\psi_0} \frac{g}{V_T} - \dot{\psi} \right)}_{\dot{\psi}_e} \right) \frac{V_T}{g} \frac{K_{RI}}{s} \tag{11}$$

General composition of the outerloop design eliminates control system's across-platform integration dependencies for a particular aircraft. Platform tailored inner loops provide effective stability augmentation for all control modes and flight conditions.

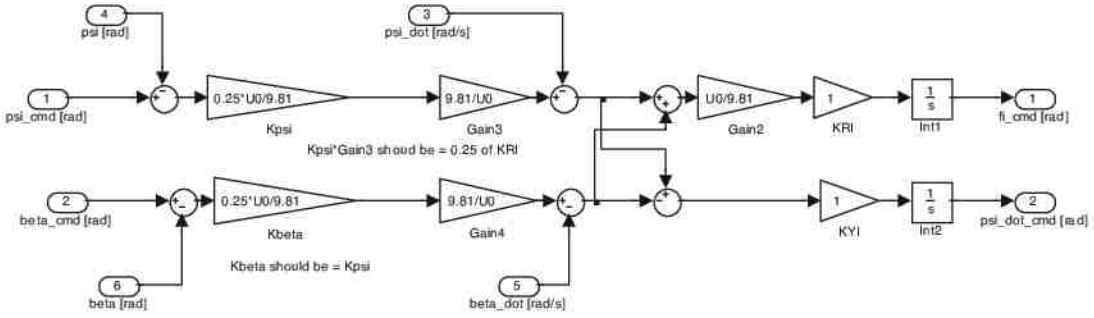

Figure 3. THCS core for lateral-directional aircraft control.

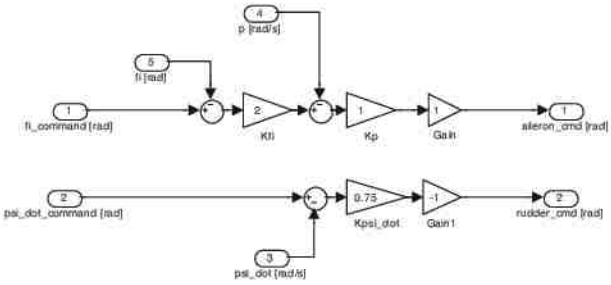

Figure 4. Aircraft specific inner loop designs.

IV. Experimental flying platform

A typical representative of a low-end general aviation single engine propeller aircraft, Socata Rally/PZL-110 Koliber, has been identified by the authors as a suitable candidate for the purpose of modeling and simulation of the TECS/THCS based controller. The rationality of the choice was not only in Koliber's availability to the research team, but also in well predictable performance characteristics and favorable unaugmented handling qualities.

Figure 5. Experimental flying platform PZL-110 Koliber.

A. Aircraft description

PZL-110 Koliber has been produced in Poland during the 1980's under the license of Morane-Saulnier. It is an all metal single engine low wing monoplane equipped with a fixed landing gear. Cockpit provides room for up to four occupants. Initial version was powered by PZL licensed 116 hp Franklin 4A-235 engine, which has been later replaced by 112/175 kW Lycoming O-320/520 engines. Koliber's have been traditionally used for enjoyable cross-country flying and flight-schools based training.

B. Linear model

Linear model of PZL-110 Koliber aircraft dynamics, for 4 selected flight states, has been used for the initial computations and testing of the TECS & THCS based flight control system. State-space models of aircraft dynamics[1] in the form of Eq. 13 and Eq. 14 have been used for the simulations

$$\dot{x} = Ax + Bu \tag{13}$$

$$y = Cx + Du \tag{14}$$

State vector: $x = \begin{bmatrix} u[m.s^{-1}] & \alpha[rad] & q[rad.s^{-1}] & \Theta[rad] \end{bmatrix}^T$, (15)

Control vector $u = \begin{bmatrix} dh[rad] & dt[rad] \end{bmatrix}^T$. (16)

Values of state and control matrixes that correspond to four particular flight states are presented in Table 1. More detailed models of aircraft and control system dynamics are included in Ref. 11, 12, 13. State space matrices C and D from Eq. 14 have the following form

$$C = \begin{bmatrix} 1 & 0 & 0 & 0 \\ 0 & 1 & 0 & 0 \\ 0 & 0 & 1 & 0 \\ 0 & 0 & 0 & 1 \end{bmatrix}, \quad D = \begin{bmatrix} 0 & 0 \\ 0 & 0 \\ 0 & 0 \\ 0 & 0 \end{bmatrix} \tag{17), (18}$$

Table 1. Particular values of state-space matrixes for four characteristics flight conditions

Config.	A				B	
1	-0.1149	-0.2350	0	-9.7987	0	0.0200
	-0.0254	-1.2766	1.0000	-0.0142	-0.1058	0.0001
	0.0027	-2.4726	-0.9682	0	-3.6408	0
	0	0	1.0000	0	0	0
	h = 250 m, γ = 2.3 deg, v = 27.8 m/s, α0 = 15.7 deg, dT0= 99.1 %, L/D = 6.1, m = 670 kg + 2x70 kg, remarks: take-off, ½ flaps.					
2	-0.0894	0.6188	0	-9.7932	0	0.0190
	-0.0210	-1.3664	1.0000	-0.0168	-0.1147	0.0001
	0.0032	-2.9479	-1.0505	0	-4.4901	0
	0	0	1.0000	0	0	0
	h = 400 m, γ = 3.0 deg, v = 30.6 m/s, α0 = 14.6 deg, dT0= 99.7 %, L/D = 7.2, m = 670 kg + 2x70 kg, remarks: climbing.					
3	-0.0561	2.8748	0	-9.8066	0	0.0144
	-0.0099	-1.8862	1.0000	0	-0.1613	0.0001
	0.0064	-6.0187	-1.4825	0	-10.6727	0
	0	0	1.0000	0	0	0
	h = 750 m, γ = 0 deg, v = 44.4 m/s, α0 = 7.1 deg, dT0= 84.2 %, L/D = 7.9, m = 670 kg + 2x70 kg, remarks: cruise.					
4	-0.0944	0.6786	0	-9.8066	0	0.0191
	-0.0210	-1.3882	1.0000	0	-0.1164	0.0001
	0.0033	-2.9910	-1.0657	0	-4.9833	0
	0	0	1.0000	0	0	0
	h = 250 m, γ = 0 deg, v = 30.6 m/s, α0 = 10.9 deg, dT0= 74.6 %, L/D = 6.8, m = 670 kg + 2x70 kg, remarks: approach, full flaps.					

V. TECS/THCS controller with linear models

The TECS controller structure shown in Fig. 1 was used to construct a controller for a linear aircraft model seen in Fig. 6. Initial TECS controller gain selection was based on authors' educated guess and subsequently manually fine-tuned to meet system's desired performance. The controllers' performance has been demonstrated in series of simulations using linearized models of aircraft dynamics and nonlinear actuators. Typical flight regimes and related configurations have been investigated. In off-line simulation, these featured: take-off, climbing, cruise at specified airspeed and final approach. Even the controller structure is compact and excellently readable, the manual tuning process has been found a lengthy and error prone procedure. The approach discussed in this chapter uses a subset of linear controllers, with Altitude Command and Speed Hold modes implemented for TECS based controller structure (Fig. 7) and Heading Command Mode for THCS controller (Fig. 8).

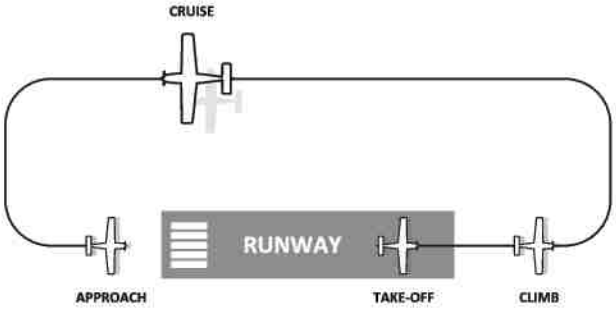

Figure 6. Simulated flight configurations.

A. Simulation scheme of TECS and THCS based linear controller

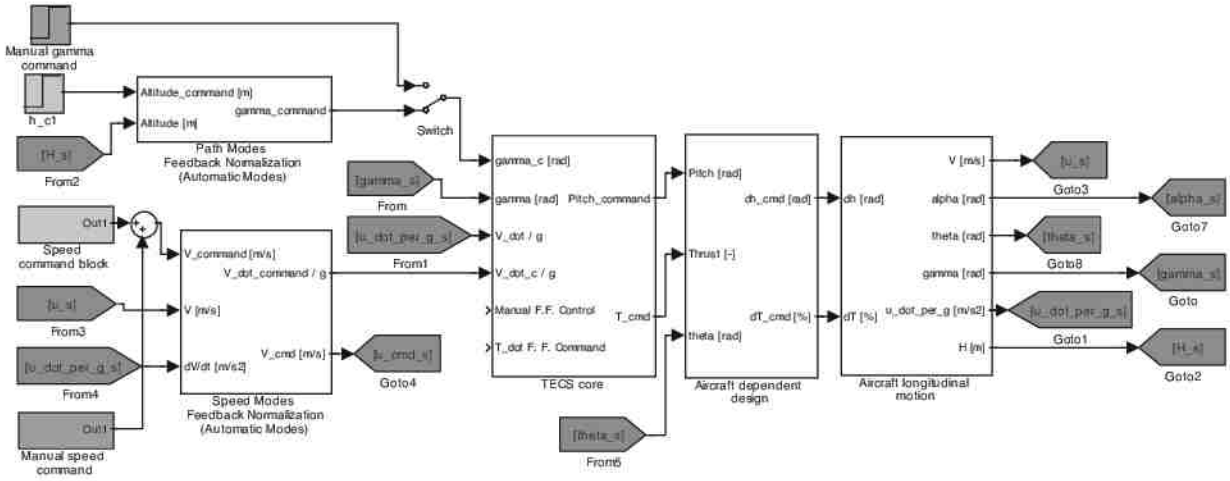

Figure 7. General structure of longitudinal control of aircraft motion based on TECS.

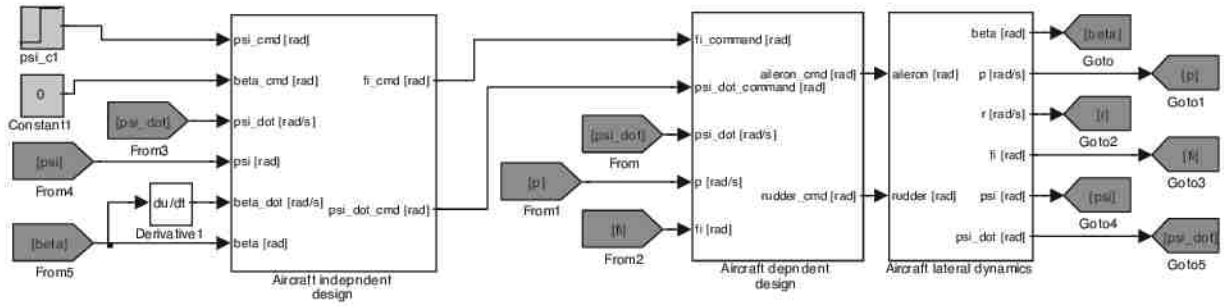

Figure 8. General structure of lateral-directional control of aircraft motion based on THCS.

B. Simulation results for longitudinal controller with TECS core.

Figure 9 depicts response of the investigated linear system in different above mentioned configurations to a step input in altitude. The desired altitude was captured with an average 1 $m.s^{-1}$ overshoot in airspeed without any significant control variable couplings.

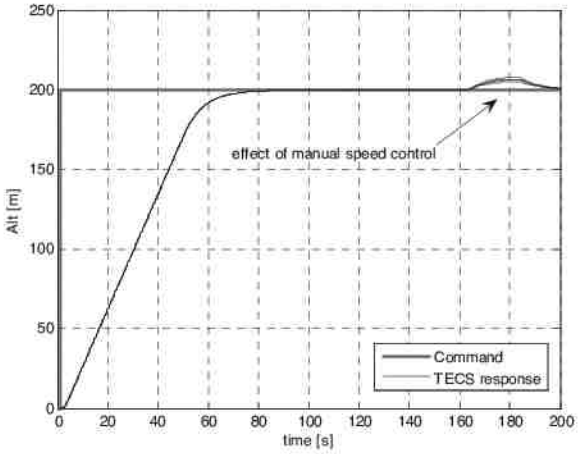

Figure 9. Altitude control with TECS.

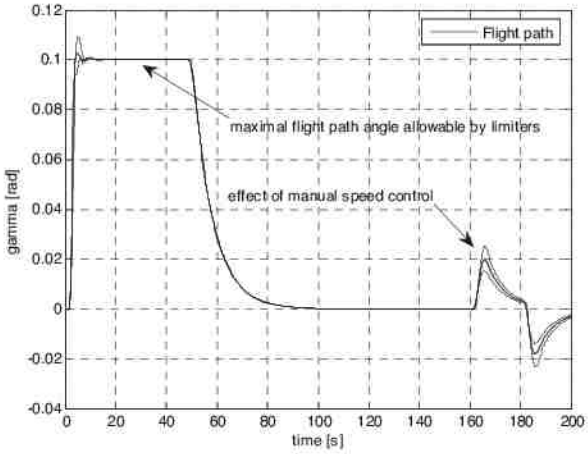

Figure 10. Flight path changes related to Fig. 9.

Series of bumps in Altitude Mode in Fig. 9 appeared as a result of manual speed inputs in simulations with various aircraft configurations. Fig. 10 correlates the influence of altitude step input and manual speed corrections on flight path angle γ, which has been, for our purposes, limited to a maximal value of 0,1rad ≈ 5,73deg. Figure 11 shows a response of linear model to a 20 $m.s^{-1}$ step demand in airspeed. Airspeed has converged to its desired value after a vertical altitude overshoot of 10 meters, without any noticeable delay. Compared to a classical SISO design TECS provides very precise airspeed stabilization (Fig. 13). Responses for analyzed configurations feature minimal overshoot and short time of regulation. Classically designed regulator causes overshoots in airspeed up to almost 10% over commanded value as seen in figure 13. Similar conclusion can be made about flight path stabilization. Also in this case the TECS responses to control input demands are more gentle and free of oscillations.

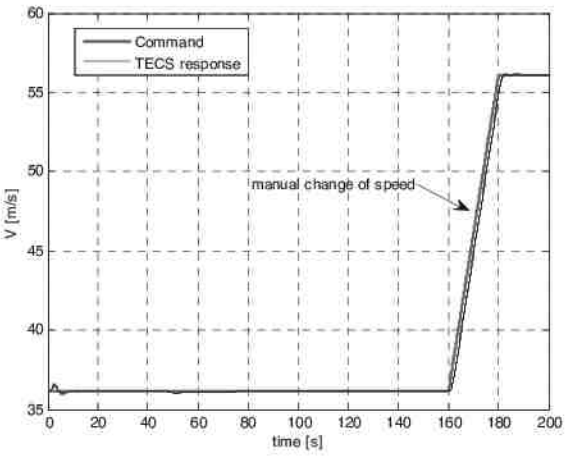

Figure 11. Changes in speed related to altitude step input of 200m as shown on Fig.9.

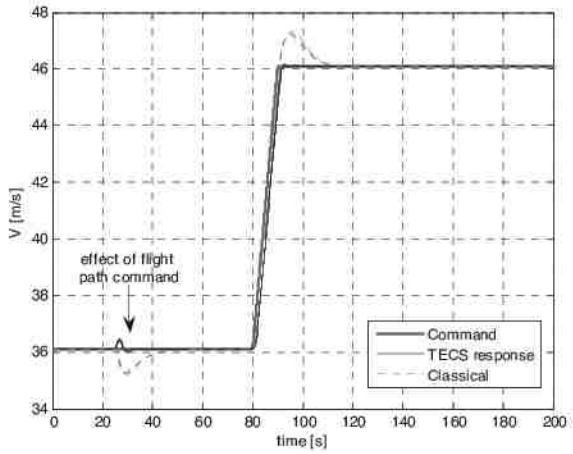

Figure 12. TECS based manual control mode of flight path vs. classical PID design.

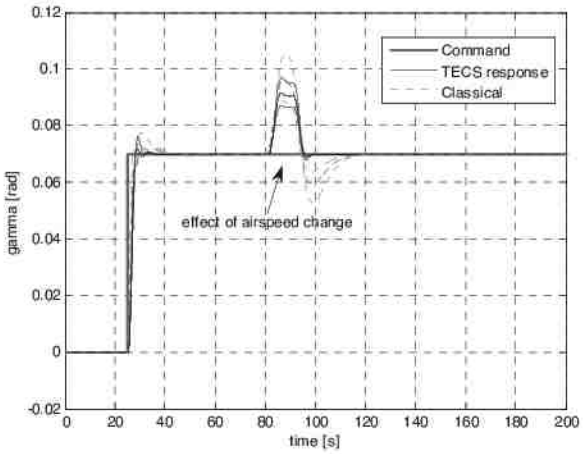

Figure 13. TECS based vs classical PID design.

C. Simulation results for lateral-directional controller with THCS core.

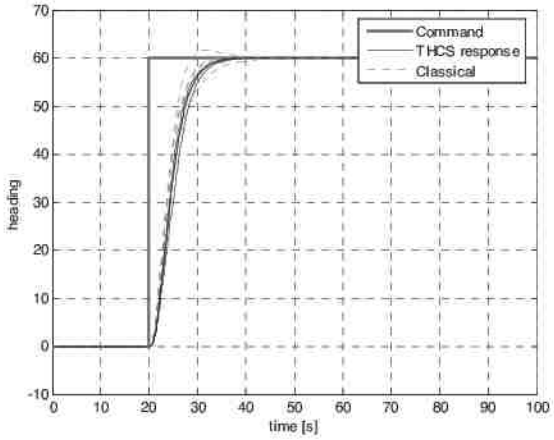

Figure 14. THCS heading control mode.

Figure 14 illustrates the response of the modeled aircraft configurations to a step input in heading. The desired heading was captured for all observed states with a negligible overshoot in roll and with an almost identical response development. Figures 14-16 show a comparison of responses for a THCS based controller and a classical SISO lateral directional controller. Roll overshoot for the classical design is substantially larger (0,08 rad) then the plotted response with THCS. More visible differences are seen on the sideslip plot (Fig. 16). The SISO controller exhibits oscillations almost twice the magnitude of THCS's. As seen in Fig 14-16 THCS lateral-directional controller performs a more precise aircraft control with less overshoot and undesired system oscillations.

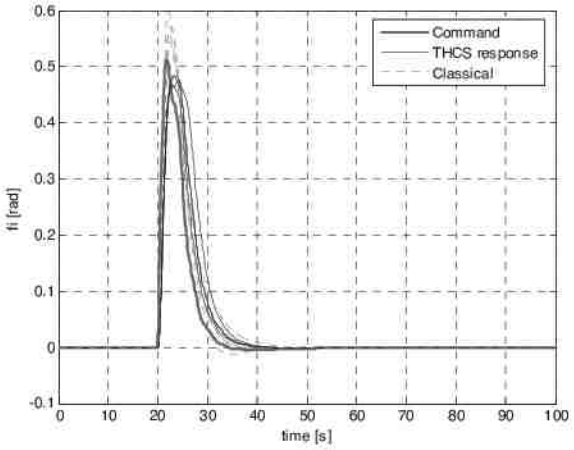

Figure 15. Changes in roll corresponding to Fig. 14.

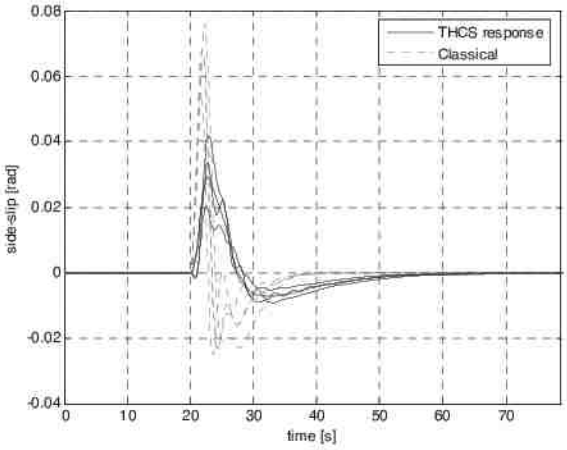

Figure 16. Side-slip response corresponding to heading command input from Fig. 14.

VI. Real time simulation of TECS/THCS controller

Simplified flight simulator was designed and built especially for testing of the TECS/THCS based flight control system (Fig. 18, Fig. 19). It showed to be a necessity due to the absence of both technical and formal possibility to modify a simulator used for pilot training. Experimental flight simulator is based on PZL-110 Koliber nonlinear aircraft dynamics with the cabin from PZL M-15 "Belfegor". DSpace rapid prototyping environment linked to Matlab/Simulink was used for the preparation of simulator's flight control system. This solution enabled coupling of chosen flight control system components with the simulator core (Fig. 17). This solution is based on CAN data bus. There are four elements connected directly to CAN. First of them is rapid prototyping environment which enables building of real-time models, eg. control laws, aircraft dynamics, atmosphere disturbances, inceptor's shaping functions, force feedback, etc.

Flight simulator software and FS/CAN interface constitute the second block. This block is responsible for visualization of surroundings, indicators and knobs operations as well as for simulation of in-build aircraft dynamics and atmosphere influences. Operator of experiment can select what kind of aircraft dynamics and atmosphere model should be used for simulation purposes: model from rapid prototyping card or model from the software module. Third and fourth blocks, connected directly to CAN, are experiment operator's console and data recorder (Fig. 20). This solution enables connecting of additional equipment to the simulator. Particular software or rapid prototyping modules can be replaced by real parts of aircraft control system. Additional actuators, indicators or other hardware modules equipped with CAN interface and CANaerospace protocol can be connected directly to the bus and can work in the loop (hardware in the loop simulation).

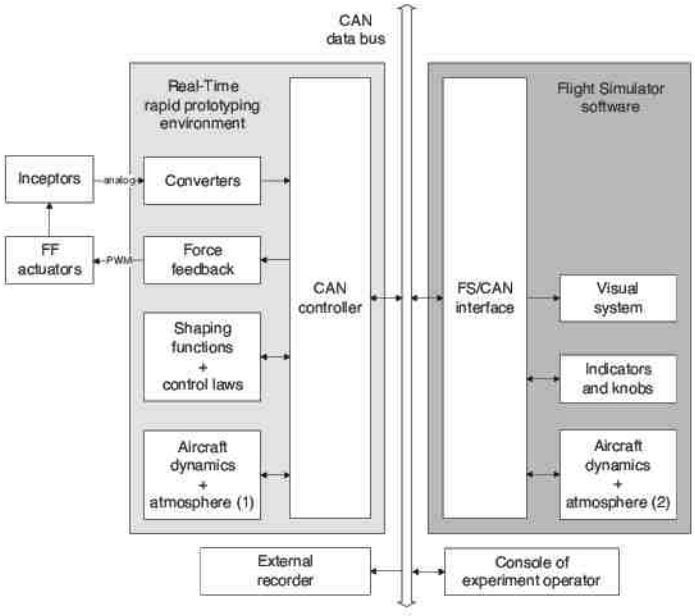

Figure 17. Block scheme of experimental flight simulator.

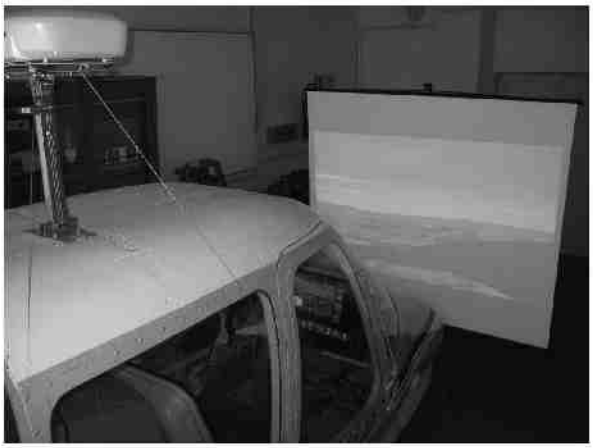

Figure 18. General view of real-time simulation environment.

Figure 19. Pilot's and Operator's workplace in a real-time simulation environment.

Results of real-time simulations of PZL-110 Koliber aircraft equipped with a TECS/THCS based autopilot are presented in figures 21-27. All simulated flights were performed in good weather conditions (weak turbulence and wind, perfect visibility). Experiments were initiated in a horizontal steady-state flight at altitude 1500[ft] and preselected heading of 180 degrees. Figures 21-24 illustrate an example of longitudinal motion control. Autopilot maintains the altitude of 1500[ft] (457[m]) during first 50 seconds of flight and then subsequently executes a commanded change of altitude to 2100[ft] (640[m]). The altitude changes smoothly by maintaining the desired altitude within a range of ±5[m] (Fig. 21). Changes in flight path related to altitude command are presented in Fig. 22. TECS flight path command is nearly identical to off-line simulation (Fig. 10), with moderate oscillations observed in flight path response between t=50 and t=90 seconds. The above mentioned effect is caused by the differences in the linear and non-linear aircraft dynamics models. The inner-loop (aircraft dependent design) coefficients have initially been tuned for the linear model, so the slight oscillations due to non-linear effects can be in the future minimized by a precision tuning process of the simulator's non-linear model. Nevertheless, the observed oscillations do not exceed ±0.012[rad] and they are virtually unnoticeable. The altitude hold task was combined with the airspeed change command between t=160 and t=220 seconds of the experiment (Fig. 23). Speed changes smoothly and continuously from 37.5[m/s] to 47.5[m/s] and doesn't essentially influence the altitude or flight path control.

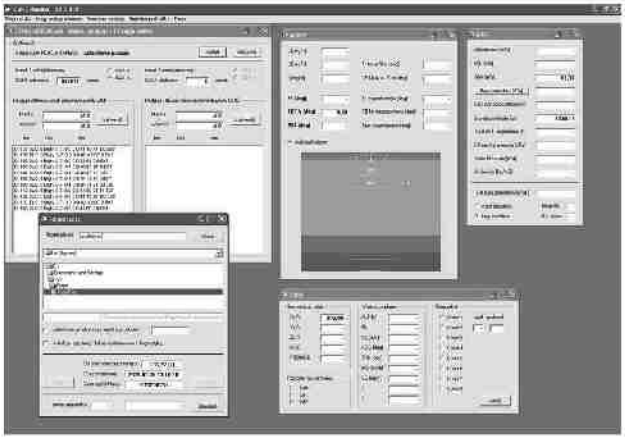

Figure 20. Window of *CAN2 Monitor* application (recording and diagnostics of CAN data bus).

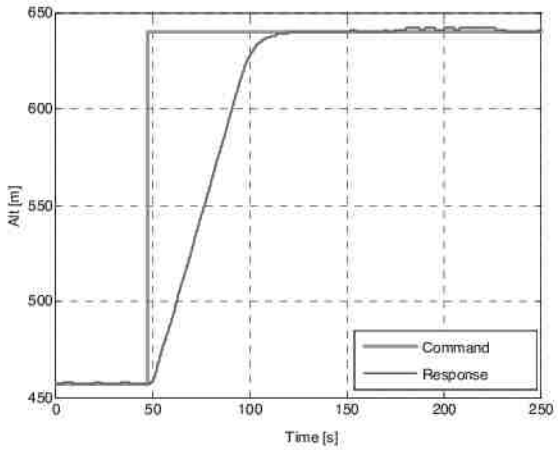

Figure 21. Altitude control with TECS/THCS.

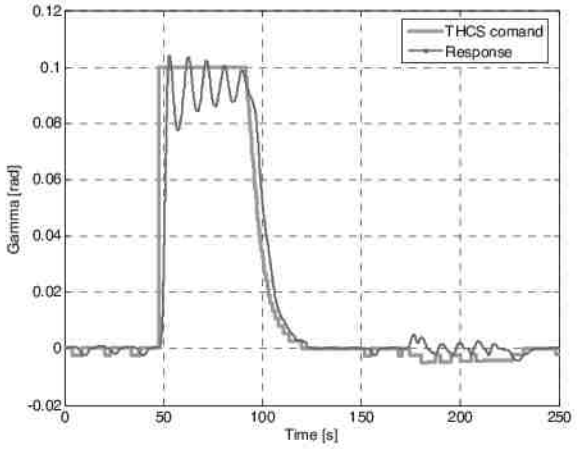

Figure 22. Flight path changes related to Fig. 21.

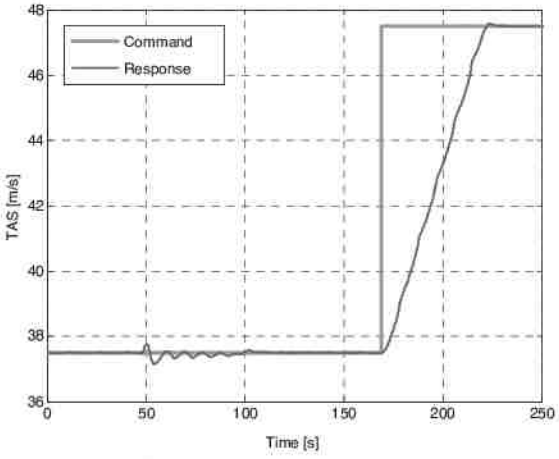

Figure 23. Speed command and changes in speed related to altitude step input as shown on Fig. 21.

Real-time simulation results for lateral-directional control are presented in figures 24-26. The aircraft holds an initial heading of 90 [deg] until t=35 seconds and is subsequently commanded to align to a new heading of 135 degrees (Fig. 24). The response of the aircraft is similar to the results obtained from the linear simulations (Fig. 14-16). Significant differences occur, after t=50 seconds, in bank angle plot only (Fig. 25). Damped oscillations are present in THCS command and they are repeated in aircraft response. It indicates that the THCS core (aircraft independent design) should be tuned additionally for a non-linear model to achieve perfect solution (the already mentioned oscillations due to nonlinear effects do not exceeds ±0.03[rad] and are virtually irrelevant). Side slip angle is stabilized during the whole time of the flight and the maximal temporary error is less than 0.03[rad].

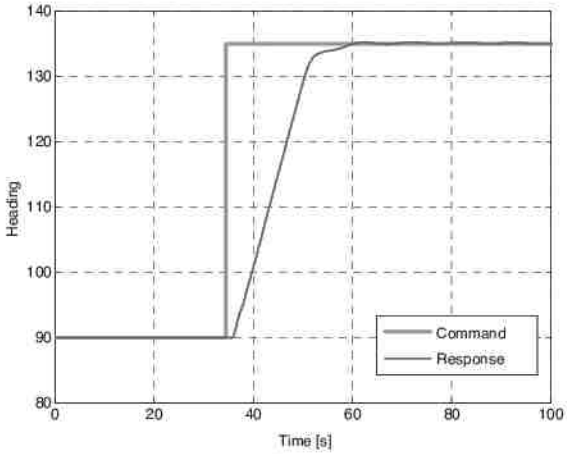

Figure 24. TECS/THCS heading control.

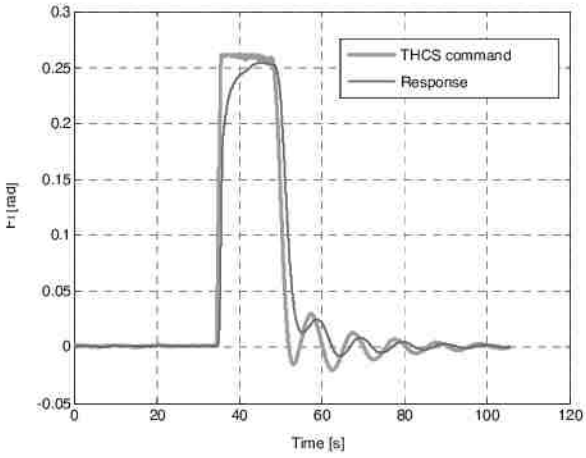

Figure 25. Changes in roll corresponding to Fig. 24.

TECS/THCS algorithms implemented to a real-time simulation environment allow for an independent control of the flight path, airspeed and heading. Graphs demonstrating simulated system's capabilities are presented in figure 27. The development of monitored system's performance confirms the expected suitability of a precise control of the three main flight parameters (solo or simultaneously). System's responses to the commanded inputs closely follow the shape of the commanding signal. Unfavorable interactions between control algorithms for longitudinal and lateral-directional motion have not been observed. Designed control laws support simultaneous control for both types of motion. The results of the nonlinear real-time simulations prove that the TECS/THCS based automatic flight control logic has a strong potential in the flight automation of low-end General Aviation aircraft.

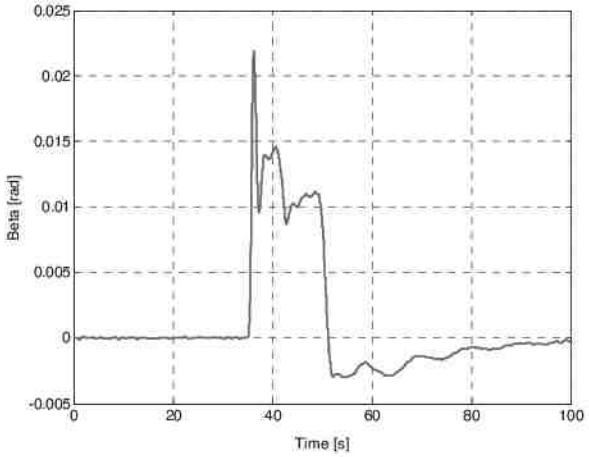

Figure 26. Side-slip response corresponding to heading command input from Fig. 24.

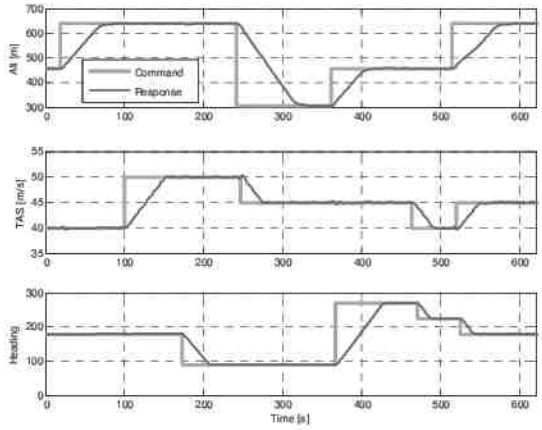

Figure 27. Simultaneous control of altitude, airspeed and heading with TECS/THCS.

VII. Conclusion

Responsible piloting requires a constant mental endeavor in monitoring the aircraft systems, prioritizing flight data and if necessary taking a corrective action under real-time constrains. This seriously contradicts with the human ability to successfully perform simultaneous data management processes in stressful conditions. Due to the lack of proper control coordination, SISO control modes never functioned satisfactorily if not properly managed by pilot or autopilot. TECS and THCS represent an elegant way of controlling longitudinal and lateral directional aircraft motion and thanks to their compact and clear structure they became authors' preferred choice over classical controllers. Nevertheless, the total energy and total heading control systems support proven analytical tools which are in line with the airworthiness certification procedure, making it transparent to an implementation processes. The effects of time delays, lost or damaged control data remain beyond the scope of this paper, but represent topics which are of high importance and remain to be investigated. Finally, the issue of robustness of the resulting controller would need to be addressed by utilization of advanced techniques that are able to cope with system's nonlinearities.

Future work on flight control system for General Aviation will focus on more rigorous testing of TECS/THCS based controllers in pilot-in-the-loop simulations and on substitution of designer's manual inputs with automatic gain search procedure introducing a suitable option for optimized future development.

Acknowledgments

This work has been supported by the "Security-Oriented Research in Information Technology" research project CEZ MŠMT, MSM 0021630528 and supported from Polish scientific founds within the framework of development project in years 2007-2010.

References

1McRuer, D., Ashkenas, I. and Graham, D., Aircraft Dynamics and Automatic Control, Princeton University Press, Princeton, NJ, 1990.

[2]Bociek, S., Gruszecki, J., "Aircraft Control Systems," Rzeszow University of Technology Press, Rzeszow, 1999.

[3]Michalew, I., Okojemow, B., Czikulajew, M., *Automatic Aircraft Control*, Maszynostrojenije, Moscow, 1987.

[4]Etkin, B., and Reid, L. D., *Dynamics of Flight – Stability and Control*, John Wiley & Sons, New York, 1996.

[5]Lambregts, A. A., "Vertical Flight Path and Speed autopilot Design using Total Energy principles," *AIAA Conference Proceedings*, AIAA Paper 83-2239CP, August 1983.

[6]Lambregts, A. A., "Fundamentals of Fly-By-Wire Augmented Manual Control", Society of Automotive Engineering, SAE 2005-01-3419, 2005.

[7]Rysdyk, R., Agarwal, R.K., "Nonlinear Adaptive Flight Path and Speed Control Using Energy Principles", *AIAA Guidnace, Navigation, and Control Conference and Exhibit*, August 2002, AIAA 2002-4440.

[8]Lambregts, A. A., U.S. Patent Application for an "Total Energy Based Flight Control System," Docket No. 6,062,513, filed 14. Sep. 1998.

[9]Faleiro, L.F., Lambregts, A. A., "Analysis and tuning of a 'Total Energy Control System' control law using eigenstructure assignment," *Aerospace Science and Technology*, No.3, 1999, pp. 127-140.
[10]Lambregts, A. A., U.S. Patent Application for an "Aircraft Lateral-Directional Control System," Docket No. 5,050,086, filed 17 Sep. 1991.
[11]Ciecinski, P., Pieniazek, J., "Aircraft Model for Purposes of Control Systems Synthesis," *Mechanics in Aviation IX Conference*, Warsaw, 2004.
[12]Rzucidlo P., *Methods of Suppression of Pilot Induced-Oscillations in Fly-By-Wire Aircraft*, Ph.D. Thesis, Rzeszow University of Technology, Rzeszow 2005.
[13]Tomczyk A., at al., *Integrated Control System for General Aviation Aircraft*, Polish State Committee for Scientific Research 8 T12C 049 20, Rzeszow, 2003.
[14]Hodgkinson, J., *Aircraft Handling Qualities, Reston*, AIAA Education Series, AIAA, VA, 1999.
[15]McCormick, B. W., *Aerodynamics, Aeronautics, and Flight Mechanics*, 2nd ed., John Wiley & Sons, New York, 1995.
[16]Tomczyk, A., "Facilitated airplane – Project and preliminary in-flight experiments," *Aerospace Science and Technology*, Elsevier, Vol. 8, No 6, 2004, pp. 469-477.

INTENTIONALLY LEFT BLANK

EVOLUTION ASSISTED FLIGHT CONTROL SYSTEM DESIGN

Peter Chudy, Jan Vlk, Petr Dittrich, Brno University of Technology, Brno, Czech Republic

Abstract

An evolution driven controller design approach has been applied to a rigid-body aircraft model of a light sport aircraft. The model comprises inertial, aerodynamic and flight dynamics related elements and the controller architecture is based on Classical Control Theory. The evolution driven concept plays a significant role in the optimization of the proposed controller structure by providing tuned controller parameters, which meet the designed fitness function criteria imposed through the optimization problem formulation. The proposed fitness function combines significant controller stability evaluation conditions into a single abstraction. The use of a robust optimization framework based on the genetic algorithms has allowed the suggested form of multi-criteria optimization definition. The suitability of the evolutionary optimization has been successfully tested on a model with rigid-body aircraft dynamics. Time-domain simulation results have shown the compliance of the tuned controller performance with its anticipated behavior.

Introduction

The evolutionary approach is a popular tool in optimization tasks of nonlinear problems. The design of a flight controller must typically satisfy a range of optimization criteria which can be later transformed into a cost function. The principal advantage of using evolution driven tools is their suitability to account for heterogeneous optimization conditions. Even though traditional techniques for solving nonlinear optimization tasks offer computationally less costly solutions, their applicability imposes higher demands in terms of cost function definition and may therefore be limited in utilization and robustness. The implemented evolutionary approach offers a robust platform, which allows tuning the controller performance to the required levels.

Evolution driven approaches got recognition in aerospace disciplines when successfully used for the optimization of high performance airfoils, efficient high lift systems or unconventional aircraft configurations. Its scientific potential has been put on display when human powered aircraft whose design elements were influenced by the outcomes of the evolutionary optimization took flight and made its public debut. The multi-criteria nature of the task formulation, which has been used for the aerodynamics, introduced the rationality of using the robust nonlinear optimization technique also on flight control related tasks [1, 2].

Rigid-Body Dynamic Model

The dynamic model used during the simulation runs was extracted from a series of flight experiments performed on an Evektor SportStar experimental aircraft equipped with a laboratory grade data acquisition system. The aircraft is shown in flight in Figure 1.

Figure 1. Evektor SportStar - Light Sport Aircraft

Measured data were subjected to parameter identification procedures, results of which were integrated into a nonlinear aircraft model structure. The identification was concluded by the model quality assurance process. Based on the initially drawn assumptions of the flight envelope margins, the model includes only basic estimates of stall and spin characteristics as post stall and spin recovery tasks were not primarily addressed in the research.

$$\begin{aligned} \dot{x} &= \boldsymbol{A} \cdot x + \boldsymbol{B} \cdot u \\ y &= \boldsymbol{C} \cdot x + \boldsymbol{D} \cdot u \end{aligned} \tag{1}$$

The implemented dynamic model in its approximated form was described by a standard linear state space model, which includes the dynamic

978-1-4799-1538-5/13/$31.00 ©2013 IEEE

matrix $\boldsymbol{A}$, input matrix $\boldsymbol{B}$, output matrix $\boldsymbol{C}$ and feed-forward matrix $\boldsymbol{D}$, as shown in Equation 1.

The actuators have been modeled as standard second order linear single input single output systems and described by a transfer function with natural frequency ω_0 and damping coefficient ξ_0, as shown below:

$$G_{Act}(s) = \frac{\omega_0^2}{s^2 + \omega_0 \cdot \xi_0 \cdot s + \omega_0^2} \tag{2}$$

The complex number s acts as the standard Laplace operator. The next part of this section deals with the longitudinal/lateral decomposition of the aircraft motion.

Longitudinal Motion

A linearized longitudinal motion state space model for steady state level flight has been obtained by making use of the dynamic matrix from Equation 4 and the input matrix presented in Equation 5. As seen in Equation 3, the longitudinal state vector x_{lon} contains the true airspeed V, the angle of attack α, the pitch angle θ and the pitch rate q. Furthermore, the input vector u_{lon} includes the elevator deflection η and the thrust lever position δ_T as seen below:

$$\begin{aligned} x_{lon} &= [V \quad \alpha \quad \theta \quad q]^T \\ u_{lon} &= [\eta \quad \delta_T]^T \end{aligned} \tag{3}$$

$$\boldsymbol{A}_{lon} = \begin{bmatrix} X_V & X_\alpha & -g \cdot cos\gamma_0 & X_q \\ Z_V & Z_\alpha & -\frac{g}{V_0} \cdot cos\gamma_0 & Z_q \\ 0 & 0 & 0 & 1 \\ M_V & M_\alpha & 0 & M_q \end{bmatrix} \tag{4}$$

The dynamic matrix consists of the linearization force elements (X_V, Z_V), force and moment variables influenced by the angle of attack (X_α, Z_α, M_α) and force and moment elements, which are functions of the pitch rate (X_q, Z_q, M_q). The constants V_0 and γ_0 refer to trim point conditions for true airspeed and flight path angle, whereas g provides the gravity acceleration.

$$\boldsymbol{B}_{lon} = \begin{bmatrix} X_\eta & X_{\delta_T} \\ Z_\eta & Z_{\delta_T} \\ 0 & 0 \\ M_\eta & M_{\delta_T} \end{bmatrix} \tag{5}$$

The input matrix includes force and moment variables as functions of the elevator deflection (X_η, Z_η, M_η) and thrust (X_{δ_T}, Z_{δ_T}, M_{δ_T}). Before proceeding to the derivation of the control law, the approximated longitudinal dynamics of the pitch angle and the pitch rate must also be introduced. These are based on Equation 6, which contains only one eigenvalue in its dynamics thus indicating a priori aperiodic stable behavior.

$$\begin{aligned} \begin{bmatrix} \dot{q} \\ \dot{\theta} \end{bmatrix} &= \begin{bmatrix} M_q & 0 \\ 1 & 0 \end{bmatrix} \cdot \begin{bmatrix} q \\ \theta \end{bmatrix} + \begin{bmatrix} M_\eta \\ 0 \end{bmatrix} \eta \\ y &= \begin{bmatrix} 1 & 0 \\ 0 & 1 \end{bmatrix} \cdot \begin{bmatrix} q \\ \theta \end{bmatrix} \end{aligned} \tag{6}$$

Lateral Directional Motion

The following equations describe the full lateral motion and show the extraction of lateral directional aircraft motion. The lateral state vector x_{lat} contains the yaw rate r, sideslip angle β, roll rate p and the bank angle ϕ. The input vector u_{lat} is composed of the aileron and rudder deflections, respectively given by ξ and ζ. Both vectors are shown in Equation 7. The dynamic and the input state space model matrices are described in Equations 8-9. The dynamic matrix of the lateral directional motion consists of linearization moment elements, which are functions of the yaw rate (N_r, L_r), force and moment variables related to the angle of sideslip (N_β, Y_β, L_β) and moment elements influenced by the roll rate (N_p, L_p).

$$\begin{aligned} x_{lat} &= [r \quad \beta \quad p \quad \phi]^T \\ u_{lat} &= [\xi \quad \zeta]^T \end{aligned} \tag{7}$$

$$\boldsymbol{A}_{lat} = \begin{bmatrix} N_r & N_\beta & N_p & 0 \\ -1 & Y_\beta & 0 & \frac{g}{V_0} \\ L_r & L_\beta & L_p & 0 \\ 0 & 0 & 1 & 0 \end{bmatrix} \tag{8}$$

The lateral directional input matrix includes the force and moment elements as function of aileron (N_ξ, Y_ξ, L_ξ) and rudder deflection ($N_\zeta, Y_\zeta, L_\zeta$).

$$\boldsymbol{B}_{lat} = \begin{bmatrix} N_\xi & N_\zeta \\ Y_\xi & Y_\zeta \\ L_\xi & L_\zeta \\ 0 & 0 \end{bmatrix} \tag{9}$$

The roll mode has been extracted directly from a full lateral directional model with its main states being the roll rate and the bank angle. The roll mode is primarily excited by the aileron deflection and it has been employed for the lateral controller design. Similar to the reduced longitudinal state space dynamics represented by Equation 6, the roll mode contains only one eigenvalue in its dynamics thus indicating a priori aperiodic stable behavior.

The roll mode equations that have been extracted from the lateral directional state space description are shown below [3]:

$$\begin{bmatrix} \dot{p} \\ \dot{\phi} \end{bmatrix} = \begin{bmatrix} L_p & 0 \\ 1 & 0 \end{bmatrix} \cdot \begin{bmatrix} p \\ \phi \end{bmatrix} + \begin{bmatrix} L_\xi \\ 0 \end{bmatrix} \xi$$
$$y = \begin{bmatrix} 1 & 0 \\ 0 & 1 \end{bmatrix} \cdot \begin{bmatrix} p \\ \phi \end{bmatrix} \tag{10}$$

Baseline Control Strategy

This chapter describes the control strategy, which allowed the design and implementation of a baseline flight controller. The main objective of the baseline controller is to ensure that the modeled aircraft successfully tracks the desired pitch angle and bank angle command signals with small static error. The implemented flight control system acts as a longitudinal and lateral autopilot providing the necessary elevator and ailerons deflections for the demanded pitch angle and bank angle given by the reference signal. Since for the presented application only the longitudinal and lateral commands are demanded, it is assumed that the rudder deflection is zero [4].

Classical Controller Design

In order to ensure that the modeled aircraft successfully tracks the desired pitch and bank angle commands, a longitudinal/lateral autopilot based on a classical control theory has been designed. The longitudinal/lateral controller structure has been inspired by the plant dynamics, thus achieving a linear input/output behavior of the closed loop system. The architecture of the implemented closed loop system contains the aircraft dynamics divided into longitudinal and lateral motion and augmented with actuator dynamics. The flight control system (FCS) includes two control loops for both the longitudinal and the lateral motion. The cross coupling effects have been neglected in this case. The cascaded longitudinal controller contains blocks for the control of the pitch angle and pitch rate. Standard PI architecture has been applied to each of the cascaded loops [5]. The whole flight control system includes a pitch angle and pitch rate controller in the longitudinal controller structure and a roll angle and roll rate in the lateral block.

The input signals of the FCS are the pitch angle command (PITCH CMD) and the bank angle command (ROLL CMD). They are transformed to the pitch rate and roll rate command signals by blocks PITCH CTRL and ROLL CTRL, which belong to the outer loop controller. The pitch rate and roll rate command signals are inputs of the pitch rate and roll rate controllers. These controllers comprise the inner loop and generate the control signals for the aircraft's elevator and aileron deflections. Figure 2 introduces a block scheme depicting the whole closed loop system. Each controller block includes classical proportional-integral controller with saturation at the output and a simple anti-windup filter. Suitable controller parameters were automatically computed by the evolutionary optimization algorithm as to fulfill the design specific criteria, which are mentioned in the following chapters. Equations 11-13 show the general mathematical description of the linear controller structure depicted in Figure 3.

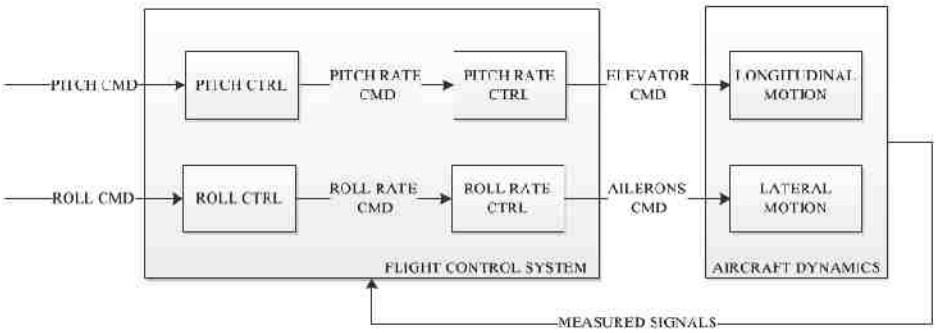

Figure 2. Closed-Loop System Scheme

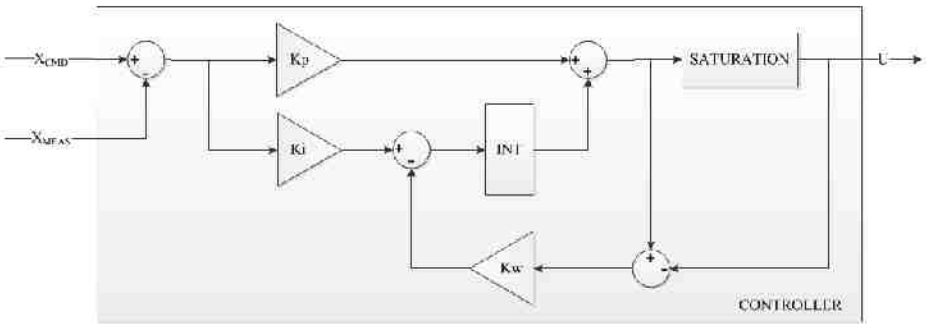

Figure 3. Controller Scheme

$$u(t) = K_p e(t) + \int_0^t [K_i e(t) - K_w d_{sat}(t)]dt \quad (11)$$

where K_p, K_i, K_w are constant parameters of the PI controllers, $e(t)$ is the error between commanded and measured signal which is given by:

$$e(t) = x_{cmd}(t) - x_{meas}(t), \quad (12)$$

and $d_{sat}(t)$ is the difference between the saturated and the non-saturated output signal:

$$d_{sat}(t) = \overline{u}(t) - u(t), \quad (13)$$

where $\overline{u}(t)$ is controller output before saturation and $u(t)$ is controller output after saturation.

Evolutionary Principles

Evolutionary Algorithms (EA) are a class of bio-inspired, stochastic search-techniques based on the principle of natural selection, which is known from biological evolution. The theory was first proposed by Charles Darwin. In contrast to the traditional optimization approaches, evolutionary algorithms operate over a population of candidate solutions rather than over a single case. Each candidate solution (called phenotype) is encoded in a population of individuals (called genotypes, genomes or also chromosomes) that represent a particular problem solved within the evolutionary algorithm. In this case, the goal is to obtain a proper controller gain combination for the Flight Control System of a light aircraft. Therefore, the candidate solution is a set of feedback gains. The process of evolution consists of a sequence of search-steps, where each step involves the creation of a new population through reproduction. It is possible to talk about generations of individuals developed over time. Every new population is created by the means of reproduction, which performs the selection of chromosomes according to their suitability to represent a solution to a given problem. This ability is expressed by a fitness function. While the genetic operators work over chromosomes, the fitness function evaluates the

candidate solutions. Since the selection operator prefers more fit genomes, there is a selection pressure motivating the evolution process to provide better outcomes. The selection pressure causes more fit individuals to live longer and allows them to create offspring, which inherits their genetic information. Selected chromosomes are then modified by the genetic (also variation) operators, which are also inspired by the relevant processes known from biological evolution. These modifications give rise to new candidate solutions forming the next generation. Note that the way of implementation and use of specific genetic operators (including selection) depends on the evolutionary algorithm and also on the problem to be solved [6].

The genetic algorithm (GA) is the most well known variant in the evolutionary approach. The genotype of every individual in the population is initialized with random gene values (using a priori information about the solution). The main loop of the algorithm begins with a corresponding phenotype of every individual in the population being evaluated and gives a fitness value according to how well it fulfills the problem objective or fitness function. Evaluation scores are used to describe how many samples of a particular individual are found in the mating pool. The actual reproduction (creation of a new population) then proceeds as follows: two individuals (parents) are randomly chosen from the mating area and their two offsprings are generated by the genetic crossing operator (recombination), which replaces the value of the selected genes between parental chromosomes. Crossing is a probabilistic genetic operator, which means that the modification of two chosen parent chromosomes is carried out only with a certain probability. A genetic mutation operator is applied after the recombination (also with a certain probability), which randomly selects a gene (or several genes) in the chromosome and generates new values (alleles) [7]. The basic GA strategy is depicted in Figure 4.

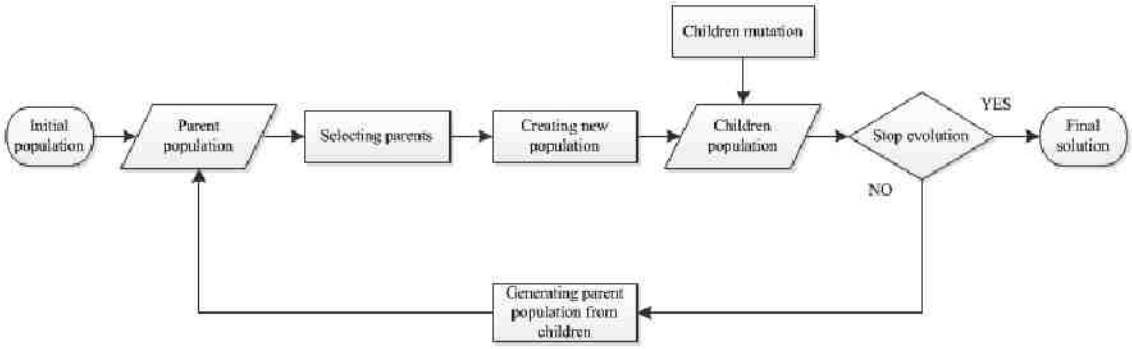

Figure 4. Basic Genetic Algorithm Block Diagram

Initializing Genetic Sets

The first step of the genetic algorithm is to create an initial population built from individuals with random genes. This population is in most cases represented by parameters of a function, which is to be optimized. A priori information used as an initial expert guess may be used in order to reduce high computation costs and in order to lead the genetic algorithm to an optimal solution much faster.

Computing Fitness Function

The fitness function represents the solution quality of every population member and its definition includes quantities, which are to be optimized. It may take a general form as its composition is related to expected limitations, interferences, behavioral trends or penalties for crossing predefined functional limits.

Selection of Best Parents

This operation is often simply called the selection, deriving from its biological origin in the natural selection. For the creation of a new population, individuals with a minimal fitness function value are employed in the majority of cases. Furthermore, the probability by which the individual

candidate solution might become parents according to their own fitness function can also be chosen.

Parents Crossover, Creating New Population

A new population is created through an interaction of parent genes chosen in the previous step. In the presented optimization framework, a mixing method has been implemented. This method uses a random part of the genotype from one parent and the rest of the genes is taken from the second parent.

Mutation Effects

Some genes of the population members might be affected by the so-called mutation process, which modifies these genes within a scope of predefined probabilities.

It is possible to use any representation for the individuals in the genetic algorithm. Individuals built from strings of bits are often used, due to inherent speed and simplicity in the implement mutation and crossover processes. It is also possible to use trees, arrays, lists or any object, but it is then necessary to define genetic operators (initialization, mutation, crossover) for any representation the user decides to employ. Figure 5 shows an individual with a binary array representation (i.e. chromosome). The operations of crossover and mutation are shown in Figure 6.

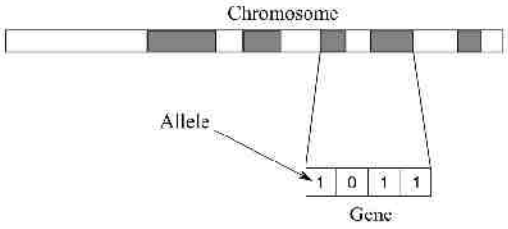

Figure 5. Binary Representation of Genetic Individual

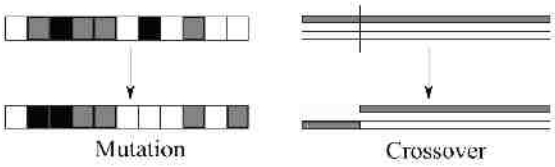

Figure 6. Genetic Mutation and Crossover

The abovementioned algorithm steps are executed until the fitness function value reaches a desired precision threshold related to a number of virtually produced generations. The implementation of the genetic algorithm includes parameters whose specification is left to the designer. These parameters include the number of initial population members, initial means and deviation of initial gains, weights of the fitness function (or a whole fitness function). Among the parameters to be defined is the number of chosen parents used for the creation of a new population, gene distribution between parents or number of children the parents can create. Almost every parameter may be affected by a predefined probability value [8].

Controller Tuning

In order to define adequate controller design parameters for the implemented rigid-body dynamic model, a simple genetic algorithm has been employed. Each chromosome in the population contains a list of controller parameter values that needs to be identified. The goal of the genetic algorithm is to find a set of controller parameter values that fulfill pitch angle and bank angle step response requirements like minimal overshoot, adequate settling time and minimal steady state error. In addition, closed-loop stability requirements (gain and phase margins) have also been taken into account. The fitness function is calculated as a weighted sum of the abovementioned quantities. The objective of the evolution driven optimization is to minimize the fitness function in order to obtain desired controller parameter values.

Stability Requirements

Two of the most common characteristics, which describe the control stability of closed loop system, are the gain margin (GM) and the phase margin (PM). Its values characterize how far from instability is the closed loop system (aircraft with the flight control system) based on a frequency response analysis of a linear system (Bode magnitude and phase characteristics). The optimal values for a stable system are GM > 6dB and PM > 45°. The flight quality measure known as the Gibson-Dropback Criterion (GDC), was also employed for the longitudinal controller tuning. This limits the pitch rate overshoot related to the attitude dropback. The value of GDC should be kept within predefined limits to avoid unwanted aircraft behavior (e.g. Pilot Induced Oscillations) [9].

Evolutionary Algorithms

The controller parameter optimization routines are implemented within a tool performing the identification of optimal control parameters for the aircraft's longitudinal/lateral motion. This tool represents an application-specific software code composed in Matlab that runs the genetic algorithm routine to tune the parameters of the airplane controller described by a set of physical quantities related to the longitudinal/lateral motion. The genetic algorithm searches for the optimal values of the parameters that represent a set of controller gains used for a given airplane.

The evolution starts with the initial values of the controller parameters specified in accordance with the settings from a similar airplane category. The functional behavior of the observed quantities is evaluated by the main characteristics of the response, overshoot (OVS), settling time (ST) and steady state error (SSE), using a weighted sum approach, which represents a fitness value for each candidate solution and is composed of a combination of controller parameters. The selection pressure leads to the optimization of the fitness values for each new generation within the genetic algorithm. If a combination of parameter values is found whose fitness value is less than a specified threshold fitness value, this parameter combination is considered being a result of the optimization process. The fitness function is defined as a weighted sum of the pitch angle and bank angle overshoot and of their steady state errors.

There are also penalization flags that should prevent unwanted system behavior (e.g. unstable system, too long or short settling time, violated GDC conditions etc.) [9]. The implemented fitness function FF is shown in the following equation:

$$FF = k_1 \cdot OVS + k_2 \cdot SSE + k_3 \cdot ST + \sum_i FLAG_i \cdot pen \quad (14)$$

The implemented penalization flags may reach values 0 or 1 (0 - the criterion is fulfilled, 1 – the criterion is violated). The penalization constant pen multiplies the sum of the penalization flags, which is numerically a large number.

Simulation Results

This chapter presents some of the simulation results obtained with the implemented rigid-body dynamic model. The initial section is dedicated to the implemented baseline controller performance as it contains the time history of the rigid-body states after one of the longitudinal motion maneuvers is executed. At the beginning of the simulation, the aircraft is considered to be in a steady state flight condition. For this particular case, the chosen flight condition is the following: altitude of 6000 ft and IAS = 90 kts. All time simulation results and plots were obtained via Simulink®, a Mathworks environment. The genetic optimization routine initiation consisted of filling the matting pool with an initial set of parameters taken from a random distribution around the a priori controller setting values. The algorithm created 100 generations of individuals within this experiment. The number of generations is a variable influencing the quality of the system behavior with a large impact on the computational cost.

Longitudinal Motion Controller

Figure 7 shows the aircraft response (blue curve) to a step input of the pitch angle (red curve). The following subplots include responses of pitch rate and elevator deflection, which are important for the computation of the flight quality and control sensitivity criterions.

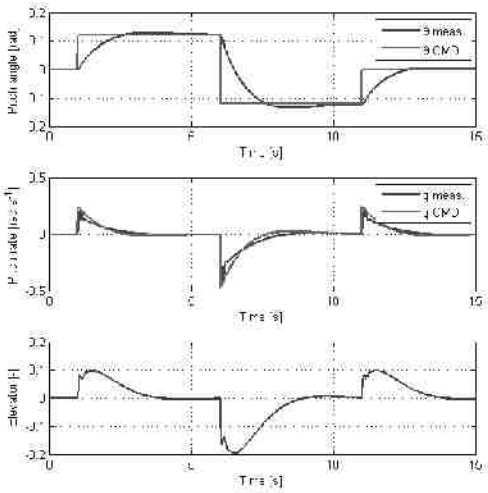

Figure 7. Longitudinal Motion Results

The optimization routine has tuned the baseline controller to a minimum response overshoot and static error (both under 1%), optimal settling time and passed flight quality and stability criteria from [9]. The optimization algorithm also minimized the dropback and pitch rate overshoot to avoid pilot induced oscillations (PIO). Figure 8 shows the progress of the longitudinal fitness function over all generations.

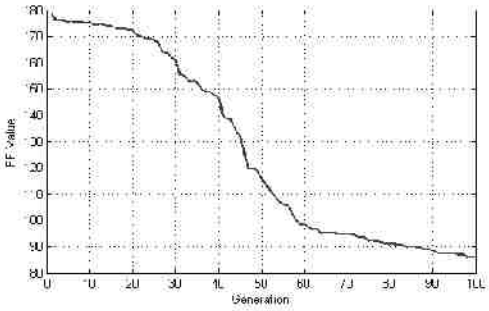

Figure 8. Longitudinal Fitness Function Progress

Table 1 displays the final controller gain settings, and performance characteristics in pitch angle step response overshoot, static error and settling time for the modeled aircraft.

Table 1. Longitudinal Controller Setting

Set of Gains			
Kp_θ	Ki_θ	Kp_q	Ki_q
1.946	0.0001	1.001	2.673
Performance Results			
Overshoot	Static Error	Settling Time	
4.982%	0.076%	1.430s	

Lateral Motion Controller

Figure 9 shows the results of the lateral motion aircraft response. The plot includes bank angle step response (blue curve) for the commanded signal (red curve). The following subplots contain the response of the roll rate and the right aileron deflection.

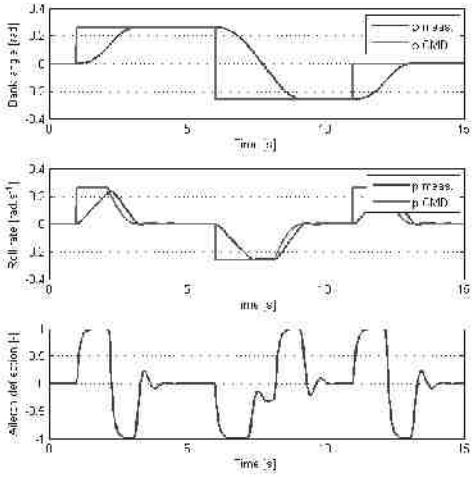

Figure 9. Lateral Motion Results

Figure 10 shows the progress of the lateral fitness function over all generations. The fitness function value tends to decrease, which is a desirable effect of the evolution driven optimization.

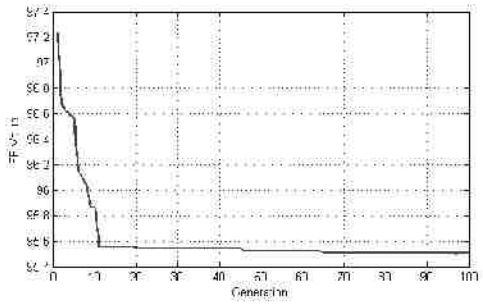

Figure 10. Lateral Fitness Function Progress

Table 2 presents the final gain settings for a roll controller and its performance results like bank angle step response overshoot, static error and settling time.

Table 2. Lateral Controller Settings

Set of Gains			
Kp_ϕ	Ki_ϕ	Kp_p	Ki_p
1.784	0.0001	0.731	0.339
Performance Results			
Overshoot	Static Error	Settling Time	
0.079%	0.096%	2.04s	

The optimization routine kept the bank angle overshoot and static error below 1% and settling time around 2 seconds, leading to a very good result.

Conclusions

A modern controller design and optimization approach for a light sport type of aircraft has been introduced and implemented. The controller design process integrates not only an evolution driven optimization technique but also makes use of a classical control design approach. The use of classical control theory enabled creating a state of the art flight control system implementation for a rigid-body aircraft model.

The evolutionary concept played a significant role in the optimization of the proposed controller structure by providing tuned controller parameters meeting the designed fitness function criteria imposed through the optimization problem formulation. The proposed fitness function combined significant controller stability evaluation criteria into a single abstraction. The suggested form of multicriterial optimization definition was allowed by using a robust optimization framework based on genetic algorithms. A suitable combination of stability criteria with robustness of the evolution driven algorithms enabled the authors to propose and fine-tune a complex control structure of a rigid-body model of a light sport aircraft. The suitability of the evolutionary optimization has been successfully tested on a set of examples, which accounted for rigid-body aircraft dynamics. Further development should account for hardware accelerated genetic optimization algorithm with real-time auto-tuning capability of an aircraft control system.

References

[1] Marinus, B.G., Influence of Parameterization and Optimization Method on the Optimum Airfoil, ICAS 2010, Nice, France, 2010.

[2] Benini, E., Ponza, R., Massaro, A., High-Lift Multi-Element Airfoil Shape and Setting Optimization Using Multi-Objective Evolutionary Algorithms, Journal of Aircraft, Vol. 48, No. 2, 2011.

[3] Lewis, B. L., Stevens, F. L., Aircraft Control and Simulation, John Wiley & Sons, 1992.

[4] Etkin, B., Reid, L. D., Dynamics of Flight: Stability and Control, John Wiley & Sons, 1995.

[5] Peter, F., Leitao, M., Holzapfel, F., Adaptive Augmentation of a New Baseline Control Architecture for Tail-Controlled Missiles Using a Nonlinear Reference Model, AIAA Guidance, Navigation and Control Conference, Minneapolis, 2012.

[6] Back, T., Evolutionary Algorithms in Theory and Practice, 2nd ed., Oxford University Press, New York, 1996.

[7] Rothlauf, F., Representation for Genetic and Evolutionary Algorithms, 2nd ed., Springer-Verlag, Berlin, 2006.

[8] Crina, G., Ajith, A., Hisao, I., Hybrid Evolutionary Algorithms, Springer, Berlin, 2007.

[9] Department of Defense, MIL-F-8785C Flying Qualities of Piloted Airplanes, Military Specification, Washington, 1980.

Acknowledgements

This work has been supported by the European Regional Development Fund in the IT4Innovations Centre of Excellence project (CZ.1.05/1.1.00/02.0070), by the Technology Agency of the Czech Republic research project "Smart Autopilot" TACR TA01010678, and by the DAAD/MSMT project 7AMB12DE004.

INTENTIONALLY LEFT BLANK

AIAA 2013-5153

Evolution Driven Controller Design for Aeroservoelastic Aircraft

Peter Chudy[1] and Jan Vlk[2]
Brno University of Technology, Brno, Czech Republic

and

Miguel Leitão[3] and Felix Stroscher[4]
Technical University Munich, Munich, Germany

An evolution driven controller design approach has been applied to an aeroservoelastic model of a large passenger aircraft. The aeroservoelastic model comprises structural, aerodynamic and flight dynamics related elements and the chosen controller architecture is based on Nonlinear Dynamic Inversion. The evolutionary concept has played a significant role in the optimization of the proposed NDI controller structure by providing tuned controller parameters which meet the designed fitness function criteria imposed through the optimization problem formulation. The proposed fitness function combines significant controller stability evaluation criteria into a single abstraction. The use of a robust optimization framework based on the genetic algorithms has allowed the suggested form of multi-criteria optimization definition. The suitability of the evolutionary optimization has been successfully tested on a set of examples, which accounted for rigid body aircraft dynamics as well as for the case with elastic structural modes. Time-domain simulation results have shown the compliance of the tuned controller performance to its anticipated behavior.

Nomenclature

$\bar{c}$	=	Mean Aerodynamic Chord	u	=	System Input
C_{ij}	=	Aerodynamic Coefficients	V_{TAS}	=	True Airspeed
F_x	=	Penalization Flag	$(\boldsymbol{V}_K^G)_B$	=	Kinematic CG Velocity Vector
$(F_P^G)_B$	=	Total Thurst Force	x	=	System State
h^G	=	Aircraft Altitude	$\boldsymbol{x}_0^G$	=	Possition Vector in NED frame
$\mathbf{I}_{BB}$	=	Aircraft Inertia	$\boldsymbol{x}_l$	=	Lag States
K	=	Baseline Feedback Gains	y	=	System Output
$\mathbf{K}$	=	Stiffness Matrix	Z_A^G	=	Aerodynamic Forces Vector
m	=	Aircraft Mass	α	=	Aerodynamic Angle of Attack
$\mathbf{M}$	=	Mass Matrix	β	=	Aerodynamic Sideslip Angle
Ma	=	Mach Number	δ_T	=	Throttle Level State
$\boldsymbol{M}_A^G$	=	Aerodynamic Moments Vector	η	=	Elevator Deflection
n_Z	=	Vertical Load Factor	$\boldsymbol{\eta}$	=	Aeroservoelastic State Vector
p^A	=	Static Air Pressure	ν	=	Pseudo-Control
q	=	Pitch Rate	ξ	=	Damping Coefficient
$\bar{q}$	=	Dynamic Pressure	$\boldsymbol{\Phi}$	=	Euler Angles
S	=	Wing Reference Area	ω_0	=	Natural Frequency
T	=	Thrust Force	$\boldsymbol{\omega}_K$	=	Kinematic Angular Rate Vector

[1] Ph.D., Faculty of Information Technology, Email: chudyp@fit.vutbr.cz, AIAA Member.
[2] Ph.D. Candidate, Faculty of Information Technology, Email: ivlk@fit.vutbr.cz.
[3] Ph.D. Candidate, Institute of Flight System Dynamics, Email: miguel.leitao@tum.de, AIAA Student Member.
[4] Ph.D. Candidate, Institute of Lightweight Structures, Email: stroscher@llb.mw.tum.de, AIAA Student Member.

I. Introduction

The evolutionary approach is a popular tool in optimization tasks of nonlinear problems. The design of a controller accounting for aeroservoelastic phenomena must typically satisfy a range of optimization criteria transformed into a cost function. The principal advantage of using evolution driven tools is in their suitability to account for heterogenous optimization conditions. Even the traditional techniques for solving nonlinear optimization tasks offer computationally less costly solutions, their applicability imposes higher demand on cost function definition and may therefore be limited in utilization and robustness. Implemented evolutionary approach offers a robust platform allowing the tuning of controller performance to required levels.

Evolution driven approaches got recognition in aerospace disciplines when successfully used for the optimization of high performance airfoils, efficient high lift systems or unconventional aircraft configurations. Its scientific potential has been put on display when human powered aircraft whose design elements were influenced by the outcomes of the evolutionary optimization took flight and made its public debut. The multi-criteria nature of the task formulation, which has been used for the aerodynamics, introduced the rationality of using the robust nonlinear optimization technique also on the flight control related tasks.[1,2]

II. Aeroservoelastic Simulation Model

In order to successfully demonstrate the potential benefits of employing evolution-based optimization approaches during the design task of aeroservoelastic aircraft controllers, a realistic nonlinear simulation model comprising both structural and rigid-body dynamics, unsteady aerodynamics and control surface dynamics has been implemented. The main purpose of this section is therefore to introduce this simulation model which is based on data derived from a conventional large passenger aircraft.

A. Structural Dynamics

The dynamic properties of a large commercial aircraft with slender load bearing structural elements have been the foundation for the aeroservoelastic modeling tasks with a state of the art Finite Element (FE) methods applied to describe its structural dynamics behaviour. The wing FE model has been rigidly connected at its root section to a node at the aircraft's modeled center of gravity (CG node). The dynamic properties of the fuselage, the tail unit and all nonstructural elements have been virtually represented by their dynamic substitutions in a form of concentrated mass elements with assigned moments of inertial located at the CG node. In order to model the aeroservoelastic effects and their relationship to the rigid-body dynamics in a representative form, the FE model has been augmented with the following components: elastic model of the tail structure, structural representative of trailing edge control surfaces located on the wing, elevator and rudder composed of shell elements. The aforementioned control surfaces have been connected to the modeled primary structure using a stiff bar and spring elements, ensuring that the control surfaces are statically decoupled from both the wing and the tail structure. The structural properties of the half-span FE model have been assessed by analyzing the symmetric and antisymmetric normal modes. For both cases, the three rigid-body modes and the first thirteen elastic modes have been computed and stored in a database containing respective eigenvectors, modal mass and stiffness matrix. Furthermore, an additional modal analysis considering movable control surfaces has been carried out by disabling rotational support around hinge axis. The modal database has then been augmented by the extracted rigid-body modes of control surfaces, which are inertially coupled to the full aircraft structural modes. As an example, the first symmetric elastic mode is depicted in Figure 1.

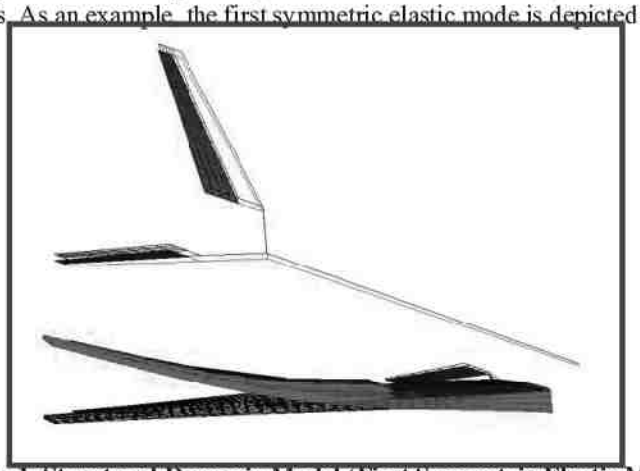

Figure 1. Structural Dynamic Model (First Symmetric Elastic Mode)

B. Unsteady Aerodynamics

The unsteady aerodynamic forces of the lifting surfaces have been taken into account by making use of the linear, subsonic panel method ZONA6.[3] The mid-surfaces of wing and tail have been discretized into aerodynamic panels, for which the so-called Aerodynamic Influence Coefficients (AIC) have been computed. These relate normal pressure distribution of the upper and lower surfaces of one panel with the dynamic motion of all other panels, represented in the frequency domain. A depiction of the employed panel model for the unsteady aerodynamic is shown in Figure 2.

In order to relate the unsteady pressure coefficients acting on the aerodynamic panels with the structural model, an infinite plate spline approach has been applied.[4] The constructed spline matrix $\mathbf{G}$, which directly relates the aerodynamic degrees of freedom with the structural physical degrees of freedom has been obtained. As a modal approach has been employed for the aeroelastic equations of motion, the unsteady pressures have been transformed into the modal space by the eigenvectors $\mathbf{\Phi}$, defined on physical degrees of freedom. The so-called Generalized Aerodynamic Forces (GAF) can then be written as follows:

$$\mathbf{GAF} = \mathbf{\Phi}^T \mathbf{G}^T \cdot \mathbf{AIC} \cdot \mathbf{G}\mathbf{\Phi}. \tag{1}$$

The required GAF have been computed for a set of reduced frequencies. In order to be able to apply them in a time-domain simulation model, these generalized forces have been approximated in the Laplace domain by making use of the minimum-state method.[5] The relationship between generalized aerodynamic forces and minimum-state matrices can be seen in the expression below.

$$\mathbf{GAF}(s) = \mathbf{A}_0 + \left(\frac{\bar{c}}{2V_{TAS}}\right)\mathbf{A}_1 \cdot s + \left(\frac{\bar{c}}{2V_{TAS}}\right)^2 \mathbf{A}_2 \cdot s^2 + \mathbf{D} \cdot \left(\mathbf{I} \cdot s - \frac{2V_{TAS}}{\bar{c}} \cdot \mathbf{R}\right)\mathbf{E} \cdot s \tag{2}$$

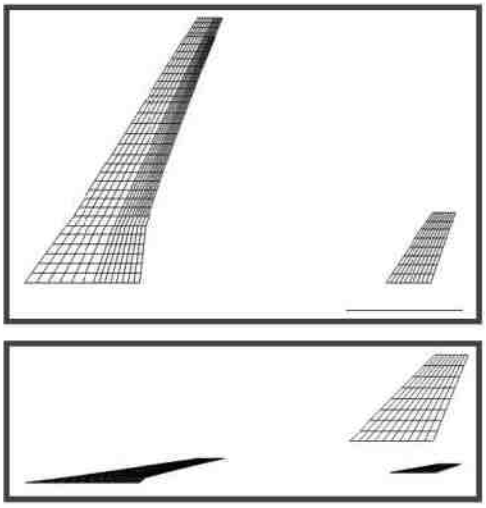

Figure 2. Aerodynamic Panel Model (Top and Side Views)

If the number of lag states is given by l, the identity matrix $\mathbf{I}$ and the diagonal matrix $\mathbf{R}$ are defined as: $\mathbf{I}, \mathbf{R} \in \mathbb{R}^{l \times l}$. The resulting minimum-state matrices $\mathbf{A}_0$, $\mathbf{A}_1$, $\mathbf{A}_2$, $\mathbf{D}$ and $\mathbf{E}$ can be further broken down by taking the nature of motion of its components into account – rigid-body modes "r", elastic modes "e" and control surface modes "c".

$$\mathbf{A}_i = \begin{bmatrix} (\mathbf{A}_i)_{rr} & (\mathbf{A}_i)_{re} & (\mathbf{A}_i)_{rc} \\ (\mathbf{A}_i)_{er} & (\mathbf{A}_i)_{ee} & (\mathbf{A}_i)_{ec} \\ (\mathbf{A}_i)_{cr} & (\mathbf{A}_i)_{ce} & (\mathbf{A}_i)_{cc} \end{bmatrix}, \qquad i = 0,1,2 \qquad \mathbf{A}_i \in \mathbb{R}^{n \times n} \tag{3}$$

$$\mathbf{D} = [\mathbf{D}_r \quad \mathbf{D}_e \quad \mathbf{D}_c]^T, \qquad \mathbf{D} \in \mathbb{R}^{n \times l} \tag{4}$$

$$\mathbf{E} = [\mathbf{E}_r \quad \mathbf{E}_e \quad \mathbf{E}_c], \qquad \mathbf{E} \in \mathbb{R}^{l \times n} \tag{5}$$

In the expressions above, n represents the total number of states and is given by the sum of rigid-body, elastic and control surface modes. All the $\mathbf{A}_2$ sub-matrices corresponding to the rigid-body and control surface modes are neglected in this framework since their modal frequency is much lower when compared to the elastic modes. This indicates that a purely unsteady s^2-proportional aerodynamics are only considered for the elastic motion (only $(\mathbf{A}_2)_{ee} \neq \mathbf{0}$). Additionally, if one assumes purely steady aerodynamic response from the rigid-body motion, its aerodynamic influence in the lag equations can also be neglected ($\mathbf{E}_\tau = \mathbf{0}$). This approximation implies that the time delays influencing the aerodynamic forces which are induced by rigid-body motion will not be considered in this document.

C. Atmosphere, Engine and Actuator Models

The simulation model makes use of a simplified atmospheric model based on the international standard ISO-2533 which is valid for an altitude range between -2 and 20 kilometers (Troposphere and Lower Stratosphere). The atmospheric model is employed to acquire important air-related physical properties which influence the modeled aircraft dynamics, such as air temperature, Mach number, dynamic pressure, etc.

The commercial aircraft model considered in the simulation possesses a total of four engines located under the wing (two per wing) which generate the necessary thrust. The total thrust force has been modeled by a linear function influenced by the throttle level state, static pressure, Mach number and aircraft altitude as seen in the expression Eq. (6). The moments generated by the propulsion are zero since all engine gyroscopic effects have been neglected. Additionally, the engine dynamics has been modeled by a first-order linear filter.

$$\left(\vec{\boldsymbol{F}}_P^G\right)_B = \begin{bmatrix} T \\ 0 \\ 0 \end{bmatrix}_B = \begin{bmatrix} f(\delta_T, \mathrm{Ma}, p^A, h^G) \\ 0 \\ 0 \end{bmatrix}_B \tag{6}$$

Regarding actuation systems, the implemented simulation model considers a total of thirteen different control surfaces: three high lift devices and two ailerons per wing, as well as two elevators and one rudder. The control surface positive deflections are defined in the conventional way, respecting the right-hand rule over the body-fixed frame. The modeled actuators are nonreversible and have been modeled by second order filters with acceleration, rate and deflection limits.[6] The actuator model takes the aerodynamic hinge moments computed by the aerodynamic model into account, as seen in the following expression:

$$\delta = \frac{\omega_0^2}{s^2 + \frac{2\xi\omega_0}{H}s + \omega_0^2} \cdot \delta_{CMD} \ , \tag{7}$$

where H is a dimensionless variable given by a nonlinear function which depends on the abovementioned aerodynamic hinge moments acting on the actuator at a particular time.

D. Rigid-Body Equations of Motion

The rigid-body equations of motion implemented in the simulation model have been obtained by making use of the standard angular and linear momentum conservation laws. Their derivation can be found in several bibliographic references.[7,8] The translational and rotational equations of motion are respectively given by the following expressions:

$$\left(\dot{\boldsymbol{V}}_K^G\right)_B = \begin{bmatrix} \dot{u}_K^G \\ \dot{v}_K^G \\ \dot{w}_K^G \end{bmatrix}_B = \frac{\sum \vec{\boldsymbol{F}}_B^G}{m} - \begin{bmatrix} p_K \\ q_K \\ r_K \end{bmatrix} \times \begin{bmatrix} u_K^G \\ v_K^G \\ w_K^G \end{bmatrix}_B \ , \tag{8}$$

$$\dot{\boldsymbol{\omega}}_K = \begin{bmatrix} \dot{p}_K \\ \dot{q}_K \\ \dot{r}_K \end{bmatrix} = (\mathbf{I}_{BB})^{-1} \cdot \sum \vec{\boldsymbol{M}}_B^G - \begin{bmatrix} p_K \\ q_K \\ r_K \end{bmatrix} \times (\mathbf{I}_{BB}) \cdot \begin{bmatrix} p_K \\ q_K \\ r_K \end{bmatrix}, \tag{9}$$

where $\vec{\boldsymbol{F}}_B^G$ and $\vec{\boldsymbol{M}}_B^G$ respectively represent the total forces and moments acting on the CG defined in the body-fixed frame. Whereas $\vec{\boldsymbol{F}}_B^G$ comprises the effects of the aerodynamics, gravity and propulsion, $\vec{\boldsymbol{M}}_B^G$ only depends on the aerodynamic effects.

Instead of following an Euler angle-based approach for obtaining the aircraft orientation, the implemented model makes uses of quaternions in order to avoid the known singularities with the pitch angle. The differential equations respective to the quaternions are provided next:

$$\dot{\boldsymbol{q}} = \begin{bmatrix} \dot{q}_0 \\ \dot{q}_1 \\ \dot{q}_2 \\ \dot{q}_3 \end{bmatrix} = \frac{1}{2} \cdot \begin{bmatrix} 0 & -p_K & -q_K & -r_K \\ p_K & 0 & r_K & -q_K \\ q_K & -r_K & 0 & p_K \\ r_K & q_K & -p_K & 0 \end{bmatrix} \cdot \begin{bmatrix} q_0 \\ q_1 \\ q_2 \\ q_3 \end{bmatrix}. \tag{10}$$

Furthermore, the quaternion constraint law ($q_0^2 + q_1^2 + q_2^2 + q_3^2 = 1$) must always be enforced.

The final set of rigid-body equations of motion provides the aircraft CG position dynamics defined in the North-East-Down (NED) Frame. The aircraft position dynamics are computed via the kinematic velocities defined in the body-fixed frame, as seen below:

$$\dot{\boldsymbol{x}}_0^G = \begin{bmatrix} \dot{x}^G \\ \dot{y}^G \\ \dot{z}^G \end{bmatrix}_0 = \mathbf{M}_{0B} \cdot \begin{bmatrix} u_K^G \\ v_K^G \\ w_K^G \end{bmatrix}_B, \tag{11}$$

where $\mathbf{M}_{0B} \in \mathbb{R}^{3\times3}$ simply defines a transformation from the body-fixed frame to the NED frame. Making use of general flight dynamics relations and neglecting all wind effects, the Euler angles and other important variables such as true airspeed and aerodynamic angles are respectively given by the Eq. (12) and Eq. (13).

$$\boldsymbol{\Phi} = \begin{bmatrix} \Phi \\ \Theta \\ \Psi \end{bmatrix} = \begin{bmatrix} \tan^{-1}\left(2\dfrac{q_1q_2 + q_0q_3}{q_0^2 + q_1^2 - q_2^2 - q_3^2}\right) \\ \sin^{-1}[-2(q_1q_3 - q_0q_2)] \\ \tan^{-1}\left(2\dfrac{q_2q_3 + q_0q_1}{q_0^2 - q_1^2 - q_2^2 + q_3^2}\right) \end{bmatrix} \tag{12}$$

$$\begin{bmatrix} V_{TAS} \\ \alpha \\ \beta \end{bmatrix} = \begin{bmatrix} \sqrt{(u_K)_B^2 + (v_K)_B^2 + (w_K)_B^2} \\ \tan^{-1}\left[\dfrac{(w_K)_B}{(u_K)_B}\right] \\ \tan^{-1}\left[\dfrac{(v_K)_B}{\sqrt{(u_K)_B^2 + (w_K)_B^2}}\right] \end{bmatrix} \tag{13}$$

E. Aeroservoelastic Equations of Motion

The aeroservoelastic equations of motion have been assembled by combining the data derived from the structural dynamics and from the unsteady aerodynamics. A second order differential equation which can easily be found in literature related to structural dynamics has been augmented with aerodynamic loads, as seen in Eq. (14).[9] The aerodynamic loads depend on the rigid-body states, elastic states, control surface states and the lag states.

$$\mathbf{M}\ddot{\boldsymbol{\eta}} + \mathbf{K}\boldsymbol{\eta} = \bar{q}\mathbf{A}_0\boldsymbol{\eta} + \bar{q}\frac{\bar{c}}{2V_{TAS}}\mathbf{A}_1\dot{\boldsymbol{\eta}} + \bar{q}\left(\frac{\bar{c}}{2V_{TAS}}\right)^2\mathbf{A}_2\ddot{\boldsymbol{\eta}} + \bar{q}\mathbf{D}\boldsymbol{x}_l \tag{14}$$

In the above expression, the vector $\boldsymbol{\eta} = [\boldsymbol{\eta}_r \quad \boldsymbol{\eta}_e \quad \boldsymbol{\eta}_c]^T$ contains the elastic states $\boldsymbol{\eta}_e$, the modified rigid-body states which are computed via a linear transformation and are defined as $\boldsymbol{\eta}_r = f(\dot{\boldsymbol{x}}_0^G, \boldsymbol{V}_K^G, \dot{\boldsymbol{V}}_K^G, \boldsymbol{\Phi}, \boldsymbol{\omega}_K, \dot{\boldsymbol{\omega}}_K)$, and the control surface states $\boldsymbol{\eta}_c = f(\boldsymbol{\delta}, \dot{\boldsymbol{\delta}}, \ddot{\boldsymbol{\delta}})$. On the other hand, the rational part in the time-domain approximation is given by a first order differential equation incorporating the so-called lag states $\boldsymbol{x}_l$, as seen next.

$$\dot{\boldsymbol{x}}_l = 2\frac{V_{TAS}}{\bar{c}}\mathbf{R}\boldsymbol{x}_l + \mathbf{E}\dot{\boldsymbol{\eta}} \tag{15}$$

Since the rigid-body and control surface states are separately computed, their contributions have been removed from Eq. (14), meaning that the elastic equations of motion shall only take the integration of the elastic and lag states into account. The final result is shown in the following expression:

$$\ddot{\boldsymbol{\eta}}_e = \left[\mathbf{M}_e - \bar{q}\left(\frac{\bar{c}}{2V_{TAS}}\right)^2 \mathbf{A}_{2e}\right]^{-1} \cdot \left[(\bar{q}\mathbf{A}_{0e} - \mathbf{K}_e)\cdot \boldsymbol{\eta}_e + \bar{q}\frac{\bar{c}}{2V_{TAS}}\mathbf{A}_{1e}\dot{\boldsymbol{\eta}}_e + \bar{q}\mathbf{D}_e \boldsymbol{x}_l\right]. \tag{16}$$

III. Baseline Control Strategy

This chapter describes the control strategy which allowed the design and implementation of a baseline controller for the aeroservoelastic model described in the previous section. The main objective of the baseline controller is to ensure that the modeled aircraft successfully tracks desired load factor command signals with small static error, even in the presence of uncertainty deriving from approximated aerodynamics and unmodeled dynamics (e.g. structural dynamics). The implemented flight control system acts as a longitudinal autopilot providing the necessary elevator deflections for the demanded load factor given by the reference signal. This section starts with the description of an approximated model which has been used for the control design and then proceeds through a brief explanation on how the control laws have been designed. Since for the presented application only the longitudinal commands are demanded, it is assumed that the aileron and rudder deflections are kept to zero and that only the symmetric elastic modes are able to influence the aircraft dynamics.

A. Model Used for Control Design

Due to the fact that the elastic modes cannot be conveniently measured in flight and are therefore not directly available to the flight control system, an approximated unsteady aerodynamics model has been obtained by making use of modern computational fluid dynamics tools. This approximated model describes the aerodynamic forces and moments acting on the aircraft structure in a particular flight regime, even though only depending on rigid-body states and on the control surface deflections, which are assumed to be available to the controller. The aerodynamic forces acting on the X-axis of the body-fixed frame are neglected by this approximation due to the nature of the limitations introduced into the aerodynamic part implemented within the aeroservoelastic model. The approximated longitudinal aerodynamic force Z_A^G and the moment M_A^G are given by the following expressions:

$$(Z_A^G)_B = \bar{q}S \cdot \left[C_{Z0} + C_{Z\alpha}\alpha + \frac{\bar{c}}{2V_{TAS}}C_{Zq}q + C_{Z\eta}\eta\right], \tag{17}$$

$$(M_A^G)_B = \bar{q}S\bar{c} \cdot \left[C_{M0} + C_{M\alpha}\alpha + \frac{\bar{c}}{2V_{TAS}}C_{Mq}q + C_{M\eta}\eta\right], \tag{18}$$

where q represents the pitch rate, η is the elevator deflection and the multiple C_{ij} with $i = \{Z, M\}, j = \{0, \alpha, q, \eta\}$ provide the respective aerodynamic coefficients. As previously mentioned, the main objective of the implemented controller is to track a given vertical load factor command $(n_Z)_C$. Taking Eq. (17) into account, the plant load factor can be approximated by the following expression:

$$n_Z = -\frac{(Z_A^G)_B}{mg} \approx -\frac{\bar{q}S}{mg} \cdot \left[C_{Z0} + C_{Z\alpha}\alpha + \frac{\bar{c}}{2V_{TAS}}C_{Zq}q + C_{Z\eta}\eta\right], \tag{19}$$

with $g = 9.81\, ms^{-2}$ representing the acceleration due to gravity. Before proceeding to the derivation of the control law, the approximated longitudinal dynamics of the angle of attack and of the pitch rate must also be introduced. These are based on the Eqs. (17) and (18) and are respectively given by:

$$\dot{\alpha} = \frac{(Z_T^G)_{\bar{K}}}{mV_{TAS}} + q \approx \frac{[(Z_A^G)_B + mg\cos\Theta]\cos\alpha - [T - mg\sin\Theta]\sin\alpha}{mV_{TAS}} + q\,, \tag{20}$$

$$\dot{q} = \frac{(M_T^G)_B}{I_{yy}} \approx \frac{\bar{q}S\bar{c}}{I_{yy}} \cdot \left[C_{M0} + C_{M\alpha}\alpha + \frac{\bar{c}}{2V_{TAS}}C_{Mq}q + C_{M\eta}\eta\right], \tag{21}$$

where I_{yy} represents the moment of inertia around the Y-axis.

B. Nonlinear Dynamic Inversion and Control Law

In order to ensure that the modeled aircraft successfully tracks the desired load factor commands, a longitudinal autopilot based on a Nonlinear Dynamic Inversion (NDI) technique has been designed. Nonlinear dynamic inversion is a control method motivated by the plant dynamics which achieves a linear input/output behavior of the closed loop system. Its main objective is to find a state transformation which is able to convert a nonlinear system of the form depicted in Eq. (22) into a linearized system by applying nonlinear state feedback.[10,11] NDI has been successfully applied in various aerospace applications and its usefulness has already been proven in some theoretical frameworks[12,13] and flight tests.[14,15]

$$\begin{aligned} \dot{x} &= f(x) + g(x) \cdot u, \\ y &= h(x). \end{aligned} \tag{22}$$

The global linearization of such nonlinear system via nonlinear feedback requires a dynamical relationship between the inputs $\boldsymbol{u}$ and the outputs $\boldsymbol{y}$. This dependency on the input can be achieved by finding the r-th output derivative where the input appears for the first time. The variable r is the so-called Relative Degree (RD) and its existence is a necessary condition for the existence of a linearizing feedback law. For this particular case, the baseline controller considers the existence of two NDI-based cascaded loops (both relative degree one), one corresponding to the fast aircraft dynamics in Eq. (21) – inner loop, and another representing the slower dynamics given by the Eq. (20) – outer loop. The architecture of the implemented baseline controller is depicted in Figure 3.

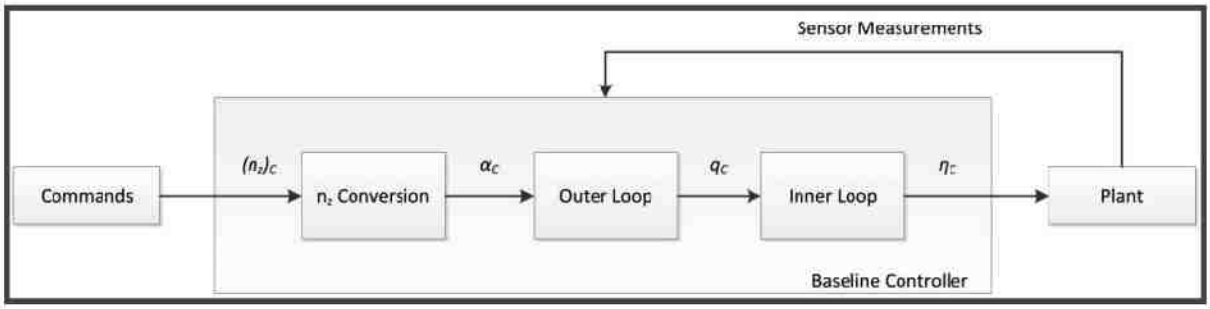

Figure 3. Baseline Controller Architecture

As seen in the schematic above, the employed NDI-based cascaded approach requires a commanded angle of attack signal. Therefore, the first step is to algebraically convert the provided vertical load factor command $(n_Z)_C$ into the corresponding angle of attack α_C. Furthermore, feedforward and feedback proportional integral (PI) control strategies have also been applied inside the block named "n_Z Conversion" in order to improve performance and avoid static error. According to Eq. (19), the commanded angle of attack is then given by:

$$\alpha_C = -\frac{1}{C_{Z\alpha}}\left[\frac{mg}{\bar{q}S}\nu_{nZ} - C_{Z0} - \frac{\bar{c}}{2V_{TAS}}C_{Zq}q - C_{Z\eta}\eta\right], \tag{23}$$

where the pseudo-control ν_{n_Z} simply consists of:

$$\nu_{n_Z} = (n_Z)_C + K_{Pn}[(n_Z)_C - n_Z] + K_{In}\int[(n_Z)_C - n_Z]dt, \tag{24}$$

with K_{Pn} and K_{In} being the controller parameters to be designed.

Now that the commanded angle of attack is known, it is possible to apply the standard NDI architecture to each of the RD1 cascaded loops. As seen in Figure 4, each of the baseline control loops contains four different components which will be briefly discussed next: reference model, linear error controller, dynamic inversion and pseudo-control hedging.

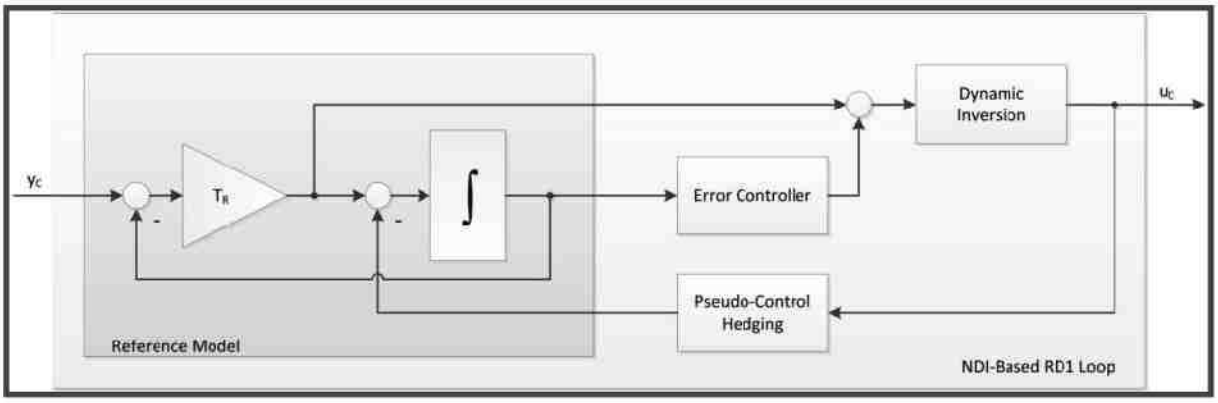

Figure 4. Architecture of a NDI-based RD1 Control Loop

1. Reference Model

Linear and nonlinear reference models have been successfully employed in many frameworks comprising NDI-based control loops.[12,13] The main purpose of implementing a reference model in such architectures is to come up with a feasible reference signal y_R based on the commanded signal y_C. The reference model is designed in a way which guarantees that the resulting reference signal can be tracked by the plant without demanding extensive and burdening control effort. For this particular control problem, both cascaded loops are RD1, which means that first order linear reference models have been selected (Figure 4). The reference model dynamics on both loops are defined by the following pair of equations:

$$\begin{aligned} \nu_R &= T_R(y_C - y_R), \\ \dot{y}_R &= \nu_R - \nu_H. \end{aligned} \tag{25}$$

where T_R is a design parameter and ν_H is the pseudo-control hedging signal which will be defined later.

2. Error Controller

In order to successfully track the designed reference signals, both control loops include a linear error controller comprising feedforward and feedback terms. The implemented baseline controller considers proportional feedback for the inner loop, whereas the outer loop comprises proportional-integral feedback in order to reduce potential static error in the angle of attack signal. The pseudo-controls for the inner and outer loops are respectively given by:

$$\nu_q = \nu_{Rq} + K_{Pq}(q_R - q), \tag{26}$$

$$\nu_\alpha = \nu_{R\alpha} + K_{P\alpha}(\alpha_R - \alpha) + K_{I\alpha}\int (\alpha_R - \alpha)dt\,, \tag{27}$$

where $K_{Pq}, K_{P\alpha}$ and $K_{I\alpha}$ are feedback gains that need to be chosen according to the defined requirements.

3. Dynamic Inversion

The block named "Dynamic Inversion" is responsible for providing the control laws for both loops. By considering the following system representation

$$\dot{y} = A \cdot u + b\,, \tag{28}$$

the approximated aircraft dynamics given by Eqs. (20) and (21) can be rewritten as:

$$\dot{\alpha} \approx \underbrace{1}_{A_\alpha} \cdot q + \underbrace{\frac{[(Z_A^G)_B + mg\cos\Theta]\cos\alpha - [T - mg\sin\Theta]\sin\alpha}{mV_{TAS}}}_{b_\alpha}, \tag{29}$$

$$\dot{q} \approx \underbrace{\frac{\bar{q}S\bar{c}}{I_{yy}} C_{M\eta}}_{A_q} \eta + \underbrace{\frac{\bar{q}S\bar{c}}{I_{yy}} \cdot \left[C_{M0} + C_{M\alpha}\alpha + \frac{\bar{c}}{2V_{TAS}} C_{Mq} q \right]}_{b_q}. \tag{30}$$

The commanded elevator deflections η_C (inner loop) and the commanded pitch rate q_C (outer loop) can thus be finally obtained by respectively inverting Eqs. (30) and (29).

$$\eta_C = A_q^{-1}(\nu_q - b_q), \tag{31}$$

$$q_C = A_\alpha^{-1}(\nu_\alpha - b_\alpha). \tag{32}$$

4. Pseudo-Control Hedging

In order to overcome the undesired effects deriving from actuator saturations, a technique named pseudo-control hedging has been employed.[16] The so called hedging signal ν_H is able to decelerate the reference model dynamics by taking the expected plant reaction deficit into account. The hedging signals which have been applied to the inner and outer loops are respectively shown in the following equations:

$$\nu_{Hq} = A_q(\eta_C - \eta), \tag{33}$$

$$\nu_{H\alpha} = A_\alpha(q_C - q). \tag{34}$$

5. Control Laws

The inner and outer control laws have been obtained by expanding equations (31) and (32) with the results of Eqs. (26) and (27) respectively. The final results are then:

$$\eta_C = A_q^{-1}\left[\nu_{Rq} + K_{Pq}(q_R - q) - b_q\right], \tag{35}$$

$$q_C = A_\alpha^{-1}\left[\nu_{R\alpha} + K_{P\alpha}(\alpha_R - \alpha) + K_{I\alpha}\int(\alpha_R - \alpha)dt - b_\alpha\right]. \tag{36}$$

IV. Evolutionary Principles

In contrast to the traditional optimization approaches, evolutionary algorithms (EA) operate over a population of candidate solutions rather than over a single case, with the candidate solutions encoded into chromosomes. Every new population is created by the means of reproduction, which performs the selection of chromosomes according to their suitability to represent a solution to a given problem. This ability is expressed by a fitness function. While the genetic operators work over chromosomes, the fitness function evaluates the candidate solutions. Since the selection operator prefers more fit genomes, there is a selection pressure motivating the evolution process to provide better solutions. The selection pressure causes more fit individuals to live longer and allows them to create offspring, which inherits their genetic information.

The genetic algorithm (GA) is the most well known variant in the evolutionary approach. Genetic algorithms work with a population of candidate solutions that represent an encoded version of the solution to a given problem. The genotype of every individual in the population is initialized with random gene values. The main loop of the algorithm begins with the corresponding phenotype of every individual in the population being evaluated and given a fitness value according to how well it fulfils the problem objective or fitness function. Evaluation scores are used to describe how many samples of a particular individual are found in the "mating pool". A simple GA uses two genetic operators known as crossover and mutation.[17-19] The basic GA is depicted in Figure 5 and will be introduced to the reader in the following paragraphs.

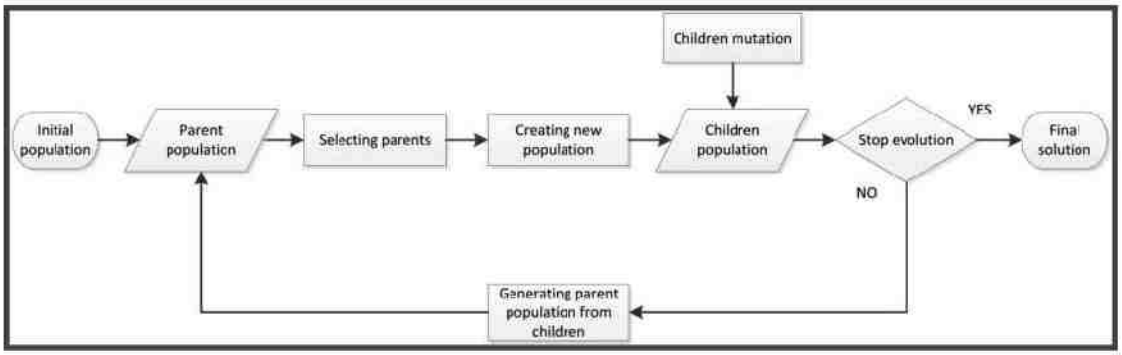

Figure 5. Basic Genetic Algorithm Block Diagram

A. Initializing Genetic Sets

The first step of the genetic algorithm is to create an initial population built from individuals with random genes. This population is in most cases represented by parameters of a function which is to be optimized. A priori information used as an initial expert guess may be used in order to reduce high computation cost and leads the genetic algorithm to an optimal solution much faster.

B. Computing Fitness Function

The fitness function represents the solution quality of every population member and its definition includes quantities, which are to be optimized. In may take a general form as its composition is related to expected limitations, interferences, behavioral trends or penalties for crossing predefined functional limits.

C. Selection of Best Parents

This operation is often simply called the selection, deriving from its biological origin in the natural selection. For the creation of a new population, individuals with a minimal fitness function value are employed in the majority of cases. Furthermore, the probability by which the individual candidate solution might become a parent according to their own fitness function can also be chosen.

D. Parents Crossover, Creating New Population

A new population is created through an interaction of parent genes chosen in the previous step. In the presented optimization framework, a mixing method has been implemented. This method uses a random part of the genotype from one parent and the rest of the genes is taken from the second parent.

E. Mutation Effects

Some genes of the population members might be affected by the so-called mutation process which modifies these genes within a scope of predefined probabilities.

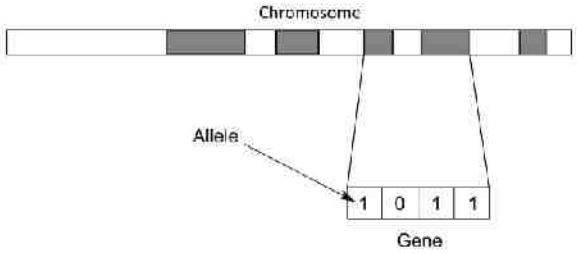

Figure 6. Binary Representation of Genetic Individual

It is possible to use any representation for the individuals in the genetic algorithm. Individuals built from strings of bits are often used, due to inherent speed and simplicity in the implement mutation and crossover processes. It is also possible to use trees, arrays, lists or any object, but it is then necessary to define genetic operators (initialization, mutation, crossover) for any representation the user decides to employ.[18] Figure 6 shows an individual with a binary array representation (i.e. chromosome). The operation of crossover and mutation are shown in Fig. 7.

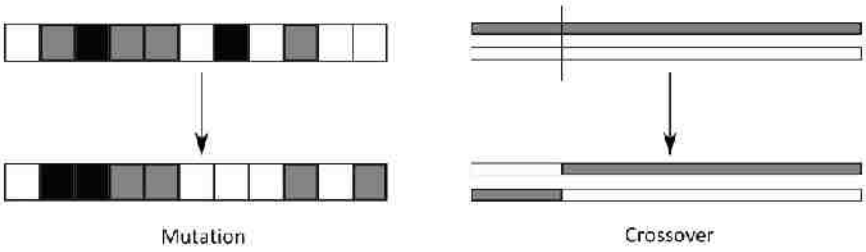

Figure 7. Genetic Mutation and Crossover

The abovementioned algorithm steps are executed until the fitness function value reaches a desired precision threshold related to a number of virtually produced generations. The implementation of the genetic algorithm includes parameters whose specification is left to the designer. These parameters include the number of initial population members, initial means and deviation of initial gains, weights of the fitness function (or a whole fitness function). Among the parameters which need to be defined is the number of chosen parents that are used for the creation of a new population, gene distribution between parents or number of children the parents can create. Almost every parameter may be affected by a predefined probability value.[19]

V. Controller Tuning

In order to define adequate controller design parameters for the implemented aerservoelastic model, a simple genetic algorithm has been employed. Each chromosome in the population contains a list of controller parameter values that needs to be identified. The goal of the genetic algorithm is to find a set of controller parameter values that fulfill some load factor step response requirements like minimal overshoot, adequate settling time and minimal steady state error. In addition, some flight qualities and control sensitivity requirements have also been taken into account. The fitness function is calculated as a weighted sum of the abovementioned quantities. The objective of the evolution driven optimization is to minimize the fitness function in order to obtain desired controller parameter values.

A. Flight Qualities and Control Sensitivity Requirements

One of the most common characteristics which describe the control sensitivity of an aircraft is the Control Anticipation Parameter (CAP). Its value characterizes aircraft controllability in longitudinal motion and is defined as the ratio of initial pitch rate acceleration to steady state value of load factor due to elevator step input.[20] To provide the pilot with a consistent „sense of control" over the entire operational flight envelope, the value of the CAP is required to remain constant. The expression used for computing the numerical value of the CAP is introduced below.

$$CAP = \frac{\dot{q}(t=0)}{n_z(t \to \infty)} = \frac{\omega_{0_{SP}}^2}{n_Z/\alpha} \tag{37}$$

The second flight quality criterion which has been employed within the controller tuning algorithm is the Gibson-Dropback Criterion (GDC) which limits the pitch rate overshoot related to an attitude dropback. The value of GDC should be kept within predefined limits to avoid unwanted aircraft behavior (e.g. Pilot Induced Oscillations).

Pitch Rate Overshoot	$\frac{q_{peak}}{q_\infty}$
Attitude Dropback	$\frac{\Delta\theta_{peak}}{q_\infty}$

Figure 8 depicts the aircraft response to a step input of the load factor n_Z. In addition to the commanded and measured load factor signals, the time response of the angle of attack α, elevator deflection η, pitch rate q and pitch angle Θ has also been included. The two subplots at the bottom contain the flight quality analysis expressed through the Gibson Dropback Criterion (GDC) and the Control Anticipation Parameter (CAP), which defines the control sensitivity of the simulated aircraft.

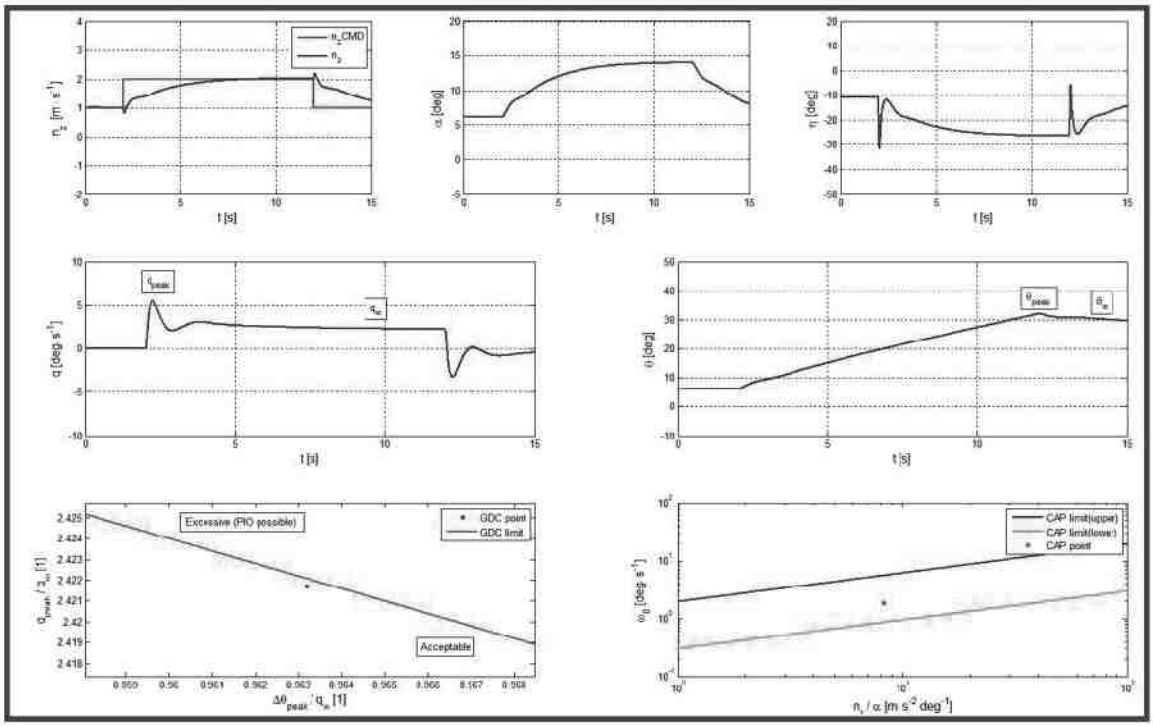

Figure 8. Ilustration of some Controller Performance Criteria (CAP, GDC)

B. Evolutionary Algorithms

A mathematical model of the aeroservoelastic problem includes a description of the longitudinal motion supported by a set of quantities related to airplane's geometrical and physical properties, unsteady aerodynamics and an atmospheric model. The controller parameter optimization routines are implemented within a tool performing the identification of optimal control parameters for the aircraft's longitudinal motion. This tool represents an application-specific software code composed in Matlab that runs the genetic algorithm routine to tune the parameters of the airplane baseline controller described by a set of physical quantities related to the longitudinal motion. The genetic algorithm searches for the optimal values of the parameters that represent a set of controller gains used for a given airplane.

The evolution starts with the initial values of the controller parameters specified in accordance with the settings from similar airplane category. The functional behavior of the observed quantities is evaluated by the main characteristics of the n_Z response, overshoot, settling time and steady state error, using a weighted sum approach which represents a fitness value for each candidate solution and is composed of a combination of controller parameters. The selection pressure leads to the optimization of the fitness values for each new generation within the genetic algorithm. If a combination of parameter values is found whose fitness value is less than a specified threshold fitness value, this parameter combination is considered being a result of the optimization process. The fitness function is defined as a weighted sum of the load factor overshoot (OVS) and of its steady state error (SSE). There are also penalization flags that should prevent unwanted system behavior (e.g. unstable system, too long or short settling time, violated CAP or GDC conditions). The implemented fitness function is shown in the following equation.

$$FF = 0{,}5 \cdot OVS + 0{,}5 \cdot SE + \left(F_{Dropback} + F_{CAP} + F_{PM} + F_{GM} + F_{ST} + F_{RT}\right) \cdot pen \tag{38}$$

Implemented penalization flags can reach values 0 or 1 (0 - the criterion is fulfilled, 1 – the criterion is violated). The sum of the penalization flags is multiplied by the penalization constant pen, which is numerically a large number.

VI. Simulation Results

This chapter presents some simulation results obtained with the implemented aeroservoelastic model. The initial section is dedicated to the implemented baseline controller performance as it contains the time evolution of rigid-body states after one of the longitudinal motion maneuvers is executed by the aircraft. At the beginning of the simulation, the aircraft is considered to be in a steady state flight condition. For this particular case, the chosen flight condition is the following: altitude of 11000ft and Ma = 0,85. All time simulation results and plots were obtained via Simulink®, a Mathworks environment. The genetic optimization routine was initialized with a set of parameters that were distributed randomly around the predefined values ($n_{z_P} = 1$, $n_{z_I} = 1$, $T_\alpha = 1$, $\alpha_P = 1$, $\alpha_I = 1$, $T_q = 1$, $q_P = 1$). The algorithm created 1000 generations of individuals within this experiment. The number of generations is a parameter subjected to change and effects the quality of system behavior and obviously the computational cost.

A. Controller for a Rigid Aircraft

Figure 9. shows the aircraft response (blue curve) to a step input of the load factor n_Z (red curve). The following subplots include responses of angle of attack α, elevator deflection η, pitch rate q and pitch angle Θ, which are important for the computation of the flight quality and control sensitivity criterions. Table 1 shows the final baseline controller gain settings and performance and stability criteria values for the rigid aircraft model. The optimization routine has tuned the baseline controller to a minimum n_Z response overshoot and static error (both under 1%), optimal settling time and passed flight quality and stability criteria. The optimization algorithm also minimized the dropback and pitch rate overshoot to avoid pilot induced oscilations (PIO).

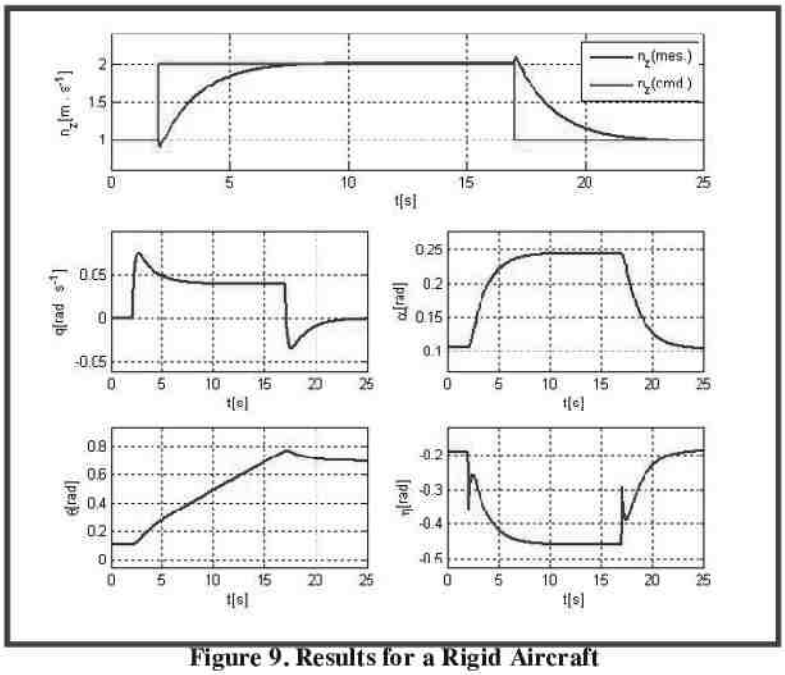

Figure 9. Results for a Rigid Aircraft

Set of Gains						
n_{z_P}	n_{z_I}	T_α	α_P	α_I	T_q	q_P
0.699	0.1078	0.363	0.338	0.0001	4.646	2.003
Stability and Performance Assessment						
Overshoot [%]	Static Error [%]	Settling Time [s]	Gain Margin [dB]	Phase Margin [°]	CAP [-]	GDC [-]
0.896	0.734	7.795	9.114	69.19	0.200	1.867

Table 1. Results for a Rigid Aircraft

B. Rigid Aircraft Controller Acting on an Elastic Aircraft

This experiment was initiated by using a set of evolutionary tuned controller parameters taken from the last optimization run and applied to the aeroservoelastic model including the aircraft elastic modes. After analyzing the simulation results, it has been found that the performance of the controller substantially degraded. The n_Z step response overshoot increased by more than 10%, similarly to the static error monitor value which shows an increase of almost 7%. Both of the evaluation quantities indicate highly undesireable behaviour. Nevertheless, the stability criterions of the gain and phase margin have been successfully met. The dynamics of the closed loop system are also very slow as the settling time reached values above 15 s . To conclude the list of monitored quantities, the pitch rate overshoot crossed the upper limit of the Gibson Dropback criterion, indicating control system's possible susceptibility to PIO.

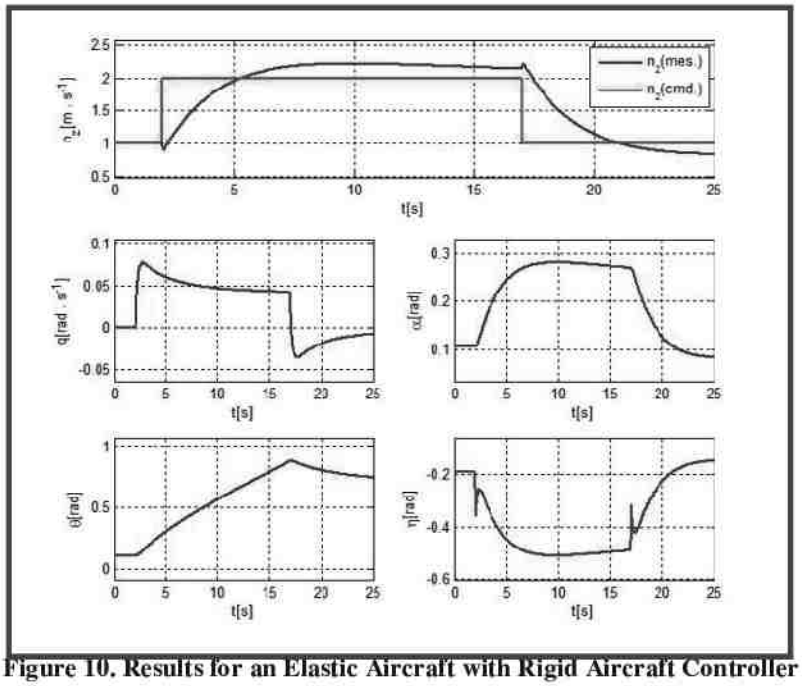

Figure 10. Results for an Elastic Aircraft with Rigid Aircraft Controller

Results in this section indicate that the controller parameter settings obtained from the evolution driven optimization on a rigid body aircraft model do not satisfy the performance criteria when directly implemented into the control system of an aeroservoelastic aircraft model. Instead of the presented non-optimal approach, the control system's internal parameters must be subjected to a new optimization run which accounts for the influences introduced throught the elastic modes of the aeroservoleastic aircraft as these modify the aircraft's dynamic response significantly.

Set of Gains						
n_{z_P}	n_{z_I}	T_α	α_P	α_I	T_q	q_P
0.699	0.1078	0.363	0.338	0.0001	4.646	2.003
Stability and Performance Assessment						
Overshoot [%]	Static Error [%]	Settling Time [s]	Gain Margin [dB]	Phase Margin [°]	CAP [-]	GDC [-]
11.50	7.584	15.16	6.199	60.43	0.188	3.120

Table 2: Results for an Elastic Aircraft with Rigid Aircraft Controller

C. Tuned Controller for an Elastic Aircraft

The concluding experiment shows some simulation results of the controller, which has been tuned for the aeroservoelastic aircraft model by the genetic algorithm introduced in chapter IV. From a performance point of view, the responses to driving manouvers identical to previous experiments indicate a siginificant improvement over the simulation results mentioned in the previous subsection. New optimization routine results have led to a modification of the baseline controller gains with a compliance to the complex cost function from equation (37). Overshoot and static error of the n_Z step response were driven close to 1% with the dropback and pitch rate overshoot which also qualified below the critical values. Detailed simulation results with a set of the tuned controller gains are shown in Fig. 11 and Table 3.

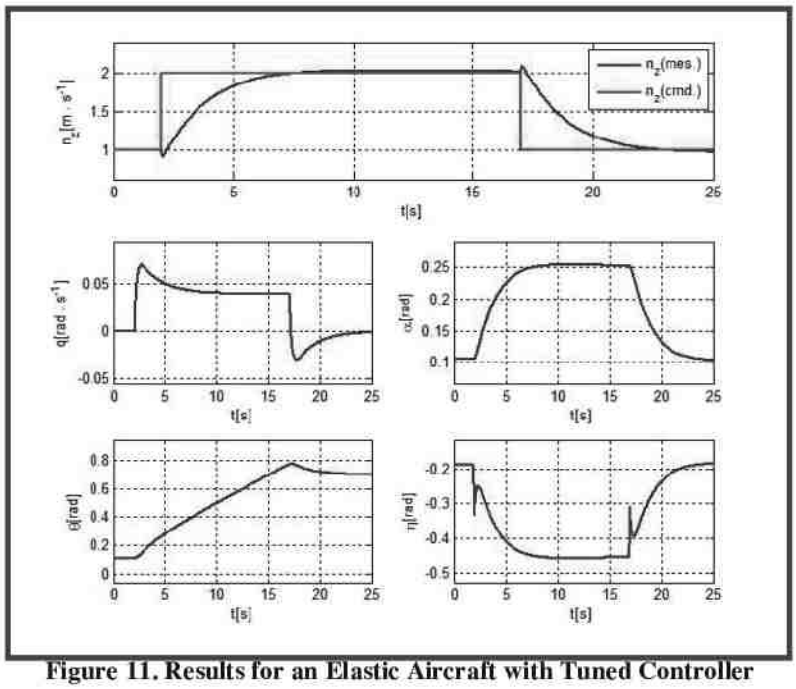

Figure 11. Results for an Elastic Aircraft with Tuned Controller

The genetic algorithm driven optimization routine shifted some of the gain values in different directions due to the changes in model dynamics introduced through the elastic states. The gains in the integral path of the n_Z and α-error controllers decreased rapidly, whereas the proportional gains of q-controller experienced an increase.

Set of Gains						
n_{z_P}	n_{z_I}	T_α	α_P	α_I	T_q	q_P
0.768	0.0001	0.321	0.165	0.0001	4.331	4.576
Stability and Performance Assessment						
Overshoot [%]	Static Error [%]	Settling Time [s]	Gain Margin [dB]	Phase Margin [°]	CAP [-]	GDC [-]
1.551	0.991	7.591	6.049	56.94	0.171	1.783

Table 3: Results for an Elastic Aircraft with Tuned Controller

VII. Conclusions

A modern controller design and optimization approach for an aeroservoelastic passenger type aircraft model has been introduced and implemented. The controller design process integrates not only an evolution driven optimization technique but also makes use of modern control design approaches as the Nonlinear Dynamic Inversion. The utilization of the NDI allowed creating a state of the art baseline control system implementation capable of handling complexities introduced through the elastic modes of an aeroservoelastic aircraft model.

The evolutionary concept played a significant role in the optimization of the proposed NDI controller structure by providing tuned controller parameters meeting the designed fitness function criteria imposed through the optimization problem formulation. The proposed fitness function combined significant controller stability evaluation criteria into a single abstraction. The suggested form of multicriterial optimization definition was allowed by using a robust optimization framework based on the genetic algorithms. A suitable combination of stability criteria with the robustness of the evolution driven algorithms enabled to propose and finetune a complex control structure of an aeroservoelastic model of a large passenger aircraft. The suitability of the evolutionary optimization was successfully tested on a set of examples, which accounted for rigid body aircraft dynamics as well as the case with elastic structural modes. The results of the presented simulations unveiled the expected differences among optimization results for a rigid aircraft and its elastic counterpart. The evolutionary optimization tool was able to handle both type of aircraft models and made the controller parameters to comply with the designed fitness function. To demonstrate the limited suitability of migrating the controller setup optimized for a rigid body aircraft model to its aeroservoelastic relative, an experiment has been proposed, results of which are presented within the paper. The direct migration of non-optimized controller settings showed to violate the designed fitness function and proved to be inferior to the controllers' whose stability has been directly influenced by the optimization process. Further development should account for hardware accelerated genetic optimization algorithm with real-time auto-tuning capability of an aircraft control system.

Acknowledgments

This work has been supported by the European Regional Development Fund in the IT4Innovations Centre of Excellence project (CZ.1.05/1.1.00/ 02.0070), by the Technology Agency of the Czech Republic research project "Smart Autopilot" TACR TA01010678, by the Clean Sky JTI research project "PALAST" Call Identifier JTI-CS-2010-5-SFWA-01-031 (Project Number 287020), and by the DAAD/MSMT project 7AMB12DE004.

References

[1]Marinus, B.G., *Influence of Parameterization and Optimization Method on the Optimum Airfoil*, ICAS 2010, Nice, France, 2010.

[2]Benini, E., Ponza, R., Massaro, A., *High-Lift Multi-Element Airfoil Shape and Setting Optimization Using Multi-Objective Evolutionary Algorithms*, Journal of Aircraft, Vol. 48, No. 2, 2011.

[3]Chen, P. C., Lee, H. W., *Unsteady Subsonic Aerodynamics for Bodies and Wings with External Stores Including Wake Effect*, Journal of Aircraft, Vol. 30, No. 5, 1993.

[4]Harder, R. L., Desmaris, R. N., *Interpolation Using Surface Splines*, Journal of Aircraft, Vol. 9, 1972.

[5]Karpel, M., *Design for Active and Passive Flutter Suppression and Gust Alleviation*, Technical Report CR-3482. NASA, 1981.

[6]Scholz, D., *Berechnung Maximal Erforderlicher Stellgeschwindigkeiten von Steuerflächen*, DGLR-JT97-083, Munich, Germany, 1997.

[7]Lewis, B. L., Stevens, F. L., *Aircraft Control and Simulation*, John Wiley & Sons, 1992.

[8]Etkin, B., Reid, L. D., *Dynamics of Flight: Stability and Control*, John Wiley & Sons, 1995.

[9]Hodges, D. H., Pierce, G. A., *Introduction to Structural Dynamics and Aeroelasticity*, Cambdrige University Press, 2002.

[10]Slotine, J. J. E., Li, W., *Applied Nonlinear Control*, Prentice Hall, 1991.

[11]Isidori, A., *Nonlinear Control Systems*, Springer, 1995.

[12]Leitao, M., Peter, F., Holzapfel, F., *Adaptive Augmentation of a Fighter Aircraft Autopilot Using a Nonlinear Reference Model*, CEAS EuroGNC Conference, Delft, The Netherlands, 2013.

[13]Peter, F., Leitao, M., Holzapfel, F., *Adaptive Augmentation of a New Baseline Control Architecture for Tail-Controlled Missiles Using a Nonlinear Reference Model*, AIAA Guidance, Navigation and Control Conference, Minneapolis, 2012.

[14]Holzapfel, F., *Nichtlineare Adaptive Regelung eines unbemannten Fluggerätes*, PhD Thesis. München, Germany, 2004.

[15]Bugaski, D. J., Enns, D. F. Elgersma, M. R., *A Dynamic Inversion Based Control with Application to the F-18 HARV*, Proceedings of the AIAA Guidance, Navigation and Control Conference, Portland, 1990.

[16]Johnson, E. N., Calise, A. J., *Pseudo-Control Hedging: A New Method for Adaptive Control*, Advances in Navigation Guidance and Control Technology Workshop, Redstone Arsenal, 2000.

[17]Back, T., *Evolutionary Algorithms in Theory and Practice*, 2nd ed., Oxford University Press, New York, 1996.

[18]Rothlauf, F., *Representation for Genetic and Evolutionary Algorithms*, 2nd ed., Springer-Verlag, Berlin, 2006.

[19]Crina, G., Ajith, A., Hisao, I., *Hybrid Evolutionary Algorithms*, Springer, Berlin, 2007.
[20]Department of Defense, *MIL-F-8785C Flying Qualities of Piloted Airplanes*, Military Specification, Washington, 1980.

INTENTIONALLY LEFT BLANK

Safety enhanced digital flight control system

Peter Chudý
Department of Computer Graphics and Multimedia, Faculty of Information Technology,
Brno University of Technology, Brno, Czech Republic, and

Andrzej Tomczyk and Pawel Rzucidlo
Department of Avionics and Control Systems, Faculty of Mechanical Engineering and Aeronautics,
Rzeszow University of Technology, Rzeszow, Poland

Abstract
Purpose – The purpose of this paper is to describe the general idea, design, and implementation of control system for general aviation aircraft which reduces pilot workload.
Design/methodology/approach – Proposed indirect flight control system framework is intended to simplify piloting, reduce pilot workload, and allow low-end general aviation aircraft to operate under deteriorated meteorological conditions. Classical control theory is used for the design of the flight control laws. Although not inherently robust, controllers with classical control logic are made sufficiently stable using a correct and updated controller structure.
Findings – Despite controversies between perception of a modern manned aerial vehicle and limitations imposed by legacy airworthiness codes it is shown that a pilot workload reducing system can be successfully implemented onboard of a low-end general aviation aircraft.
Research limitations/implications – Hi-level control laws and optimization of handling qualities can lead to unfavourable and unpredictable forms of man-machine interactions, e.g. pilot-induced oscillations.
Practical implications – General aviation aircraft are mostly flown by a single pilot, who could benefit from an intelligent system or "virtual copilot" assisting in or supervising the aircraft's safe operation under any conditions. Aircraft with this capability represents a next step in the evolution that might ultimately lead to trajectory-based free-flight concept of aircraft operations.
Originality/value – The paper introduces a safety enhanced digital flight control system on board small general aviation aircraft.

Keywords Safety measures, Flight control, Control systems, Aircraft

Paper type Research paper

1. Introduction

For decades, general aviation (as all noncommercial, nonmilitary flying is officially categorized) has been hampered by the expense and time required to get a pilot's license and the instrument rating required for flight in less-than-ideal weather. The complexity of operating and navigating a high-performance light-plane, and the dangers posed by weather, mechanical problems, and inevitable pilot carelessness pave a logical frame for a pilot workload reducing system.

Indirect flight control system (IFCS) allows utilization of complex and highly sophisticated functions aimed at increasing the flight safety and performance. IFCS represents a control technology that transforms a simplistic control surface commanding into a sophisticated motion control process. The anticipated future growth of the general aviation market arises from the social needs for individual transportation. IFCS provides the essential ingredient for delivering an easier to handle, safer, operationally attractive and environmentally friendly airplane to the general aviation industry. NASA research programs such as the Advanced General Aviation Transportation Experiment – AGATE and Small Aircraft Transportation System – SATS predicted significant growth potential for a future airborne transportation system capable of flexible point-to-point deliveries (AGATE, 2008; SATS, 2008).

IFCS, also known as fly by wire (FBW), originated in the "analog" military application traced back to the WWII Mistel Project (Tomayko, 2000). The perception of the FBW technology as a simple extension of an autopilot is generally misleading and underestimates its full potential. Even the simplest FBW system replaces the mechanical signaling of the control surface actuators by electronic signaling with little or no control augmentation. By comparison, the high-end FBW schemes include augmented control design that requires utilization of inertial and air data sensors, onboard computers, flight software, high speed data-buses and their respective interfaces. Modern digital flight control technologies greatly improve handling qualities and flight safety compared to the even best naturally stable, non-control system augmented, aircraft designs.

The current issue and full text archive of this journal is available at
www.emeraldinsight.com/1748-8842.htm

Aircraft Engineering and Aerospace Technology: An International Journal
81/5 (2009) 416–423
 [ISSN 1748-8842]
[DOI 10.1108/00022660910983699]

This work has been supported by the "Security-Oriented Research in Information Technology" research project CEZ MŠMT, MSM 0021630528 and the "Development of the Indirect Control System for Handling Qualities Shaping of General Aviation Aircraft" financed partly by The Polish State Committee for Scientific Research in the years 2003-2006. The authors would like to thank them for their financial support.

2. Digital flight control strategy

There are several key advantages leading to a successful implementation of a IFCS strategy. IFCS offers an optimization of aerodynamic performance, and a reduction in maintenance and flight crew training requirements by providing unified flight decks, automated and instantly accurate handling qualities tuning, and a host of flight safety enhancements. The last mentioned area represents a substantial advantage in relieving crew workload. By providing integrated protection against exceeding airspeed and aircraft attitude limits, for example, the digital flight control system (DFCS) implementation reduces the risk of an inadvertent control loss due to pilot error or environmental conditions. Installation of an electronic control system directly promotes a synergistic process of avionics system integration. Of course, IFCS must maintain aircraft's basic handling characteristics and flight envelope protection features, in order to avoid the need for costly retraining and possible pilots' errors in the unlikely event of platform failures.

The main advantage of a DFCS is the ability to influence the flight characteristics at every point of the flight envelope using appropriate flight control laws. Utilization of a DFCS allows implementation of complex algorithms, capable of modifying the inherent dynamic behavior, suppressing turbulence effects, and resulting in increased passenger and pilot comfort throughout the flight. Flight envelope protection is an important feature of IFCS allowing full and even extreme control inputs without the danger of violating the aircraft's inherent control limits or structural overload. Overall, safety improvements primarily due to reducing a pilot's routine operational workload demands create concomitant benefits of allowing more time for pilot awareness of often neglected navigational and other cockpit management tasks (Lambregts, 2005). Digital flight control allows quick and flexible implementation of configuration changes and has significant potential for further development. An interesting aspect of the IFCS is the ability to reduce direct operating costs due to system's high reliability and resulting low-maintenance features.

3. System architecture

A sophisticated FBW control design can be seen as an automatic control system with specialized input devices in the form of pilot's control inceptors. To take maximum advantage of ever changing state of the art hardware and software technologies, considerations must be given to the system architecture's functional design. Simplicity often results into safety enhancements based on the wildly held premise: "What isn't present can't fail".

Initial analog electronic devices and mechanical instruments technological limitations have been overcome by high speed and safe digital data processing technologies integrated within state of the art avionic systems. Basic research for development of requested functional design changes not only overcame the identified insufficiencies in the previous systems, but also led to resultant technologies with better functional integration characteristics that naturally include flight envelope protection and elimination of excessive complexity. These technologies continue to evolve for these reasons into safer and more efficient flight control designs.

A. Identified key requirements for a IFCS

- *Operational reliability and safety.* This requires utilizing automated onboard air space separation logic with a real time health monitoring capability, implying efficient emergency diagnostics and in-flight software supported reconfiguration capability.
- *Carefree handling.* This requires easy handling in all operational flight modes and under any weather conditions (manual, automated air traffic management), supported by a human centered cockpit design with ergonomic displays and controls.
- *Environment friendly.* This requires an optimized aircraft design featuring advanced lightweight structural design, stability and control, and advanced aerodynamics. Optimization of aircraft operations consequently results in reduction of perceived noise levels and emission concentrations by allowing flexible flight path definition.
- *Economy of scale.* This requires the affordability of commercially available components manufactured in large numbers, which meet strict aviation regulation requirements and allow for efficient utilization of resources (e.g. maintenance, installation, etc.).

Future operations in high-traffic density flight areas require advances in air traffic management (ATM). This encourages a substitution of the state of the art tactical instructions issued by air traffic controllers with an autonomous trajectory-based ATM environment. Carefree handling is considered to be a key attribute of the IFCS framework. A majority of general aviation aircraft are being operated under the private operator's rules generally known as FAR Part 91. The accident rate in this specific segment has achieved a level that is approximately 25 times higher then general aviation fleet operated in accordance with commercial airliners standards. The higher safety level in the later case, however, is not without significant cost. The reduced accident rate seems more a function of increased operational complexity and a requirement for highly qualified pilots and maintenance staff than many other factors which makes transferring this same standard globally to general aviation aircraft, *ipso facto*, economically prohibitive.

Another important dimension of IFCS is closely related to the concept of flight training. Examples from the commercial airline industry show improved safety and efficiency records as a result of, among other factors, complex avionic systems implementation. These are, however, prone to sudden failure which oftentimes results in performance degradation. Various failure scenarios are thus periodically exercised and simulated as a part of ongoing pilot training. The concept of system integrity, or lack thereof, however, strongly flies in the face of the requirement for a carefree handling. An airborne system dedicated to individual point to point deliveries simply cannot exhibit or be prone to significant changes in handling characteristics when operating in emergency modes. The development of simpler and better integrated system designs that are generic in architectural structure, in future aircraft development projects would lead to remarkable cost reductions. These reductions would come from a myriad of areas, including the lower procurement cost of stand alone flight control system and time penalties associated with overall system design process. Figure 1 shows the overall system architecture of a compact DFCS IFCS. At the core of the depicted system is a precise and accessible instrumentation and sensors (global positioning system – GPS, inertial

Figure 1 General structure of IFCS architecture

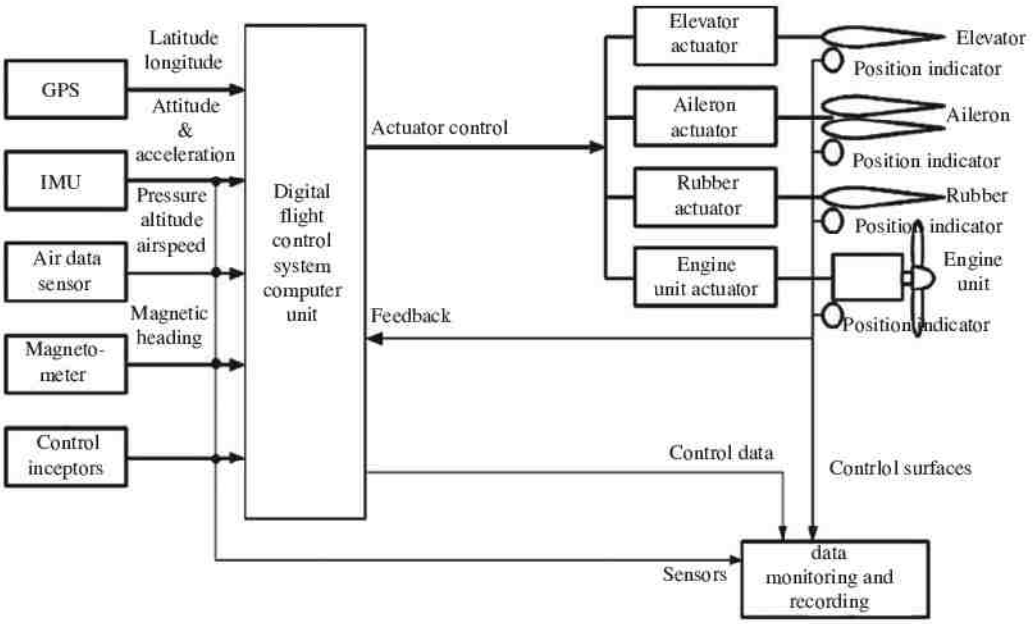

measurement unit, and Air Data Computer – ADC). The computer platform processes the input data from these sensors and, in accordance with predefined flight control laws imbedded in its software algorithms, initiates control inputs activating electromechanical actuators operating control surfaces, high-lift devices, and thrust unit settings.

4. Controller design

The design approach adopted within this framework is based on the classical control theory, which uses feedback of measurable variables fed to the controllers based on proportional, integral and derivative gains tuned to obtain the required performance characteristics. The method, however, is not inherently robust. Many different operating conditions need to be simulated and iteratively adjusted in order to achieve desired level of robustness. Classical control methods were the only methods available for many years. Their use within the aviation industry includes applications, such as piloted flight control, autopilot, and auto-stabilization units in the form of pitch and yaw dampers. The main advantage of this design methodology is that it has been well proven and a large amount of knowledge exists about its actual implementation (McRuer *et al.*, 1990). The principal disadvantage is the large amount of prior knowledge concerning the operational characteristics of the controlled system. The techniques used in the design process generally require knowledge of a system (linear) parameters model at a given operating point together with the input variables used to generate the required outputs. For a system whose behavior is well understood, the methodology is quite suitable an efficient. As the system's complexity grows and becomes more dynamic in nature, however, you begin to experience a fair degree of uncertainty in its application. For an aircraft application, the required inputs are the principal control surfaces (elevator, ailerons, and rudder), supplemented with the engine controls.

By linearising the aircraft model in steady and level flight, the longitudinal and lateral equations of motions can be decoupled in a convenient way for use independently in the design process. For each aircraft model component, the inner loops are designed first using linear analysis, primarily using robustness, comfort, and performance criteria. The controller's inner and outer loops can thus be split into longitudinal and lateral ones with no interaction between the two. The inner loops are used to provide the necessary stability augmentation while the outer loops regulate the augmented aircraft's flight path performance.

5. Simulation

Simulation plays a key role in facilitating the effects of control parameter variations during the DFCS controller design procedures. Linear simulations are used as a starting base within the initial design stages, subsequently followed by the full non-linear simulations dedicated to "fine tuning" the system and providing the controller's final check. A block diagram of a simulation system is depicted in Figure 2. The intention of this procedure is to prove that the controller's performance in the non-linear domain exhibits an acceptable behavior, which is in accordance with declared design goals. Pilot's inceptors used for a simulation process feature joystick, rudder pedals, and a thrust lever. Simulation of the surrounding environment, atmospheric models, aircraft's

Figure 2 Simulation scheme

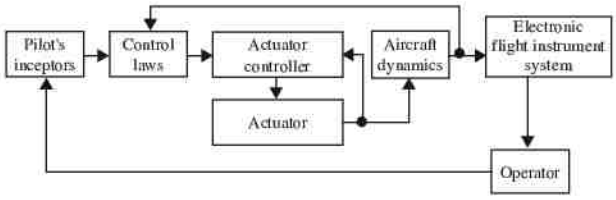

Aircraft Engineering and Aerospace Technology: An International Journal
Volume 81 · Number 5 · 2009 · 416–423

dynamic model, and actuator controllers run as routines on the main simulator computer, connected to an electronic flight deck simulator and an actuator model representing a real aircraft's installed unit. This configuration allows for analyses of the investigated system in both manual and automatic mode of operation. Simulations can show, for example, whether a particular controller change affects the ride quality. This effect can be achieved and manipulated by careful selection and alternation of system variables. The principal emphasis of the simulation is to justify designers' satisfaction with desired controller robustness criteria. A trade off between robustness, comfort and performance results in controller settings which exhibit acceptable overall balance.

6. Experimental IFCS design

Even FBW is a popular and an extensively used term addressing physical dimension of its implementation; "indirect flight control system" describes more precisely the intended mode of aircraft control where the pilot commands an aircraft implicitly via an onboard computer system. An IFCS serves primarily the purpose of shaping the control properties of an aircraft regardless of its natural responses. The aircraft is thus virtually automatically controlled, with the pilot entering desired flight parameters to the system's control computers by means of control inceptor displacements.

The main goal of the IFCS project was to improve flight safety through active adjustments in handling qualities of general aviation aircraft, by making use of an intuitively ergonomic flight control system. Future IFCS equipped aircraft will originate into a new general aviation class that targets improved safety and operational efficiency – safe flying airplane or facilitated airplane – FA (Tomczyk, 2004).

Indirect flight control system

The basic idea of the project was to employ an indirect software-based flight control system characterized by a high degree of integrated automation, leading to a safe and pilot friendly general aviation aircraft. The indirect control methodology does not eliminate a human pilot from the control loop, just alters its role to a flying platform manager. User-friendly control system affects the handling qualities of an aircraft in a way that flight control becomes more intuitive and flying safer. Pilot retains the critical role of a decision maker, while the control system performs sequences of control tasks to execute pilot's intentions, or suggests an optimal method of implementing his decisions. IFCS, frequently perceived as a virtual copilot/assistant, integrates simplified aircraft handling with autopilot functions, and reduces the complexity of interactions in flight regimes. Its flight envelope protection feature monitors aircraft configurations, attitudes and power settings, and assists avoiding an "unintentional" loss of control. General functional properties of the proposed system have been presented at the SAE/AIAA World Aviation Congress, Los Angeles, CA, 1998 (Tomczyk, 1999). The main functional characteristics of the system are best described by a continuous stabilization of attitude orientation of an aircraft and guidance (for example, flight along a selected path at constant altitude). The pilot can influence the flight state at any moment by displacing the side-stick (SI) for a manual control following the general rule: if pilot does not take any action (SI in neutral placement), the preplanned flight plan is executed, or, previous safe flight conditions are maintained.

A closer description of the experimental IFCS is presented in Figure 3. The system relies on three independent flight control computers (CC-x) that control redundant electromechanical actuators. During a flight, pilot selects a control option (control mode) using a control mode selector panel and then controls the aircraft with a SI and throttle lever.

The main sources of information related to aircraft's attitude come from the attitude and heading reference systems (AHRS). Flow field related parameters are measured and interpreted by ADC. Low cost ADC and two versions of AHRS (one based on a fiber optic gyro, the other on MEMS technology) were used for the design and installation of the IFCS. Navigation system consisted of an integrated receiver GNS-530 (GPS, VOR, ILS and COMM) and backup receiver GPS-35. This combination assured proper navigation and created a basis for future instrument-assisted landing trials. "Other measurements" present remaining sensors and systems, including engine monitoring instrumentation. Functional core elements were installed in a double pack in order to achieve system's desired hardware redundancy. Integration of the system was established by a triple digital, low cost, bi-directional databus network CAN-2 (CAN1H – high-speed bus, CAN2L and CANL3 – low speed, higher reliability buses) which connected all system elements with the control computers. A direct mechanical linkage was applied for an emergency control of the engine. In a case of the experimental system malfunction, if all three controlling computers or all three CAN-2 network lines fail, or a total malfunction of the ADC/AHRS occurs, an emergency direct control of actuators via independent pulse-width modulation (PWM) signaling (PWM line) generated in the SI module enables sufficient maneuvering capability to provide time and space for a safe deployment of an onboard rescue parachute system. This feature was implemented due to the experimental/risky nature of the project and would be disabled in future fully operational versions of the IFCS. The described IFCS experimental installation featured a maintenance computer, which has been connected to the system to complete the maintenance tasks, testing or adjustments of the system.

Since future operations of IFCS rely heavily on a high degree of operational reliability, diagnostic systems that monitor and evaluate IFCS's health have been developed and further refined based on the flight test evaluations.

The method for controlling the experimental installation of IFCS was determined on the basis of rules established for the following control complexity levels:

- *Normal control.* All features of the IFCS are employed and work flawlessly.
- *Emergency control.* Displacement of aerodynamic control surfaces directly proportional to the SI displacement.

A change of control level would be reported by an onboard diagnostic system if imperfect operations of crucial elements of control system emerge. Emergency control in the experimental version of the IFCS was intended to be used in emergency cases only, for reaching a safe area where parachute rescue device could be activated.

Figure 3 Structure of the experimental IFCS

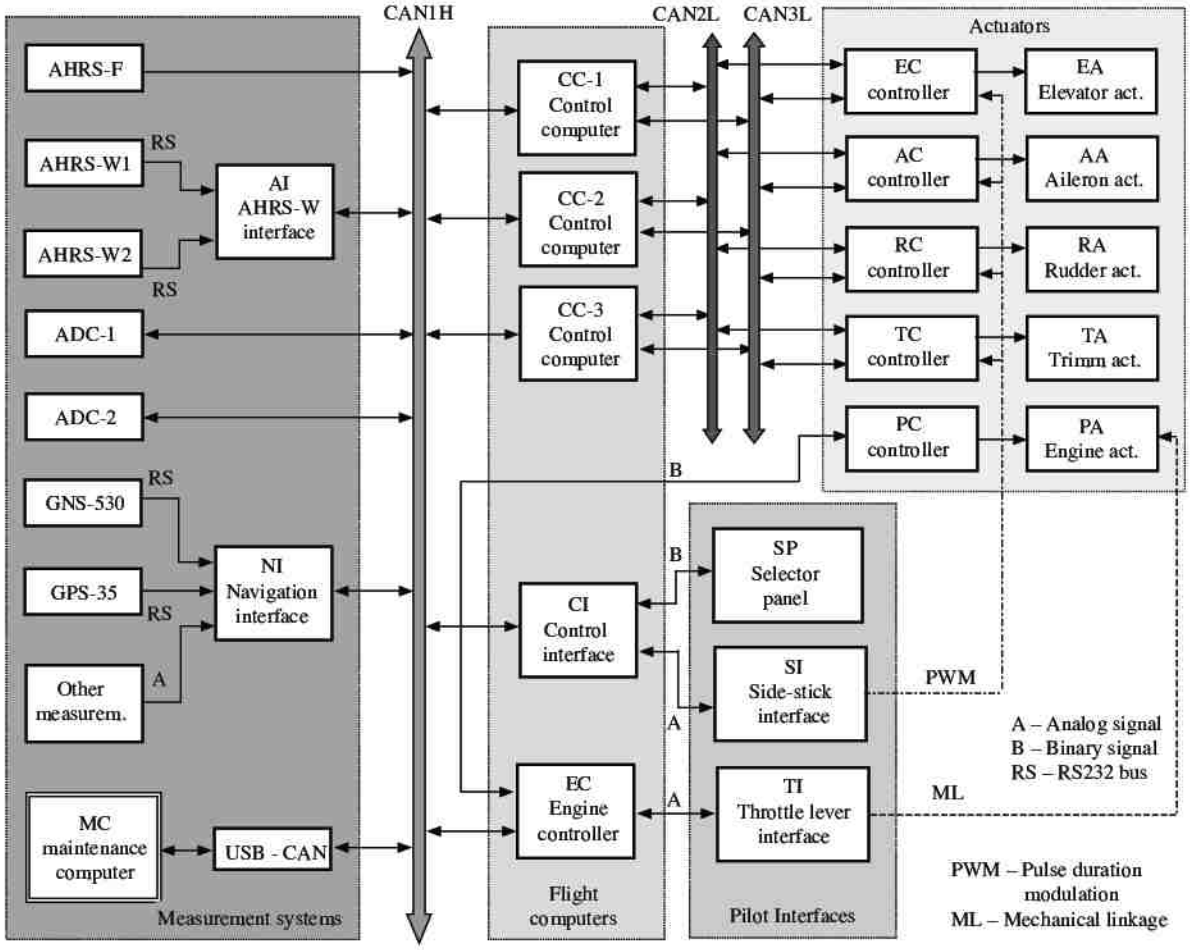

7. IFCS technology demonstrator

An experimental IFCS was designed, built, and tested (Figures 4 and 5). All basic modules of the system were designed by the research team, build and pre-tested in laboratory conditions. The proposed control laws were initially verified in a flight simulation experiment before their actual implementation onboard of the PZL-110 test aircraft. A highly challenging concept related to the IFCS is the pilot induced oscillations (PIO) phenomena. The results obtained from the PIO detector show no PIO tendency in

Figure 4 Test platform PZL-110 "Koliber" aircraft; preparation to in-flight tests (left), and cockpit (right)

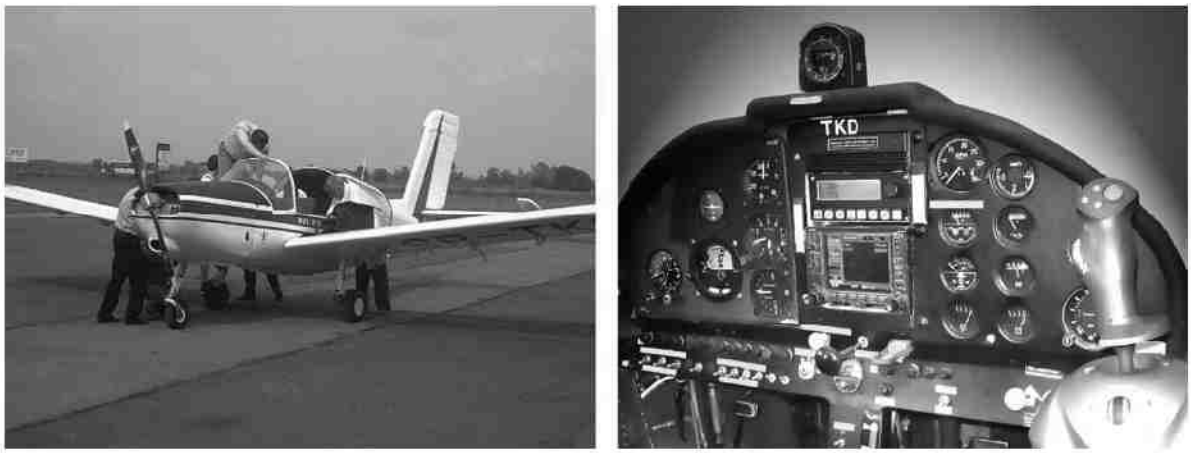

Figure 5 VUT-100 Cobra Aircraft (left) and twin-engine EM-11 Orka aircraft

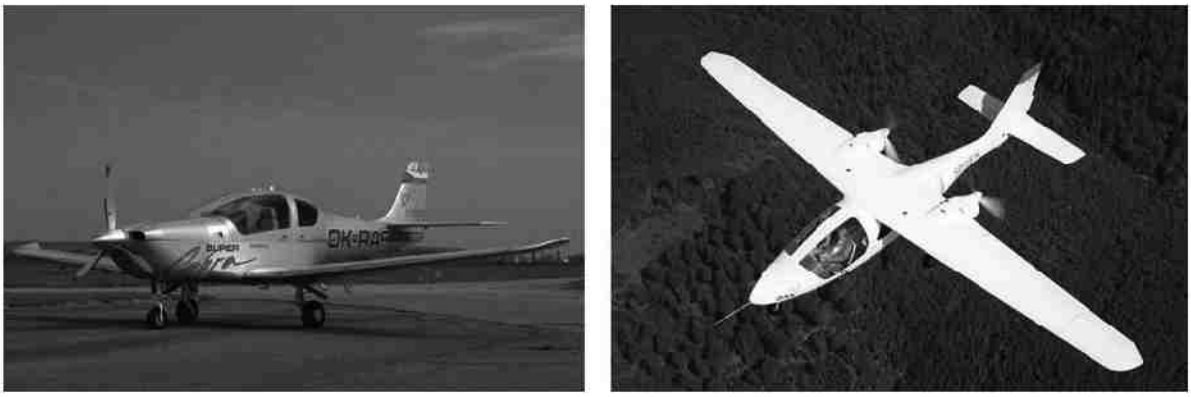

longitudinal motion during simulations of the experimental aircraft. Results of analytical criteria, which enable prediction of susceptibility to oscillations in general aviation aircraft, ground simulation-based experiments and flight tests, have been the subject of previous research (Rzucidlo, 2006).

Successful hardware implementation of indirect flight control design led to series of flight tests (Tomczyk, 2004). Emergency direct flight control mode has been thoroughly examined during the initial test flights and reportedly found to be difficult to cope with. Even unpleasant for regular flight operation, the emergency mode provided for extra "flyable" time for eventual safe activation of parachute rescue system. The normal flight mode, due to its automatic aircraft attitude stabilization features, provided the pilots with a comfortable flight experience.

Exemplary in-flight test results of IFCS are presented in Figures 6 and 7. Objectives of presented experiments were stabilization of roll and pitch angles. Manual mode allows pilots a safe and direct control in emergency situations. Flight control computers (FCCs), digital data buses and measurement units are being bypassed in this particular mode. Control signal is transmitted directly from SI (without response shaping), through PWM signals to the actuators. It is obvious that manual stabilization of the flight regime is possible, but requires effort some piloting skills resulting in a higher cockpit workload (Figure 6). Left chart presents measurements obtained from AHRS whereas SI deflections responsible for longitudinal (dh_s) and lateral (dl_s) motion are presented in right chart.

Normal mode enables a carefree control of the aircraft. Control signals are shaped and processed in the FCCs. It can be seen (Figure 7) that pitch and roll stabilization process is more precise and pilot is less engaged in control (mild longitudinal and lateral motions of SI). Between 1,000 and 1,100 s two "peaks" can be observed in left chart of Figure 7. The first peak was induced by an intentional disturbance (fast and wide motion of SI), the later peak was caused by a superposition of atmospheric gust and release of SI.

Significant PIO were not observed during flight tests so far, but that does not mean that the aircraft is PIO free. The power of actuators installed onboard the PZL-110 was insufficient, especially during aggressive maneuvers. An aircraft equipped with a powerful actuation system can be much more susceptible to this phenomenon in some cases (possibility of rapid maneuvers) and can be resistant to some forms of PIO on the other hand (better man-machine coupling). The flight envelope of the experimental PZL-110

Figure 6 Pitch and roll stabilization in emergency control

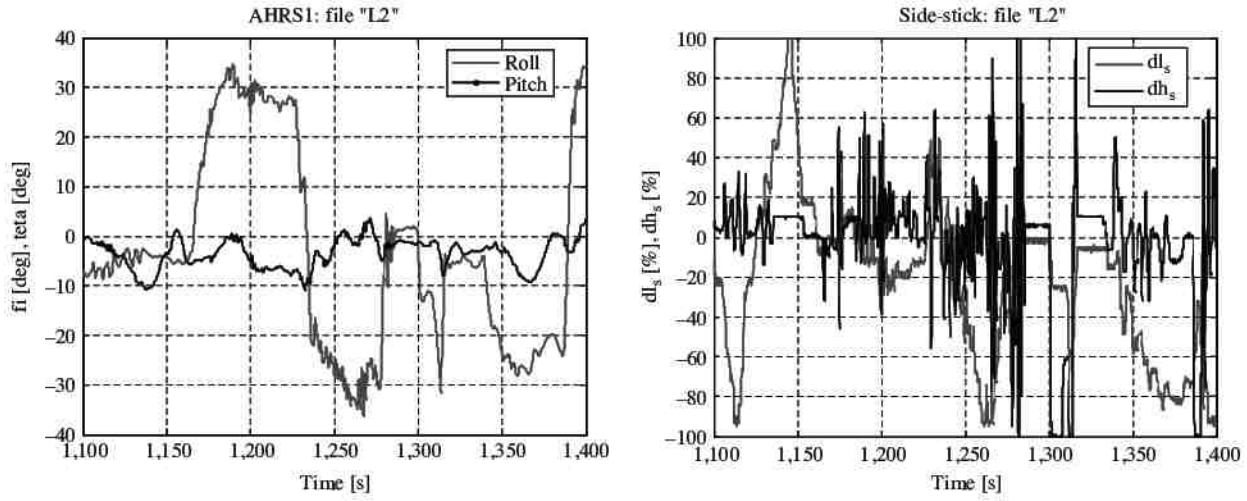

Figure 7 Pitch and roll stabilization in normal mode

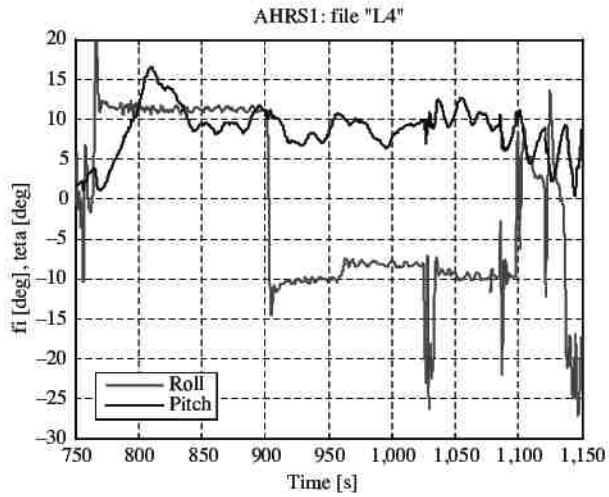

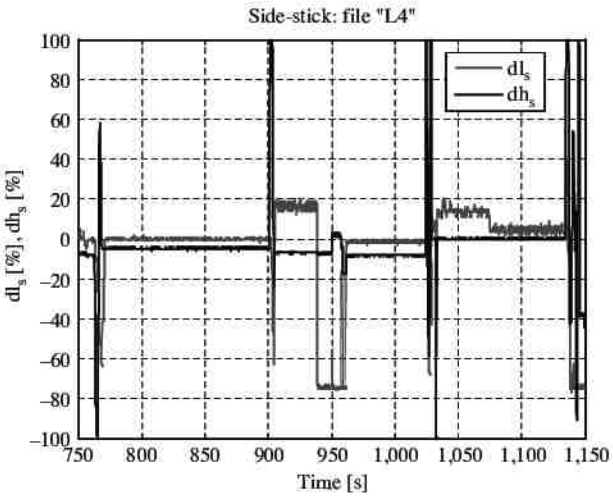

aircraft was limited for the obvious reason of safety. All tests were conducted in the summer and autumn seasons only. Flights were also limited because of economic reasons. It was practically impossible to test the control system under all possible flight conditions, system configurations, trigger events, and human behavior.

Results of performed flight tests confirmed simulation-based estimates. Rather high expenses for the flight tests caused, that only the main properties of the flight control system were in-flight verified. More sophisticated experiments using a modified flight simulator Alsim AL-200 multi-crew cooperation, routinely used for pilots training at Rzeszow University of Technology (RUT), are currently being formalized. Evaluations of control law designs for different aircraft as Socata TB-20 Trinidad, Piper Seneca II, or Beech King Air 200 will provide an additional verification capability.

Experiments show a positive role of human-aiding automation in introducing safe single-crew flight operations. Presented research addresses recommendations related to new types of pilot training and certification procedures as a result of emerging requirements on new types of piloting skills. A new version of IFCS is evaluated for a future application onboard of the VUT 100 Cobra and EM-11 Orka, which are currently being certified by the aviation authorities.

8. Conclusions

IFCS must maintain intended aircraft's handling characteristics and flight envelope protection features in order to avoid costly retraining demand and possible pilot errors in the unlikely event of platform failures. Introducing a safety enhanced DFCS into general aviation industry justifies the innovative idea of light aircraft flight envelope protection. This framework addresses reduction of pilot error induced accidents caused by loss of situational awareness and unintended stalls and spins resulting there from.

Classical control methods are most commonly used in aerospace applications. Although not inherently robust, controllers with classical control logic can be made sufficiently stable using a correct and updated controller structure. These deterministic structures are analyzable and also convenient for certification processes. The relatively low number of components makes failure assessment and testing a straightforward task. The principal disadvantage of classical control approaches is the time required to perform the overall design process. If an outline design is at hand, this time can be dramatically reduced. In order to support the design procedure, however, a significant amount of knowledge concerning the particular aircraft and its characteristics is required. Transition from mechanical to DFCSs is an evolutionary and qualitative improvement from designing simple systems to designing systems that are safe and highly economical across a myriad of general aviation aircraft platforms. A system's functional degradation in handling qualities is simply an unacceptable simplification of the design task.

References

AGATE (2008), Advanced General Aviation Transport Experiment, available at: www.nasa.gov/centers/langley/news/factsheets/AGATE.html (accessed July 18, 2008)

Lambregts, A.A. (2005), "Fundamentals of fly-by-wire augmented manual control", SAE 2005-01-3419, Society of Automotive Engineering, Warrendale, PA.

McRuer, D., Ashkenas, I. and Graham, D. (1990), *Aircraft Dynamics and Automatic Control*, Princeton University Press, Princeton, NJ.

Rzucidlo, P. (2006), "Laboratory and preliminary in-flight tests of electromechanical actuators", SAE Paper 2006-01-2414.

SATS (2008), Small Aircraft Transportation System, available at: www.nasa.gov/lb/vision/earth/improvingflight/sats_danville.html (accessed June 10, 2008)

Tomayko, J.E. (2000), "Computers take flight", available at: www.nasa.gov/centers/dryden/pdf/182985main_DFBW_rev1.pdf (accessed June 8, 2008)

Tomczyk, A. (1999), "Concept for simplified control of general aviation aircraft", paper presented at the 1998 World Aviation Conference, Anaheim, CA, SAE/AIAA Paper No 985551, *SAE 1988 Transactions, Journal of Aerospace*.

Tomczyk, A. (2004), "Facilitated airplane – project and preliminary in-flight experiments", *Aerospace Science and Technology*, Vol. 8 No. 6, pp. 469-77.

Further reading

Etkin, B. and Reid, L.D. (1996), *Dynamics of Flight – Stability and Control*, Wiley, New York, NY.

Hodgkinson, J. (1999), "Aircraft handling qualities", *AIAA Education Series*, American Institute of Aeronautics and Astronautics, Reston, VA.

McCormick, B.W. (1995), *Aerodynamics, Aeronautics, and Flight Mechanics*, 2nd ed., Wiley, New York, NY.

Rzucidlo, P. and Tomczyk, A. (2008), "Prediction of susceptibility of small aircraft to pilot-induced oscilations", *SAE Transactions: Journal of Aerospace*, SAE Paper 2007-01-3804.

About the authors

Peter Chudý received his MSc in 2001 and PhD in 2004 from Faculty of Mechanical Engineering, Brno University of Technology. His specializations are aeroelasticty and computational flight dynamics. He is a Researcher and Lecturer at Brno University of Technology since 2004. His research interests are modeling and simulation of flight dynamics, and DFCSs. He is the author of over 20 scientific papers and conference proceedings. Peter Chudý is the corresponding author and can be contacted at: chudyp@fit.vutbr.cz

Andrzej Tomczyk received his MSc degree in 1970 from Faculty of Mechanics and Thermal Engineering, Warsaw University of Technology, Degree of Doctor of Technical Sciences in 1976 from the Institute of Fundamental Technical Research of the Polish Academy of Sciences, and in 2000 he received his DSc degree from Military Academy of Technology, Warsaw. He has been working at the Rzeszow University of Technology (RUT) since 1976 and conducting research and design work connected with the synthesis of manual (SAS and CAS), automatic (autopilot) flight control systems, and fly-by-wire control system for executive airplanes. He has published over 90 papers in scientific journals and conference proceedings, and he is the author of two books, and co-author of three patents in the area of aeronautics. He is a member of American Institute of Aeronautics and Astronautics since 2001.

Pawel Rzucidlo received his MSc in 2001 and PhD in 2005 from Faculty of Mechanical Engineering and Aeronautics, RUT. His specialization is aircraft control systems. He is a Researcher and Lecturer at RUT since 2001. His research interests are aircraft control with an emphasis on interactions between human and machine. He is the author of over 30 scientific papers and conference proceedings and author of one book.

Simulation and prototyping of FCS for sport aircraft

Karol Rydlo
Brno University of Technology, Brno, Czech Republic

Pawel Rzucidlo
Rzeszow University of Technology, Rzeszow, Poland, and

Peter Chudy
Brno University of Technology, Brno, Czech Republic

Abstract

Purpose – The presented paper aims to describe the general idea, simulations and prototyping process of an assisting flight control system (FCS) for light sport aircraft (LSA). The proposed FCS framework is intended to simplify piloting, reduce pilot workload, and improve system's reliability and handling qualities of manual flying.

Design/methodology/approach – Assisting flight control strategy integrates mechanical and digital FCS into a synergic platform, combining the high reliability of mechanical controls with the computation and actuation power introduced through a single line digital FCS. Concepts drawn from classical control theory along with flight envelope protection algorithms have been used throughout the design of the flight control laws. A prototype of the assisting FCS has been subjected to validation trials during series of hardware-in-the-loop simulations.

Findings – Despite controversies between the pilots' perception of a modern aircraft and limitations imposed by the legacy airworthiness codes, it has been shown that a pilot assisting and workload reducing control system can be successfully implemented on board of a LSA while satisfying the expectations on a state-of-the-art equipment meeting required level of safety defined by the current legislation.

Research limitations/implications – A transition between specific flight modes as well as nonlinearities in the FCS may lead to unfavorable and unpredictable forms of aircraft-pilot interactions. The number of accessible flight control modes should be therefore limited to the most significant ones.

Practical implications – Sport aircraft are mostly flown by a single pilot, who could benefit from the pilot assisting FCS as the system has the potential to supervise the aircraft's safe operation in various flight conditions.

Originality/value – Introducing an assisting FCS on board of a LSA through an innovative approach which utilizes hidden and unused resources of modern digital automatic FCSs while respecting the limitations imposed through the weight and cost sensitive nature of the LSA market.

Keywords Assisting flight control system, Hardware-in-the-loop, Light sport aircraft, Prototyping, Simulations

Paper type Research paper

Nomenclature

Definitions, acronyms and abbreviations

ADC = Air data computer
AGL = Above ground level
AHRS = Attitude heading and reference system
ALT = Altitude
ATC = Air traffic control
CAN = Control area network
CTRL = Controller
EFIS = Electronic flight instrument system
EM = Electro-mechanical
FCC = Flight control computer
FCS = Flight control system
FMS = Flight management system
GPS = Ground positioning system
HDG = Heading
HIL = Hardware in the loop
HLD = Hold
IAS = Indicated airspeed
LSA = Light sport aircraft
MSL = Mean sea level
NAV = Navigational
PFD = Primary flight display
TRK = Track
VFR = Visual flight rules
VS = Vertical speed

Introduction

Introducing aircraft categories intended solely for private use and individual operations revitalized the light aviation market and opened it to a new class of customers. Piloting an aircraft is a demanding task, where a safe execution of flight requires a constant mental effort. This effect is magnified by the

The current issue and full text archive of this journal is available at **www.emeraldinsight.com/1748-8842.htm**

Aircraft Engineering and Aerospace Technology: An International Journal
85/6 (2013) 475–486

[ISSN 1748-8842]
[DOI 10.1108/AEAT-10-2012-0186]

Received: 29 October 2012
Revised: 13 March 2013
Accepted: 1 January 2013

Aircraft Engineering and Aerospace Technology: An International Journal
Volume 85 · Number 6 · 2013 · 475–486

operational experience of dangers associated with inadequate piloting skills and insufficiencies in pilot training. Improvements in this matter have been rather gradual thanks to trainers with exceptional stick and rudder skills passing these on to new pilots. Safety enhancing avionics equipment has been introduced through technological innovations flowing from proven "good enough" solutions. Innovations in avionics integrated dispersed indicators on the instrument panel with a virtual/synthetic terrain and intuitive guidance cues. Nevertheless, even the increase in pilot's situational awareness, achieved through the integration, has not eliminated the danger of entering an unsafe flight regime (McRuer *et al.*, 1997; Stanton *et al.*, 2001). An inspiration to overcome the effects associated with pilots' fatigue, unfavorable stress reactions or a low level of flying skills may come from high workload cockpits equipped with an advanced digital flight control technology (Carter and Stoliker, 2000; Stachowiak and Bosworth, 2004; Bauer *et al.*, 2007). Nevertheless, the fly-by-wire FCSs with an active flight envelope protection utilized onboard of the state of the art military and transport aircraft are complex technological products with a narrow downscaling potential into the price sensitive market of light sport or general aviation (Tomczyk, 2004). The required level of redundancy and physical dimensions of a full fly-by-wire installation are explainable for large aircraft designs, but are cost prohibitive solutions with a substantial weight penalty considering the operational concept of sport and leisure flying.

Even the light aircraft community does not speak the same language of safety. On one hand, there is a logical motivation for a continuous production of nonaugmented aircraft with a direct mechanical FCS, which by many opinions provides the pilot with the unique sport experience the community promotes, on the other hand, is the previously stated attitude that distracts potential new buyers who are looking for a safe point-to-point delivery platform.

Assisting FCS

Principles

An assisting FCS combines the industry accepted solutions in mechanical flight controls, automated flight and digital avionics with three fundamental modes of operation: free manual flight, active pilot's assistant and an autopilot. This is achieved through a parallel integration of the electromechanical actuation units to the primary mechanical FCS, including an auto-throttle system (Chudy *et al.*, 2009). General structure of proposed control system is shown in Figure 1. The presented approach enables an intermediate step of an assistant mode, which provides the pilot with a sufficient authority to execute a manual flight while introducing tactile cues to the mechanical controls by means of the electromechanical actuators. From a user experience level, the pilot is provided with a feedback she/he is familiar with since the training days with a flight instructor. One of the vital parts of the system is the correct definition of the supported flight modes and their interpretation by the onboard automation.

The design on the CTRL structure uses the stability evaluation principles know from the classical control theory. Hence the phase and gain margins may be estimated based on the tools available for the linear, time invariant systems. Other criteria, known as the settling time, control anticipation parameter, etc. have been used for the CTRL tuning and optimization.

Active pilot's assistant mode

Active pilot's assistant is introduced by the control strategy which interacts with the pilot when she or he attempts to exceed predefined limits. The FCS remains in a standby mode when the actual flight parameters remain within the intended design margins. Exceeding at least one the design limits activates the FCS which in turn engages the dedicated actuators and/or the auto-throttle (Figure 2).

In the scenario described above, the FCS behaves as a virtual flight instructor, leaving the pilot with an option to adjust to the cues generated by the active virtual assistant in order to execute the flight within the safe flight envelope or to disregard the automated advices. Throughout the entire duration of the flight, it is the pilot who has the final authority to overdrive the tactile cues generated by the FCS or to disable the active assistant at every moment of the pilotage. The assisting mode was designed with the capability to advise the pilot to maintain the monitored flight parameters within predefined limits, but was not intended to provide for a safe aircraft recovery from an unusual attitude. Limits protected during the assisted flights are following:

- IAS: 80-105 kts.
- ALT: not less than 1,000 ft AGL and not more than 10,000 ft.
- VS: min. −900, max. 900 ft min^{-1}.
- Bank angle: min. −30, max. 30°.
- Pitch angle: min. −15, max. 10°.
- Pitch rate: max. 10°s^{-1}.
- Roll rate: max. 10°s^{-1}.

CTRL blocks of active pilot's assistant mode detect, when defined limits of particular flight parameters are being exceeded and thereafter enable the actuation system. The identification of the actuation initiation is executed through the implemented dead zone blocks, which activate the EM actuators (clutches) along with PID CTRLs that generate control signals for particular actuators. Electromechanical actuators are disengaged when flight parameters fall back into predefined boundaries.

Autopilot mode

The implemented control logic draws upon the assumptions and considerations described in the following section. The FCC, a balanced set of sensors, data communication network and user interface elements (flight displays) are operational in every control mode as opposed to the electromechanical actuators and the autopilot panel which remain inactive during the unassisted free manual flight. While being in the manual flight regime, the control surface actuators, as well as the auto-throttle module are disengaged at all time as opposed to the autopilot mode with the EMAs working continuously. The scheme of the digital autopilot includes a control system block with the autopilot flight control laws based on the classical control theory (Etkin and Reid, 1996). Control algorithms designed for the digital FCS are grouped into three formal levels: inner loop, outer loop, and navigation and flight management as shown in Figure 3. The inner loop is responsible for the stabilization of basic flight parameters, such as the pitch and bank angle, indicated air speed (IAS) as well as for the turn coordination and side-slip compensation. Part of the inner loop includes the pitch force CTRL (pitch force CTRL) that is designed to reduce the force/moment loading at the elevator's EMA stepper motor through the

Figure 1 General structure of the assisting FCS

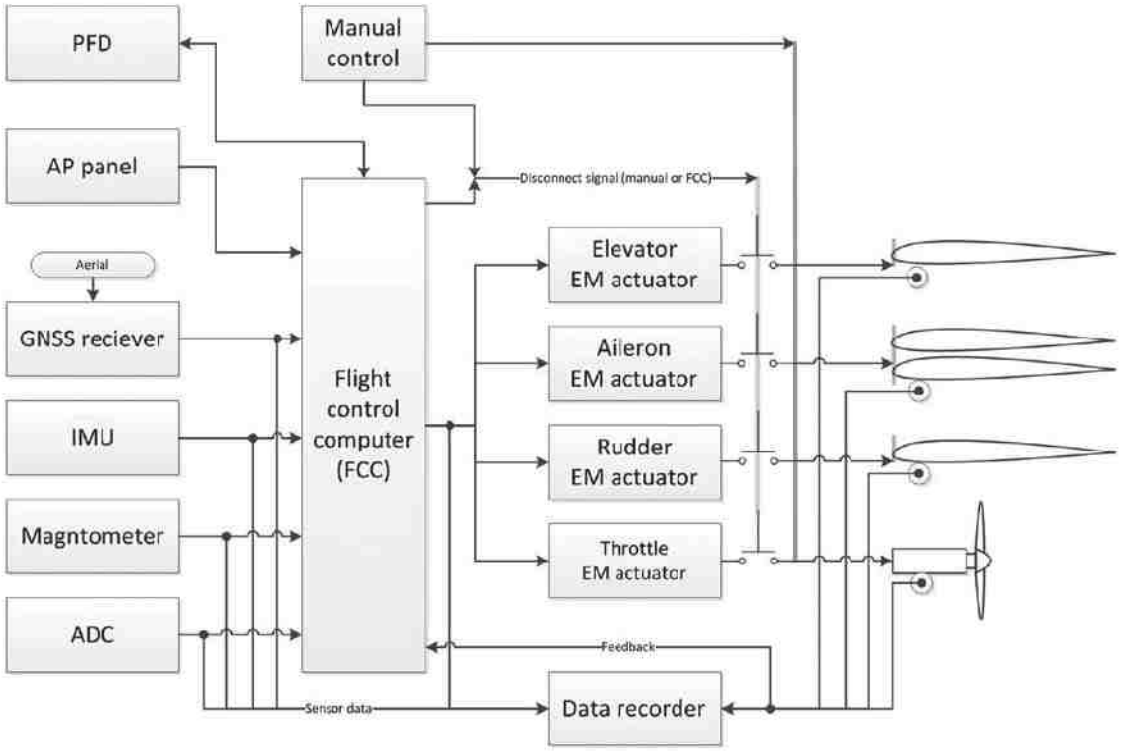

setting of the longitudinal trim. The pitch CTRL takes into account the cross-feedbacks from the roll and airspeed stabilization loops. Similarly, the IAS CTRL uses the cross-feedback from the pitch channel. The outer loop layout consists of three CTRLs arranged in two separate channels: vertical speed (VS) and ALT in the longitudinal motion, heading and track (HDG/TRK) in lateral motion. In the navigation mode the HDG/TRK CTRL stabilizes the ground track. In the manual mode, the pilot can select stabilization of the ground track or magnetic heading. The ALT CTRL stabilizes the ALT. The pilot may select required VS in both manual and automatic navigation modes. The NAV CTRL block is responsible for the horizontal and vertical navigation on particular air route sections. The FMS block manages specific sections defined by a set of waypoints.

CTRL blocks of the autopilot mode contain modified PID CTRLs which include variable gains in the proportional paths and account for the saturation of integrators. The cross-couplings from pitch, roll and IAS in the inner loops are executed within the proportional blocks. Rate limiting elements on the inputs of the selected CTRLs (pitch, roll) reduce their rapid responses. Saturation blocks limit the inputs and outputs of the inner loop CTRLs as well as the input of the vertical speed CTRL in the outer loop.

Compliance with legislation

Considering the relatively high accident rate in the amateur flying a rationale for a pilot assisting tool remains an attractive approach to alleviate the effects of insufficiencies in training, limited experience and unintentional flight into adverse weather conditions. Even the LSA category revitalized the new aircraft market through the introduction of attractive and easy to operate products supported by a favourable legislation, the safety aspects remained unchanged. Considering the FAA requirements and respective ASTM standards (ASTM F2245-11) for the LSA designs, following conclusions affecting the architecture of the assisting FCS may be drawn:

- Having a digital FCS as a parallel implementation to the primary flight control structure does not jeopardize the overall reliability of the system as the electromechanical actuators may be disabled/disengaged or overdriven by the pilot.
- The EFIS infrastructure is extended to an automatic flight executable level by the inclusion of electromechanical actuation of control surfaces and throttle.
- As the LSA are operated mostly under the day/night VFR rules, the level of sophistication/redundancy of the sensor, computational and actuation units may be kept within the scope of a simplex system.

Therefore, the FCS was designed as a single line system without additional redundancy and parallelism considerations. These assumptions were derived from the user case definition, assuming a support of VFR operations only and including a manual override capability as similar logic have been applied to successfully marketed LSA autopilot designs. The envelope protection zone was intentionally "limited" so the pilots are assisted throughout a typical touring/cross-country flying and the on-board installation does not call for a bulky actuation system, with a redundant disconnect capability.

The targeted application segment does not require the designers to show compliance with the certification standards typical for FAR part 23 aircraft. Nevertheless, best practices

Figure 2 The control scheme for an active pilot's assistant mode

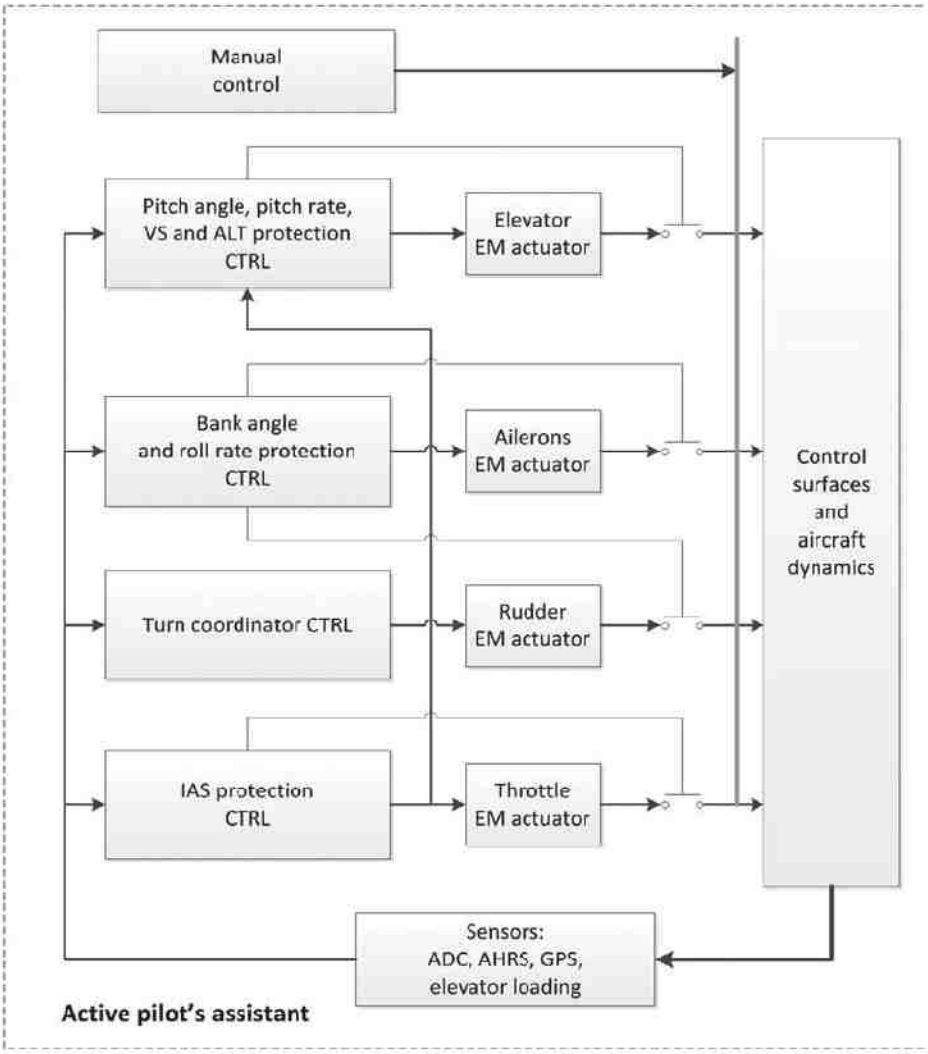

drawn from MISRA C, C++, RTCA-DO178, ARP 4754 are implemented into the coding process and are used by the authors throughout their work.

Prototyping of system components

Control algorithms

Complete algorithms for the control, navigation and flight management have been implemented within a real-time rapid prototyping environment and depending on the selected mode, emulate following configurations:

- manually controlled mechanical FCS;
- mechanical system controlled by an autopilot; and
- active pilot's assistant (assisted control).

The rapid-prototyping environment featured a set of standard I/O interfaces. Hardware as well as software layers of inputs and outputs were compatible with the prototyped autopilot module. This solution enabled convenient modifications to the real-time rapid prototyping environment and prototyped autopilot hardware within the flight simulator environment.

Autopilot mode selection panel

The autopilot mode selection panel shown in Figure 4 is a peripheral device primarily intended for light aircraft installations. The implemented functional logic allows for the selection and setting of flight parameters needed for a successful execution of an automatic flight. The panel's hardware includes a microcontroller of the MC9S08 family, LED displays, switches, rotary encoders and CAN drivers. Selectable parameters include IAS, ALT/ALT HLD (ALT hold), VS, HDG or TRK (course/track). The remaining options feature the activation of the auto-throttle and the autopilot control modes. The values of airspeed IAS are displayed in knots [kts] with the initial value set to 80 kts, as demonstrated following the panel activation. The chosen value respects the selectable min/max airspeed limits as implemented within the autopilot flight control laws. For steady horizontal flights in clean configuration, the recommended max. selectable airspeed is limited to a value of 105 kts. To account for the uncertainties and nonlinearities in the system's description, a 10 percent safety margin was included into the < min.; max. > IAS limits.

Figure 3 Control scheme of the autopilot mode

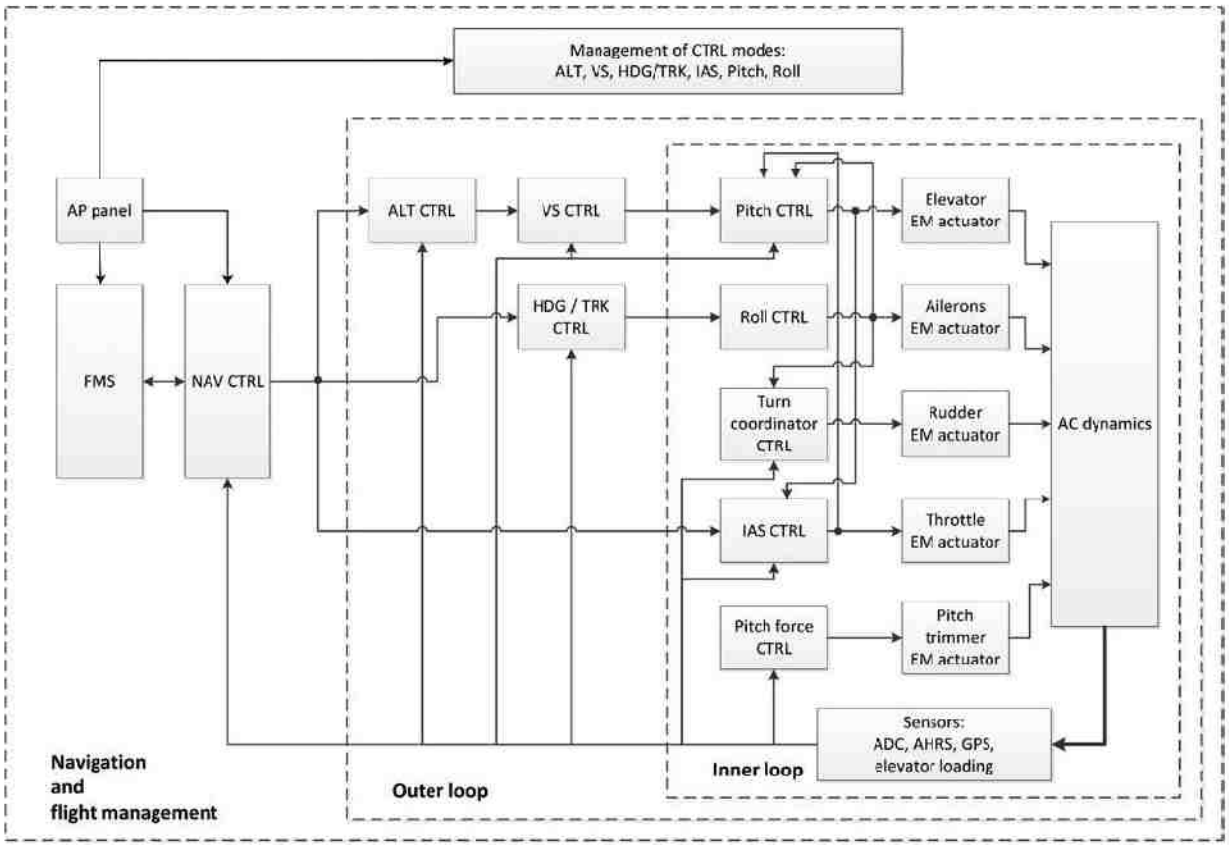

Figure 4 Autopilot mode selection panel (left) and panel's schematics

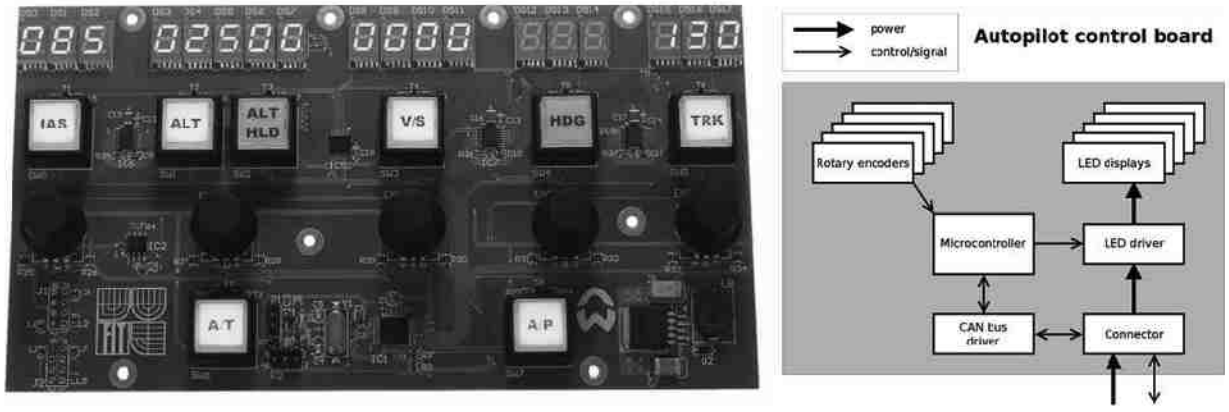

The next selectable value is the ALT displayed in feet. The initial ALT value was pre-set by design to 2,000 ft, with a minimum operationally safe ALT being limited to 1,000 ft above the ground level (AGL) and max. ceiling of 10,000 ft. The ALT selector/encoder was configured to operate with an ALT increment of 100 ft. The value of the vertical speed was also subjected to limitations arising from the dynamics of the flying system to a safe envelope of $< -900, 900 >$ ft min^{-1}. The VS increment reflects the operational experience and has a value of 100 ft min^{-1}. The remaining navigation quantities operated via the mode selection panel are HDG and TRK, whose initial values after the activation were defined to be 0°. The full scope of the selectable values for both cases covers the interval $< 0°, 359° >$, with an increment of 1°.

Flight displays

A state-of-the-art light aircraft instrument panel typically features a "glass-cockpit" installation with a host of backup analogue instruments. Advances in electronics, software design, accessibility of sophisticated testing tools and market availability of new avionics made the integrated flight displays

Aircraft Engineering and Aerospace Technology: An International Journal
Volume 85 · Number 6 · 2013 · 475–486

suitable for a larger scale implementation. Figure 5 shows an intuitive PFD installed into the SimStar's flight deck (Chudy *et al.*, 2010).

The flight displays are typically used for a compact and intuitive visualization of flight related quantities as previously done in an isolated fashion by the means of individual analogue instruments (Popelka and Paces, 2012). This assumption indicates the amount of data that need to be processed by the PFD's processor unit in order to allow the software application to generate an intuitive representation of the aircraft state. A PFD typically presents the measured values of airspeed (IAS), ALT, vertical speed (VS), pitch and roll angles, HDG and GPS related navigation data presented in the form of a synthetic terrain or a moving 3D map. Further display enhancements include data related to the on-board power network, propulsion quantities and the flight control unit's status reports.

The designed system features a direct implementation of a terrain database with the option of the database being further improved and updated. The AGL ALT is calculated using the digital terrain model and the outputs from a GNSS receiver (GPS + GLONASS) equipped with EGNOS corrections. The preselected safe minimal AGL value accounts for the possible imperfections in the vertical position estimates and the quality of the terrain data. The inclusion of additional sensors would lead to an additional complexity and cost penalty, which could render the system implementation cost prohibitive.

Electromechanical actuators

Implemented electromechanical actuators use the CANaerospace communication protocol as an interface to the FCS. The mechanical implementation of the electromechanical actuators includes a stepper motor with a custom built gearbox and an optional electromagnetic clutch. The control board electronics consists of a COTS microcontroller, stepper motor driver, galvanically isolated CAN driver, switch and high precision rotary potentiometer serving as a source of angular position information.

The configuration shown in Figure 6 was used throughout the design, implementation and verification phase of the actuation units. The potentiometer used as a source of feedback signal is not shown. A physical implementation of the CTRL and feedback structure was introduced to actuators serving the primary flight control surfaces (elevator, aileron, rudder) and an auto-throttle unit attached to the propulsion system. The actuator operating the elevator trim tab was not physically included into the HIL simulation, but was substituted by a virtual model.

HIL experiments

SimStar lab

The transition from mathematical abstraction of an assisting FCS to a rapid prototyping and experimental flight testing environment should allow for a pilot and hardware-in-the loop simulations on a suitably adapted ground-based flight simulator (Rogalski *et al.*, 2009). Modifying a state-of-the-art certified professional flight simulators is a feasible option, but at the same time a challenging task considering the number of difficulties related to the simulator's withdrawal from the training process, loss of product certificate, potential violations of proprietary data protocols, differing hardware standards, etc. A more flexible and accessible solution is to utilize a purposely built experimental simulation equipment. This proposed solution has been achieved in a light aircraft simulation lab designed and built at Brno University of Technology (Chudy *et al.*, 2010). The simulation framework of this lab accommodates different simulation modes, from commercial products to hand coded simulation and control software.

The SimStar is a light aircraft flight simulator based on the cockpit section of an Evektor SportStar (Figure 7) and equipped with SportStar's 6 DOF nonlinear dynamic model (Evektor-Aerotechnik, 2009). Due to the simulator's open architecture and its built-in hardware-in-the-loop capability, experimental hardware may be integrated and tested within the SimStar. The application of CAN network and CANaero communication protocol (Stock, 2006), allows this solution to be compatible and open to other on-board systems. SimStar thus enables HIL simulations of hardware units equipped with suitable CAN CTRLs (Chudy and Rzucidlo, 2012). The simulator's architecture also supports data recording that is primarily used to store the time histories of simulated flights. The HIL simulation environment integrates peripheral

Figure 5 SimStar's cockpit section (left) and schematics of PFD

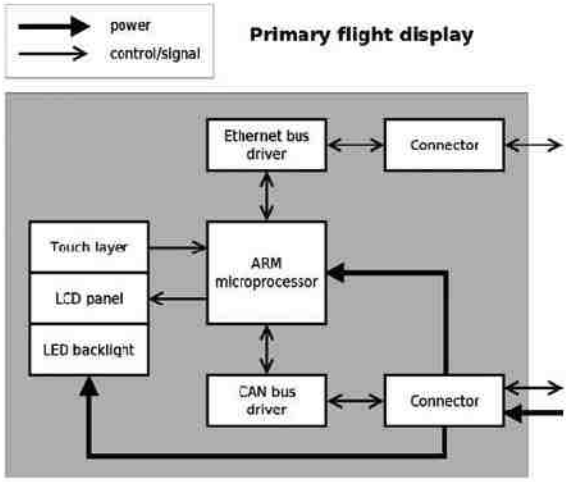

Figure 6 Actuator equipped with a controller (left) and its schematics

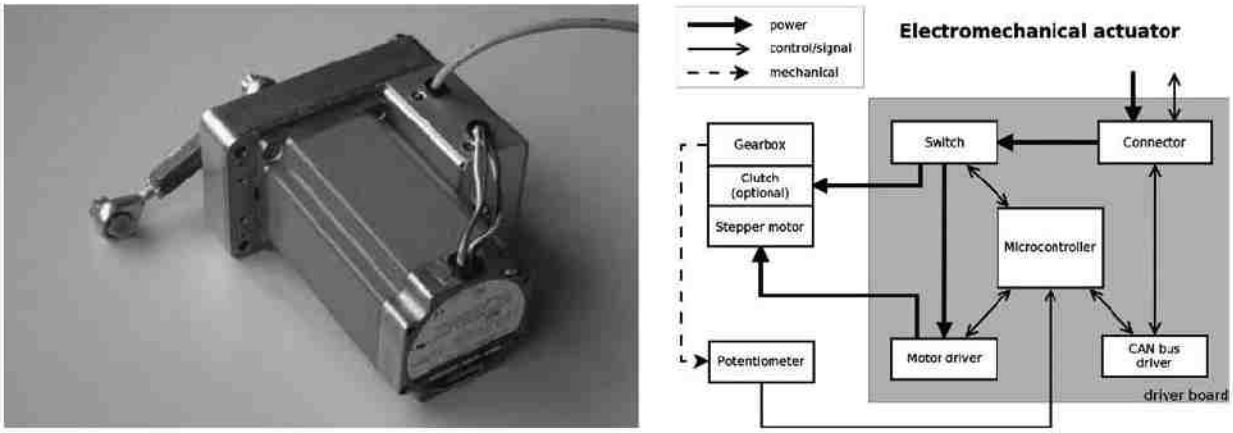

Figure 7 SimStar's cockpit section (left) and the lab during a flight simulation

devices connected to the simulation network through the CANaerospace protocol as shown in Figure 8.

The dynamic model used for the simulations was extracted from a series of flight experiments performed on an Evektor SportStar experimental aircraft equipped with a laboratory grade data acquisition system. Measured data were subjected to the parameter identification procedure, results of which were integrated into a nonlinear aircraft model structure.

Figure 8 SimStar's HIL architecture with functional blocks

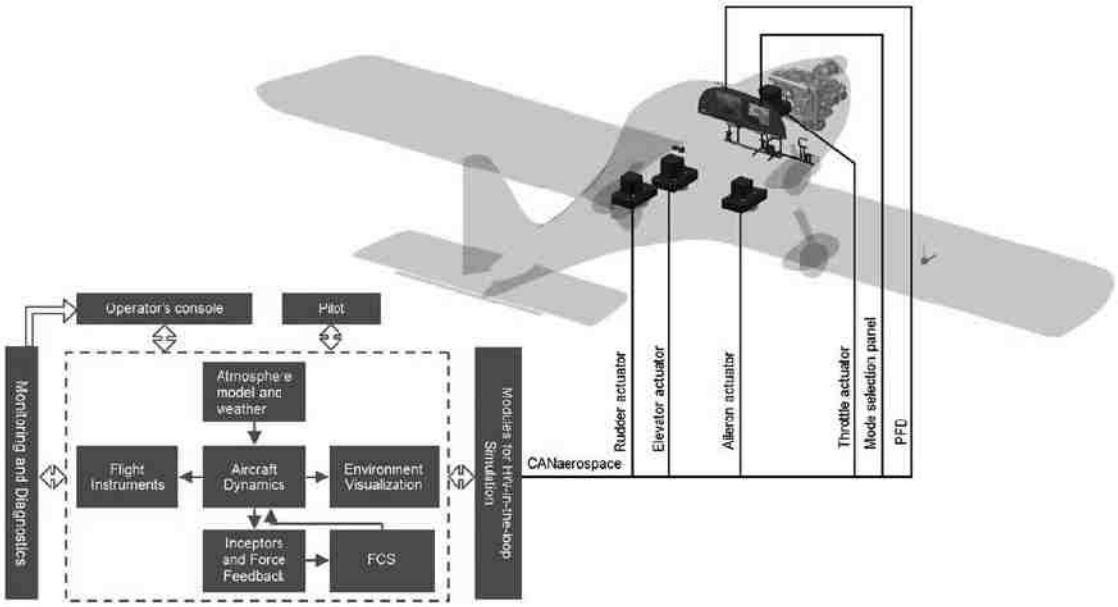

Aircraft Engineering and Aerospace Technology: An International Journal
Volume 85 · Number 6 · 2013 · 475–486

The identification was concluded by the model quality assurance process. Based on the initially drawn assumptions of the flight envelope margins, the model included basic stall and spin characteristics as post stall and spin recovery tasks were not primarily addressed in the research.

Active pilot's assistant – results of selected experiments

The pilot in the loop simulations of the assistant mode have been performed in the area of EPRZ airport (Figure 9). The flight plan assumed a manual take-off and subsequent climbing to 3,000 ft MSL. After passing the 1,000 ft AGL mark, the pilot changed the control mode to the "virtual assistant". First section of the simulated route was executed as a typical cross-country flight. After passing the first waypoint, the pilot was instructed to test particular limits of the envelope protection. Performed test included listed manoeuvres:

- turn right and next turn left with maximal attainable bank angle;
- descending and climbing with maximal attainable pitch angle;
- rapid roll (roll rate limit test);
- rapid pitch manoeuvre (pitch rate test);
- combinations of turning and climbing (test of mixed limits);
- steady descend and climb (test of VS limit); and
- full and idle throttle in horizontal flight and at various combinations of turning/climbing (test of IAS protection).

After the tests of the flight envelope protection the pilot initiated an approach to EPRZ airport, with the flight assistant mode being switched off after passing the last waypoint. The simulated flights have been performed in calm air conditions as well as in the presence of moderate turbulence. Figure 10 shows the recorded MSL and AGL ALT during the simulation runs. As shown in the figure, the pilot attempts to overcome the protected 1,000 [ft] AGL level in flight no 1 between the timestamps 1,200-1,400 s. In the other cases, the flights have been performed over the threshold of the protected level. Achieved bank and pitch angles are presented in Figures 11 and 12, with haptic cue activations indicated by the red dash-dotted ellipses. The assisting FCS protected the preselected envelope limits allowing only short or small overshoots. Overshoots were efficiently damped out in the longitudinal motion (Figures 11 and 12). Low amplitudes of sustained oscillations have been observed in the lateral motion. These were related to strong nonlinearities and had a form of limit cycles (Valentin and Biannic, 2003). This phenomenon can be observed in between 920 and 960 s in Figure 11, as the pilot attempts to permanently overcome the protected bank angle. The behaviour cannot be classified as pilot-induced oscillation, as the operator's activity is not executed in an opposite phase to the bank angle (Van der Weerd, 2000; Mitchell *et al.*, 2003). These oscillations are marginal if the pilot follows the advisory system's recommendations (850-880 s).

The simulated turbulence effects have not significantly influenced the required level of the envelope protection. From operational point of view, a demanding situation emerged for the case of angular rate limitations as shown in Figures 13 (timestamp: 800-1,000 s) and 14 (timestamp: 700-950 s). Short-period changes of roll rate reached double the limits and this effect appeared to be significant in a turbulent atmosphere (Figure 14). Results of IAS and VS protection are satisfactory and qualitatively comparable with the bank and roll angle limitations. Subjective opinions of the test pilots regarding the operational suitability of the proposed system were largely positive and supporting. The virtual assistant does not jeopardize handling qualities within the protected envelope; whereas outside the safe flight envelope the FCS provides an intuitive stimuli to direct the flight crew back to the safe margins (as comparable to the flight instructor's inputs).

Figure 9 Recorded tracks of manual flights with assistant mode

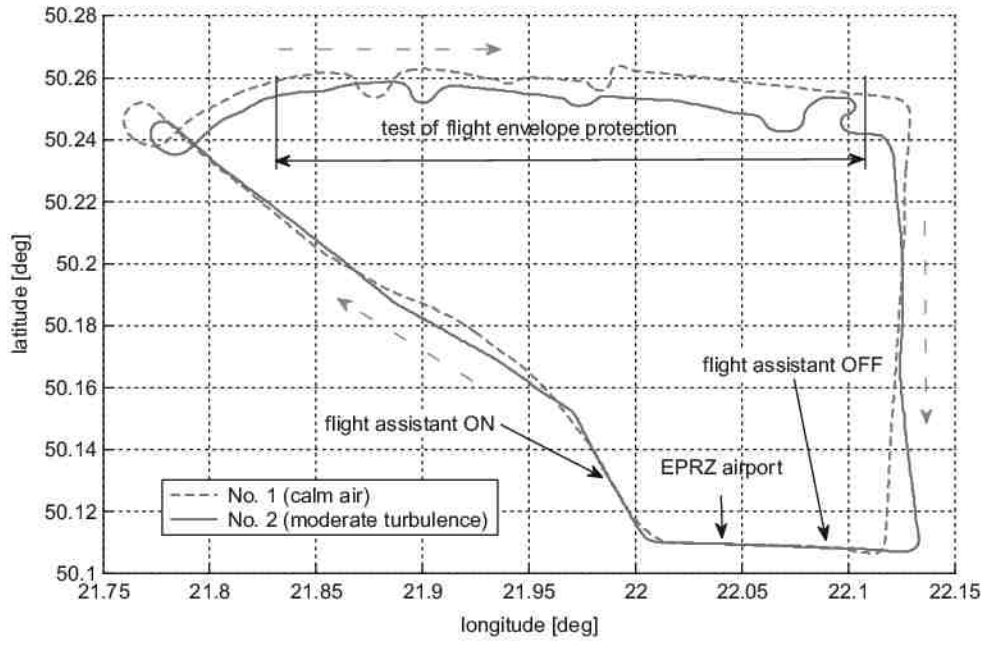

Figure 10 AGL and MSL ALT related to Figure 9

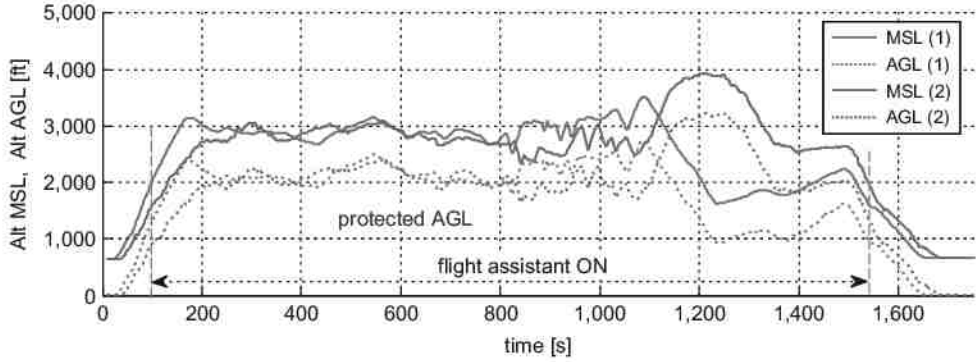

Figure 11 Pitch and bank related to Figures 9 and 10 (flight no. 1, calm air)

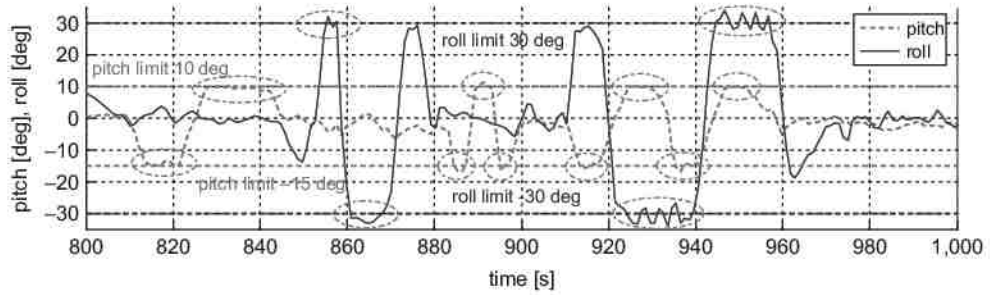

Figure 12 Pitch and bank related to Figures 9 and 10 (flight no. 2, moderate turbulence)

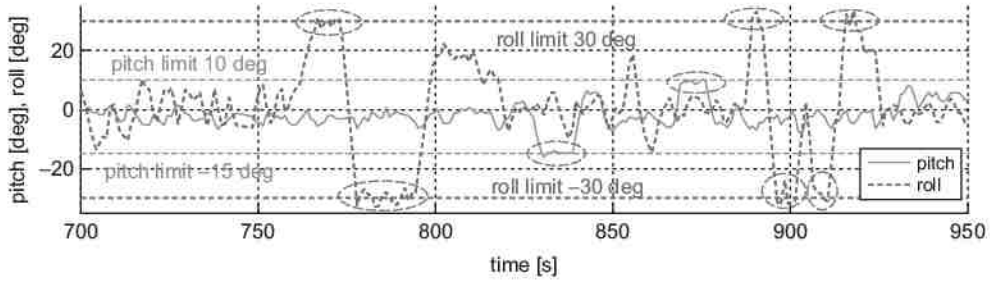

Figure 13 Angular rates related to Figures 9-11 (flight no. 1, calm air conditions)

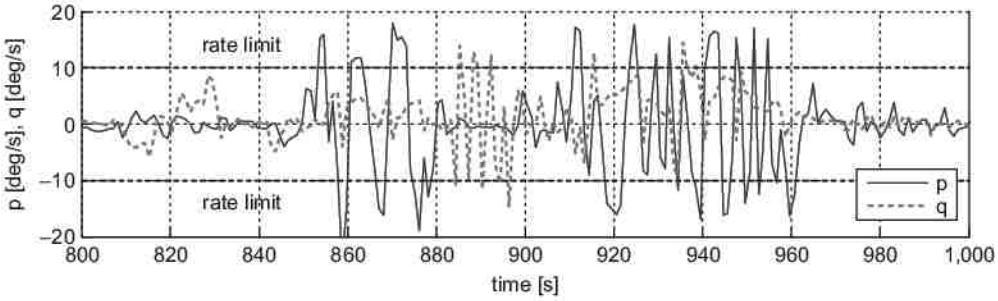

Additionally, the instances of the active pilot's assistant mode activation have been shown in Figures 11 and 12. Actuator generated forces reached a power range from 15 to 200 N. A closer in-depth study of the simulated time histories is temporarily not accessible mainly due to limitations of the measurement system. The handling qualities in the range of active pilot assistant mode have been estimated with the use of Cooper-Harper scale.

Figure 14 Angular rates related to Figures 9-10 and 12 (flight no. 2, moderate turbulence)

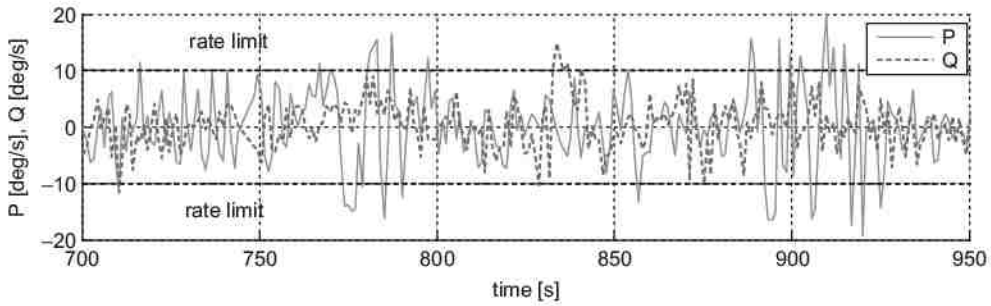

Autopilot mode – selected experiments

Series of experimental evaluations have been performed using the SimStar Lab within two of the simulated flights. The planned and the real tracks are shown in Figure 15, with the recorded flight path shown in Figure 16. The mission profiles of the flights were selected to demonstrate the stability of the CTRL and the ability to define complex flight trajectories through a mode selection panel and the upload of predefined air routes into the PFD. An important aspect of the simulation was the definition of characteristic atmospheric conditions for specific flights. The first simulated flight has been performed in calm air conditions, followed by a low turbulence environment introduced throughout the subsequent second flight. The simulation results are demonstrated through the time history plots of ALT, IAS, VS, pitch and roll angles which provide a quick visual guide for the assessment of system's stability and

Figure 15 Automatic flights with manually executed take-off and landing (EPRZ-EPML-EPRZ route)

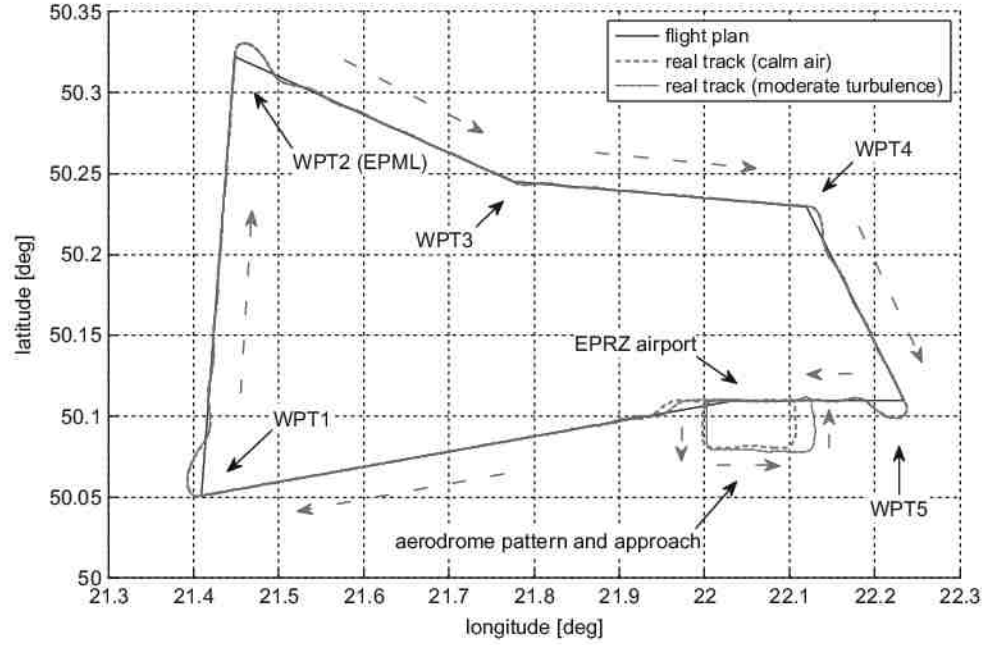

Figure 16 AGL and MSL ALT related to Figure 15

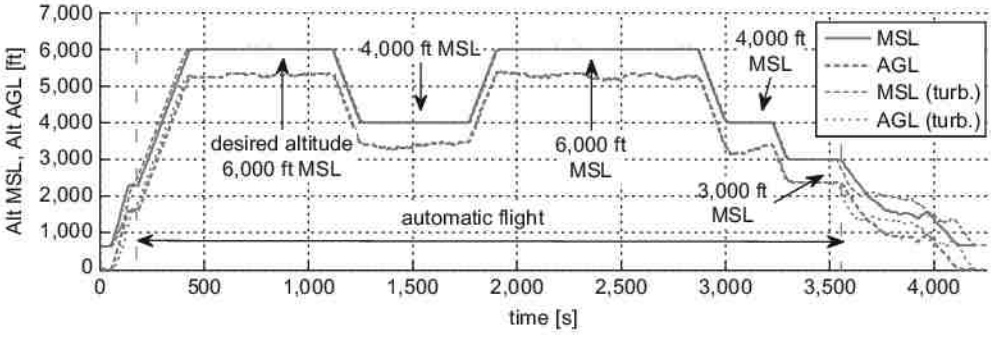

Aircraft Engineering and Aerospace Technology: An International Journal
Volume 85 · Number 6 · 2013 · 475–486

performance characteristics. The simulated flight duration was approximately 1 hour and 10 minutes.

The automatic FCS has been activated in both flights, in about 2 minutes after the take-off and over the 2,000 ft MSL threshold (Figure 16). The FCS stabilized the aircraft precisely at the desired ALT levels of 3,000, 4,000 and 6,000 ft MSL. The climb and descend were executed with an established vertical rate of 900 ft min^{-1} (Figure 17). The deviations in VS reached up to 200 ft min^{-1} during the flight in a simulated turbulent atmosphere (Figure 18). The IAS has initially been stabilized, depending on the route section, at 80, 90 or 95 kts (Figures 17 and 18). The variations in pitch angle for both flights are shown in Figure 19, with the FCS limiting the maximal values similarly to the active pilot's assistant mode.

Conclusion

The advantage of an assisting FCS design based on the classical control laws is in the moderate complexity of the resulting CTRL structure and the ability to support the design by proven analytical tools compatible with the airworthiness certification procedures, which makes it an ideal candidate for a cost effective implementation on board of state of the art LSAs. The described control strategy integrates a smart FCS to the LSA's mechanical circuits, enabling improved comfort and safety by maintaining high reliability standards along with the capability of manual recreational/sport flying. The advisory character of the system represents a technological innovation by mimicking human piloting techniques and provides the flight crew with an intuitive

Figure 17 IAS and VS related to Figures 15 and 16 (calm air conditions)

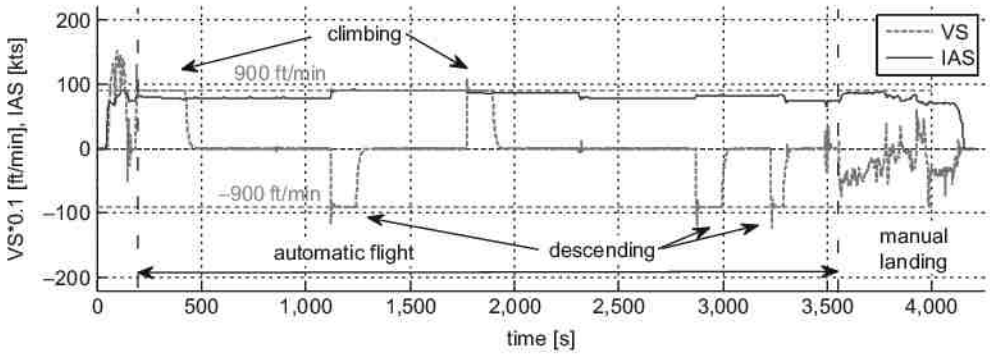

Figure 18 IAS and VS related to Figures 15 and 16 (turbulent atmosphere)

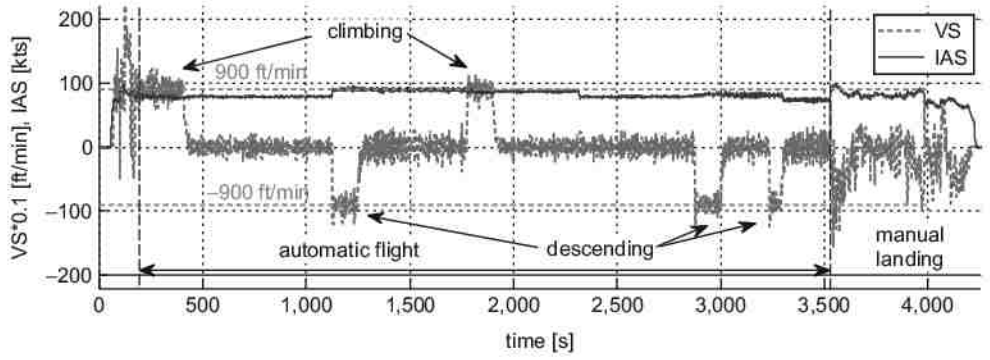

Figure 19 Pitch roll angle related to Figures 15-18 (calm air conditions as well as turbulent atmosphere)

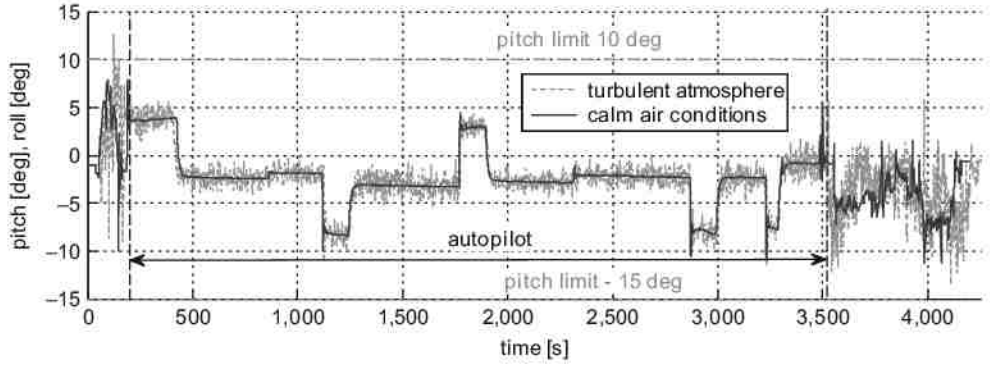

flight envelope protection interface. In all aspects of the increased level of the on-board automation, it is the pilot in command who has the final authority over the FCS's commands/interventions. Presented concept benefits a typical LSA pilot by introducing a virtual co-pilot, enabling cockpit workload reduction and a redirection of pilot's focus to careful navigation and communication with the ATC stations. When transitioning from the manual to a fully automatic flight, the system continues watching and protecting the safe flight envelope by commanding respective control surfaces and auto-throttle unit. By introducing the assisting flight control concept to the LSAs, the pilot will be provided with a flight safety enhancing system with selectable level of envelope protection based on their preferences and immediate expectations. This, along with advanced graphical user interfaces, synthetic vision systems and augmented reality will introduce new level of user experience, increased comfort and a commitment to a safer execution of flight.

The level of technological innovation was referred to the LSA segment reflecting all its limitations in cost, redundancy and power and weight penalties of complex architectures (Goyer, 2010). A MIL grade active stick, or FAR 23, 25 compliant technology would introduce a technological advancement at a price tag that would prohibitively increase the price of the flying equipment.

References

Bauer, C., Lagadec, K., Bes, C. and Mongeau, M. (2007), "Flight control system architecture optimization for fly-by-wire airliners", *Journal od Guidance Control and Dynamics*, Vol. 30 No. 4, pp. 1023-1029.

Carter, J.F. and Stoliker, P.C. (2000), *Flying Quality Analysis of a JAS 39 Gripen Ministick Controller in an F/A-18 Aircraft, Raport NASA/TM-2000-209024*, NASA Dryden Flight Research Center, Edwards, CA.

Chudy, P. and Rzucidlo, P. (2012), *Analysis of Interactions Between Pilot-Operator and Advanced Flight Control System, Solid State Phenomena*, Vol. 180, Trans Tech Publications Ltd, Zurich, pp. 101-108.

Chudy, P., Rzucidlo, P. and Tomczyk, A. (2009), "Safety enhanced digital flight control system", *Aircraft Engineering and Aerospace Technology*, Vol. 81 No. 5, pp. 416-423.

Chudy, P., Rzucidlo, P. and Zemcik, P. (2010), "Affordable light aircraft flight simulators", paper presented at AIAA Meeting Papers on Disc, Renton, VA, Vol. 15, No. 9.

Etkin, B. and Reid, L.D. (1996), *Dynamics of Flight – Stability and Control*, Wiley, New York, NY.

Evektor-Aerotechnik (2009), *Aircraft Operating Instructions for SportStar Light Sport Aircraft*, Evektor-Aerotechnik, Brno.

Goyer, R. (2010), "Envelope protection comes to GA", *Flying Magazine*, November 3.

McRuer, D., Clement, W., Thompson, P. and Magdaleno, R. (1997), *Aviation Safety and Pilot Control: Understanding and Preventing Unfavourable Pilot-Vehicle Interactions*, Committee on the Effects of Aircraft-Pilot Coupling on Flight Safety, National Academy Press, Washington, DC.

Mitchell, D.G., Doman, D.B., Key, D.L., Klyde, D.H. and Leggett, D.B. (2003), "The evolution, revolution, and challenges of handling qualities", paper presented at Atmospheric Flight Mechanics Conference and Exhibit, Austin, TX.

Popelka, J. and Paces, P. (2012), "Performance of smart sensors standards for aerospace applications", *Electrical Review*, Vol. 88 No. 01a, pp. 229-232.

Rogalski, T., Tomczyk, A. and Kopecki, G. (2009), "Flight simulator as a tool for flight control system synthesis and handling qualities research", *Solid State Phenomena*, Vol. 147-149, pp. 231-236.

Stachowiak, S. and Bosworth, J. (2004), "Flight Test Results for the F-16XL With a Digital Flight Control System", NASA/TP-2004-212046, NASA Dryden Flight Research Center, Edward, CA.

Stanton, N., Chambers, P. and Piggott, J. (2001), "Situational awareness and safety", *Safety Science*, Vol. 39 No. 3, pp. 189-204.

Stock, M. (2006), *CAN Aerospace, Stock Flight Systems*, Revision 1.7, Berg, Germany.

Tomczyk, A. (2004), "Facilitated airplane – project and preliminary in-flight experiments", *Aerospace Science and Technology*, Vol. 8 No. 6, pp. 469-477.

Valentin, S. and Biannic, J.-M. (2003), "Limit cycle detection & migration in pulse-modulated feedback systems", paper presented at AIAA Guidance, Navigation, and Control Conference, Austin, TX.

Van der Weerd, R. (2000), *Pilot-Induced Oscillations Suppression Methods and Their Effects on Large Transport Aircraft Handling Qualities*, Delft University Press, Delft.

About the authors

Karol Rydlo obtained MSc degree in 2012, Faculty of Informatics Masaryk University, specialization: computer graphics. Karol Rydlo has been Researcher at Brno University of Technology since 2011. Karol Rydlo's research interest includes modeling and simulation of flight dynamics and digital flight control systems.

Pawel Rzucidlo obtained MSc degree in 2001 and PhD degree in 2005, Rzeszow University of Technology, Faculty of Mechanical Engineering and Aeronautics, specialization: aircraft control systems. Pawel Rzucidlo has been Researcher and Lecturer at Rzeszow University of Technology since 2001. Pawel Rzucidlo's research interest includes aircraft control with an emphasis on interactions between human and machine. Pawel Rzucidlo is author of over 50 scientific papers and conference proceedings and author of two books. Pawel Rzucidlo is the corresponding author and can be contacted at: pawelrz@prz.edu.pl

Peter Chudy obtained MSc degree in 2001 and PhD degree in 2004, Brno University of Technology, Faculty of Mechanical Engineering, specialization: aeroelasticity, computational flight dynamics. Peter Chudy has been Researcher and Lecturer at Brno University of Technology since 2004. Peter Chudy's research interest includes modeling and simulation of flight dynamics and digital flight control systems. Peter Chudy is author of over 20 scientific papers and conference proceedings.

PROTOTYPING FRAMEWORK FOR DIGITAL FLIGHT CONTROL SYSTEMS

Peter Chudy, Jan Vlk, Petr Dittrich, Brno University of Technology, Brno, Czech Republic

Abstract

Hardware-in-the-loop simulations are indisputably perceived as an integral part of the avionics design and development process. This paper describes a prototyping framework, which has been employed to develop a digital autopilot for a light sport aircraft. Related simulation processes have been performed on two different ground-testing levels. The first level consisted of a laboratory grade development and testing phase, which supported the initial functional estimate of the designed and implemented autopilot features. The subsequent testing level already included the embedded autopilot system installation on board of the test aircraft. System prototyping was performed at the light aircraft simulation lab SimStar at the Brno University of Technology. Additional ground simulations were employed to verify and ground test the operational suitability of the designed autopilot flight control system elements. The implemented hardware units were connected into the simulation network using the CANaerospace communication protocol. Simulations focused on the real time automatic flight modes operational scenarios and confirmed the anticipated performance of the autopilot design features.

Introduction

Progress in aircraft technology has led in recent years to a significant reduction of light aircraft ownership and operational costs. Unfortunately for the light aircraft industry, the public opinion often questions the comfort and safety of the light aviation transport concept when compared to the professionally operated commercial airliners or business jets. The inexperienced pilots with limited training are ill prepared for solving critical situations related to bad weather conditions or in-flight failures and emergencies. Therefore, new technologies aimed at comfort and safety improvements are quickly being introduced to the lower segments of light aviation (GA, LSA). These technologies are generally built around Commercial off-the-shelf (COTS) components and require a conveniently lower level of certification effort compared to the complex systems found on military aircraft or airliners. However, even these rapidly emerging solutions require thorough testing during the design, development and preproduction stages. In order to verify the design suitability of the autopilot's components, a prototyping framework as the one proposed throughout the paper has been developed. The prototyping framework contains the following components: SimStar simulator, dynamic model of the Evektor Sportstar aircraft, autopilot peripherals and flight control system. These will be presented in next paragraphs.

Prototyping Framework

The transition from flight control system's mathematical modeling into rapid prototyping environment towards experimental flight testing should account for pilot and hardware-in-the loop (HIL) simulations on a suitably adapted ground based flight simulator. Modification of a state-of-the-art certified professional flight simulator is a feasible, but at the same time challenging task considering the number of difficulties related to the simulator's withdrawal from the training process, loss of product certificate, potential violations of proprietary data protocols, different hardware standards, etc. A more flexible and accessible solution seemed to be a purposely-built experimental simulation equipment. Therefore, a light aircraft simulation lab SimStar has been established at the Brno University of Technology. The prototyping framework accommodates different simulation modes, from commercial products as X-plane to hand coded simulation and control software [1, 2].

Simulator

The various modules and subsystems of the SimStar simulator have been grouped into functional blocks as shown in Figure 1. The modular design of the simulator hardware and software architecture allows for a direct integration or sharing of different flight models.

978-1-4799-1538-5/13/$31.00 ©2013 IEEE

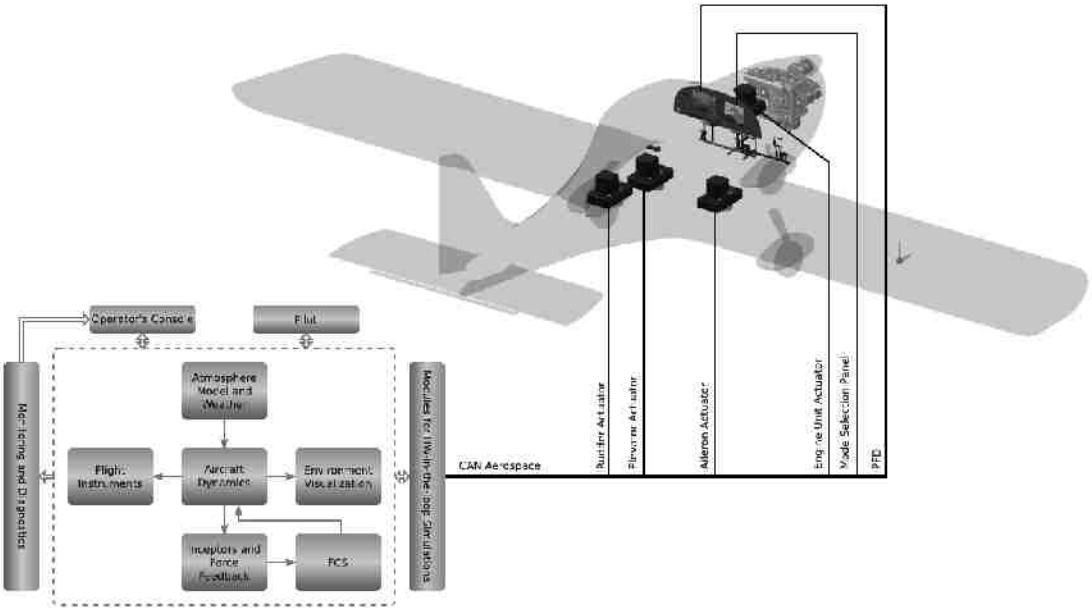

Figure 1. SimStar's Architecture Design with Functional Blocks

These models can be shared through the Matlab/Simulink or via direct upload of the aircraft's dynamic model. The simulator is by default equipped with a nonlinear aircraft dynamics model of the Evektor SportStar light aircraft [1]. The peripheral modules of the simulator shown in Figure 1 are connected by CAN databus [1]. Application of the CAN network and CANaerospace communication protocol described in [3] makes this solution compatible and open to other on-board systems.

Figure 2. SimStar's Cockpit Section

The SimStar simulator (see Figure 2) enables HIL simulation of electromechanical actuators, control panels and inceptors equipped with CAN controllers [4].

Dynamic Model

The dynamic model used during the simulation runs was extracted from a series of flight experiments performed on an Evektor SportStar experimental aircraft equipped with a laboratory grade data acquisition system. Measured data were subjected to the parameter identification procedure, results of which were integrated into a nonlinear aircraft model structure. A model quality assurance process concluded the identification. Based on the initially drawn assumptions of the flight envelope margins, the model included basic stall and spin characteristics as post stall and spin recovery tasks were not primarily addressed in the research.

Rigid-Body Equations of Motion

The derivation of the rigid-body equations of motion is based on the momentum conservation laws. Let H be an angular momentum, then the angular moment time variation equals the sum of all external moments acting on the body.

$$\frac{d\vec{H}}{dt} = \sum M = \frac{d}{dt}(\vec{r}^{P}(t) \times \vec{V}^{P}(t) \cdot m) \qquad (1)$$

As the angular momentum is simply given by the expression $H = I \cdot \omega$, where I is the inertia matrix and $\omega = [p_K \quad q_K \quad r_K]^T$ is the angular rate vector, it is possible to define the time variation of angular rates via the following expression:

$$(\dot{\vec{\omega}}_K)_B = I_{BB}^{-1} \cdot (\vec{M}_T^G) - (\vec{\omega}_K)_B \times I_{BB} \cdot (\vec{\omega}_K)_B, \qquad (2)$$

where $\vec{M}_T^G$ is the total momentum acting on the aircraft Center of Gravity (CG). A simplified form of the momentum equation is shown in Eq. 3. The reason for such a simplification is the fact that the external forces do not contribute to the creation of additional moments around the CG.

$$\begin{bmatrix} \dot{p}_K \\ \dot{q}_K \\ \dot{r}_K \end{bmatrix} = I_{BB}^{-1} \cdot \begin{bmatrix} L_A^G \\ M_A^G \\ N_A^G \end{bmatrix}_B - \begin{bmatrix} p_K \\ q_K \\ r_K \end{bmatrix}_B \times I_{BB} \cdot \begin{bmatrix} p_K \\ q_K \\ r_K \end{bmatrix}_B \qquad (3)$$

In the expression above, the vector $[L_A^G \quad M_A^G \quad N_A^G]^T$ represents the aerodynamic moments acting on the aircraft CG. The following expression depicts the inertia matrix, which is required for the computation of the angular rates.

$$I_{BB} = \begin{bmatrix} I_{XX}^G & -I_{XY}^G & -I_{XZ}^G \\ -I_{XY}^G & I_{YY}^G & -I_{YZ}^G \\ -I_{XZ}^G & -I_{YZ}^G & I_{ZZ}^G \end{bmatrix} \qquad (4)$$

A similar procedure has been employed for deriving the translational equations of motion. The time variation of the linear momentum is equal to the sum of the external forces acting on the rigid aircraft, as introduced in Eq. 5.

$$\frac{d\vec{p}}{dt} = \sum \vec{F} = \frac{d}{dt} \int \dot{\vec{r}}^{P}(t) \cdot \rho(t) \cdot dV \qquad (5)$$

The following equation represents a vector in the Body-Fixed Frame, rotating at an angular rate ω:

$$\left(\frac{d(\cdot)}{dt}\right)_I = \left(\frac{d(.)}{dt}\right)_B + \omega \times (\cdot), \qquad (6)$$

where subscripts I and B refer to the Inertial and the Body-Fixed Frame, respectively. Eqs. 7-8 show the translational equations of motion in a vector description of the Body-Fixed Frame.

$$(\dot{\vec{V}}_K)_B = \frac{1}{m} \cdot (\vec{F}_T^G)_B - (\vec{\omega}_K)_B \times (\vec{V}_K)_B \qquad (7)$$

where $(\vec{V}_K)_B = [u_K \quad v_K \quad w_K]_B^T$ is the velocity vector defined in the Body-Fixed Frame and $\vec{F}_T$ is a vector containing the influence of all external forces acting on the aircraft C.G. Equation 8 provides a more detailed view on the translational dynamics.

$$\begin{bmatrix} \dot{u}_K \\ \dot{v}_K \\ \dot{w}_K \end{bmatrix}_B = \frac{1}{m} \begin{bmatrix} X_A^G + X_P^G + X_G^G \\ Y_A^G \\ Z_A^G \end{bmatrix}_B - \begin{bmatrix} p_K \\ q_K \\ r_K \end{bmatrix}_B \times \begin{bmatrix} u_K \\ v_K \\ w_K \end{bmatrix}_B, \qquad (8)$$

where X_A, Y_A, Z_A, X_P, X_G are aerodynamic (index A), propulsion (index P) and gravity (index G) forces acting on the aircraft CG. There are many ways to express the aircraft's attitude between the Body-Fixed and Inertial Frames. One of the most common ways is through the Euler angle description. This description has however been avoided due to possible singularities arising while crossing a pitch angle value of $\pm\pi/2$. Therefore, the presented implementation of the dynamic model uses the quaternion approach as described by Eq. 9.

$$\begin{bmatrix} \dot{q}_0 \\ \dot{q}_1 \\ \dot{q}_2 \\ \dot{q}_3 \end{bmatrix} = \frac{1}{2} \cdot \begin{bmatrix} 0 & -p_K & -q_K & -r_K \\ p_K & 0 & r_K & -q_K \\ q_K & -r_K & 0 & p_K \\ r_K & q_K & -p_K & 0 \end{bmatrix}_B \cdot \begin{bmatrix} q_0 \\ q_1 \\ q_2 \\ q_3 \end{bmatrix} \qquad (9)$$

Equation 10 introduces the condition, which the quaternions have to fulfill.

$$q_0^2 + q_1^2 + q_2^2 + q_3^2 = 1 \qquad (10)$$

Equation 11 describes the standard Euler angles (bank angle ϕ, pitch angle θ, yaw angle ψ) by means of quaternions and trigonometric functions.

$$\begin{bmatrix}\phi\\ \theta\\ \psi\end{bmatrix}=\begin{bmatrix}\tan^{-1}\left(2\cdot\frac{q_1\cdot q_2+q_0\cdot q_3}{q_0^2+q_1^2-q_2^2-q_3^2}\right)\\ \sin^{-1}[-2\cdot(q_1\cdot q_3-q_0\cdot q_2)]\\ \tan^{-1}\left(2\cdot\frac{q_2\cdot q_3+q_0\cdot q_1}{q_0^2-q_1^2-q_2^2+q_3^2}\right)\end{bmatrix} \tag{11}$$

The last important information about the aircraft position defined in the NED-frame is expressed according to the abovementioned velocity vector $(\vec{V}_K)_B$ and the transformation matrix $\boldsymbol{M}_{OB}$. The position vector includes the x_{NED} and y_{NED} coordinates, as well as the h_{AGL}.

$$\begin{bmatrix}\dot{x}^G\\ \dot{y}^G\\ \dot{z}^G\end{bmatrix}=\boldsymbol{M}_{OB}\cdot\begin{bmatrix}u_K^G\\ w_K^G\\ w_K^G\end{bmatrix}_B=\boldsymbol{M}_{BO}^{-1}\cdot\begin{bmatrix}u_K^G\\ w_K^G\\ w_K^G\end{bmatrix}_B, \tag{12}$$

where x, y, z provide the position in the NED-frame. In order to express the velocity vector in the aerodynamic frame, it is necessary to consider the wind velocity vector $\vec{V}_W$. This vector has to be transformed form the body-fixed frame to the NED-frame as shown in Eqs. 13-14.

$$(\vec{V}_A)_B=(\vec{V}_K)_B-(\vec{V}_W)_B \tag{13}$$

$$\begin{bmatrix}u_A^G\\ v_A^G\\ w_A^G\end{bmatrix}=\begin{bmatrix}u_K^G\\ w_K^G\\ w_K^G\end{bmatrix}_B-M_{BO}\cdot\begin{bmatrix}u_W^G\\ w_W^G\\ w_W^G\end{bmatrix}_O \tag{14}$$

$$\begin{bmatrix}V_{TAS}\\ \alpha_A\\ \beta_A\end{bmatrix}=\begin{bmatrix}\sqrt{(u_A^G)_B^2+(v_A^G)_B^2+(w_A^G)_B^2}\\ \tan^{-1}\left[\frac{(w_A^G)_B}{(u_A^G)_B}\right]\\ \tan^{-1}\left[\frac{(v_A^G)_B}{(u_A^G)_B^2+(w_A^G)_B^2}\right]\end{bmatrix} \tag{15}$$

The true airspeed V_{TAS}, angle of attack α_A and sideslip angle β_A are defined using the aerodynamic velocity vector components u_A, v_A, w_A and are required for the Flight Control System design [5].

The identification of flight parameters has been accomplished using elements of modeling, simulation and numerical optimization. Significant contribution in acquiring results of desired precision has been introduced through a correct model structure and its mathematical description. Validation of the dynamic model has been performed via comparison of the numerical simulation results with measured flight test data under the constraints of equal initial conditions. Figure 3 shows time histories of modeled and measured data for flight conditions at 3000 ft, true airspeed 95 kts and CG forward location.

In order to support the flight control system prototyping process with a convenient implementation of linear stability evaluation criteria, linearized dynamic models have been extracted from a full nonlinear model at various flight conditions (airspeed, altitude, mass and inertia characteristics) and formulated as state space models composed of four matrices $\boldsymbol{A}$, $\boldsymbol{B}$, $\boldsymbol{C}$, $\boldsymbol{D}$ introduced below.

$$\begin{aligned}\dot{x}&=\boldsymbol{A}\cdot x+\boldsymbol{B}\cdot u\\ y&=\boldsymbol{C}\cdot x+\boldsymbol{D}\cdot u\end{aligned} \tag{16}$$

where $\boldsymbol{A}$ is the state matrix, $\boldsymbol{B}$ is the input matrix, $\boldsymbol{C}$ is the output matrix and $\boldsymbol{D}$ is the matrix of direct input output relation, x is the state vector, u is the input vector and y the vector of system outputs.

$$\boldsymbol{A}=\begin{bmatrix}X_V & X_\alpha & -g\cdot cos\gamma_0 & X_q\\ Z_V & Z_\alpha & -\frac{g}{V_0}\cdot cos\gamma_0 & Z_q\\ 0 & 0 & 0 & 1\\ M_V & M_\alpha & 0 & M_q\end{bmatrix} \tag{17}$$

The dynamic matrix consists of the linearization force elements (X_V, Z_V), force and moment variables influenced by the angle of attack (X_α, Z_α, M_α) and force and moment elements, which are functions of the pitch rate (X_q, Z_q, M_q). The constants V_0 and γ_0 refer to trim point conditions for true airspeed and flight path angle, whereas g provides the gravity acceleration.

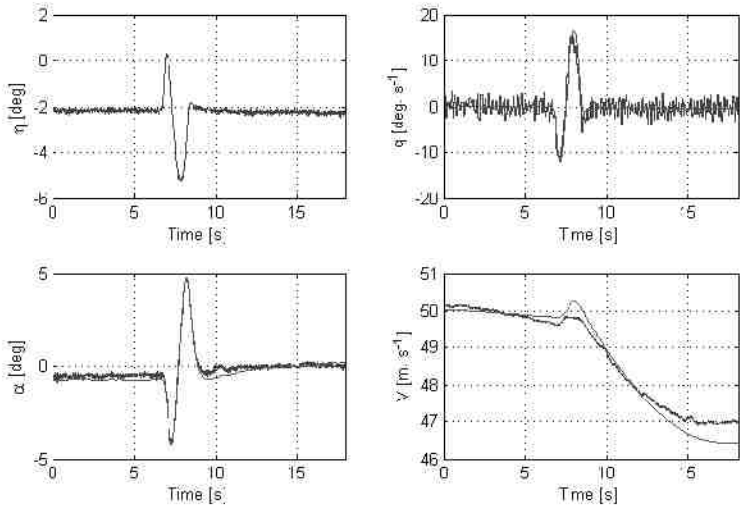

Figure 3. Time Histories of Modeled and Measured Data

The input matrix from Eq. 18 includes force and moment variables as functions of the elevator deflection (X_η, Z_η, M_η) and thrust (X_{δ_T}, Z_{δ_T}, M_{δ_T}).

$$\boldsymbol{B} = \begin{bmatrix} X_\eta & X_{\delta_t} \\ Z_\eta & Z_{\delta_t} \\ 0 & 0 \\ M_\eta & M_{\delta_t} \end{bmatrix}, \tag{18}$$

with vectors $\boldsymbol{x}$ and $\boldsymbol{u}$ having the following form:

$$\boldsymbol{x} = [V \quad \alpha \quad \theta \quad q]^T, \; \boldsymbol{u} = [\eta \quad \delta_t]^T \tag{19}$$

Considering full state feedback, the matrix $\boldsymbol{C} \in \mathbb{R}^{4\times4}$ is simply given by the identity matrix, whereas the matrix $\boldsymbol{D} \in \mathbb{R}^{4\times2}$ is a zero matrix with the corresponding dimensions [6].

Autopilot Peripherals

Peripherals shown in Figures 4 – 7 have been the principal elements controlled via CANaerospace protocol and investigated in the simulation. The aim was to subject the digital and electromechanical components to virtual operational scenarios typically encountered during light aircraft flight operations.

Figure 4. Primary Flight Display Layout

Figure 5. SimStar's Cockpit with 2 PFDs

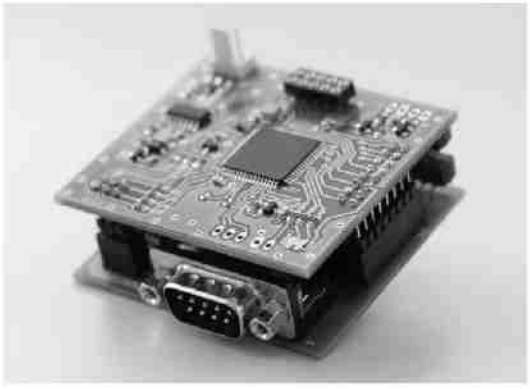

Figure 6. Actuator Controller Board

Figure 7. Actuator Assembly

One of the digital peripherals implemented for the laboratory level HIL simulations was an intuitive Primary Flight Display (PFD) shown in Figure 5 as integrated into the SimStar's instrument panel. The integrated PFD is built around an embedded computer system with a state-of-the-art multicore processor, equipped with an integrated display unit and a touch sensor layer. Visualization of flight related air data, navigation and system quantities requires a substantial amount of data that need to be processed by the PFD's processor in order to allow the software application to generate an intuitive image of the aircraft state to the pilot. The implemented intuitive PFD screen layout design, including the visualization of the measured values of Airspeed (IAS), Altitude (ALT), Vertical Speed (VS), Pitch and Roll angles, Heading (HDG) and GPS related navigation data presented in a form of synthetic terrain or moving 3D map, is shown in Figure 4. Further display enhancements include data related to the on-board power network, propulsion quantities and the flight control unit's status reports. PFD's connectivity to the communication network was accomplished via the implementation of the CAN aerospace communication protocol.

The second of the implemented peripherals was a set of digitally controlled electromechanical actuators shown in Figure 6 and Figure 7. The mechanical assembly of the electromechanical actuator includes a stepper motor with a custom built gearbox with optional electromagnetic clutch. The control board electronics consists of COTS microcontroller, stepper motor driver, galvanically isolated CAN driver and a switch. This configuration is supported by an external high precision rotary potentiometer used as a source of angular position information. In order to utilize the potential of the digital control, the following main operational functions have been implemented on the electromechanical actuator's microcontroller:

1) position measurement of an electromechanically actuated control surface,
2) commanding of the stepper motor through the stepper motor driver,
3) commanding of the electromechanical clutch (optional),
4) monitoring of the state outputs at the drivers integrated circuits,
5) communication using the CANaerospace protocol through the CAN data bus driver.

This scheme has been used throughout the design, implementation and verification phases of the actuation units. A physical implementation of the controller and feedback structure was introduced to the actuators serving the primary flight control surfaces (elevator, aileron, rudder) and the auto-thrust unit attached to the propulsion system. Actuators operating the elevator and trim tab were not physically included into the HIL simulation, but have been replaced by their respective virtual models.

CAN aerospace implementation on SimStar introduced a convenient integration capability to the simulation framework as standardized components communicating on the CAN aerospace level have been seamlessly integrated into the network.

Control Schemes

The control scheme includes a flight control system block with the autopilot flight control laws based on Classical Control Theory [7]. The prototyped control algorithms have been grouped into three formal levels: inner loop, outer loop, navigation and flight management as shown in Figure 8.

The inner loop is responsible for the stabilization of basic flight parameters, such as pitch and bank angle, Indicated Air Speed (IAS) as well as for turn coordination and sideslip compensation. Part of the inner loop includes a pitch force controller (pitch force CTRL) that is designed to reduce the force/moment reacting on the elevator's electromechanical actuator stepper motor. Pitch force CTRL operates the longitudinal trimmer to minimize the electromechanical actuator's loading. The pitch controller takes into account the cross-feedbacks from roll and air speed stabilization loops. Similarly, the IAS controller uses the cross-feedback from the pitch channel. The outer loop consists of three controllers in two separate channels, VS and ALT in longitudinal, HDG/TRK in lateral [8, 9].

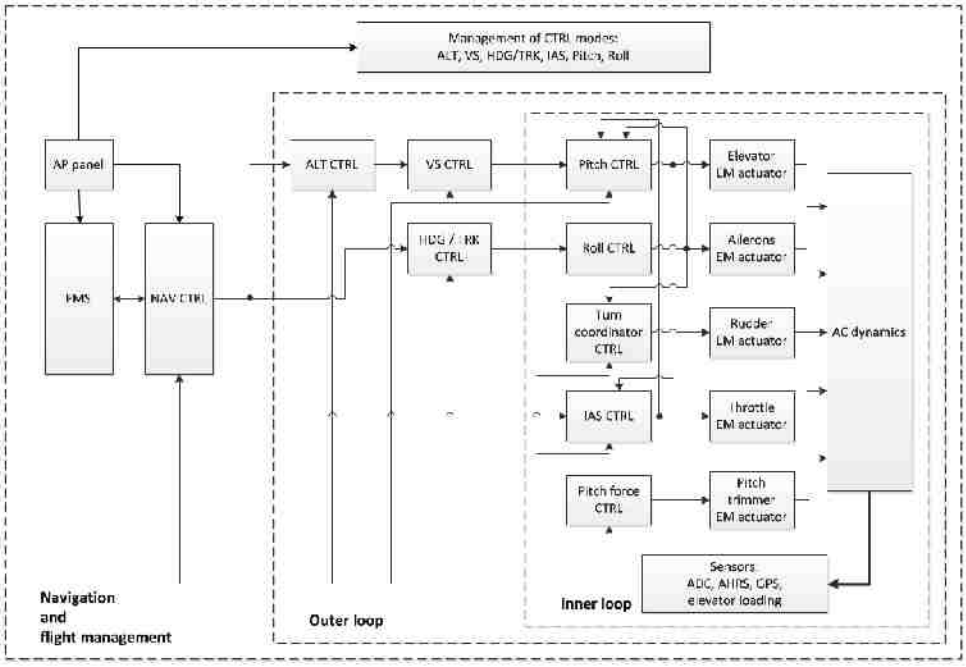

Figure 8. Autopilot Control Scheme

In navigation mode, HDG/TRK CTRL stabilizes ground track. In manual mode, the pilot can select stabilization of ground track or magnetic heading. ALT CTRL stabilizes the altitude in a way that the pilot can select required VS in both manual and automatic navigation mode. Blocks FMS and NAV CTRL are responsible for computing desired heading and altitude, which is the main input for the FCS Outer loop. They primarily contain the navigation logic, which affects computation of desired heading angle and automatic switching between waypoints in the flight plan [4]. Controller blocks of the autopilot mode contain modified PID controllers, which include variable gains in the proportional, integral and derivative paths and account for the saturation of integrators. The cross couplings from pitch, roll and IAS in the inner loops are executed within the proportional blocks. Rate limiting elements on the inputs of the selected controllers (pitch, roll) reduce their rapid responses. Saturation blocks limit the inputs and outputs of the inner loop controllers, as well as the input of the vertical speed controller in the

outer loop. Simple anti-windup filters for every controller with saturation on the output have also been implemented.

Options of autopilot selection modes:

1) Automatic navigation – primary navigation function where the pilot defines the waypoints through a Multifunction Flight Display.
2) Stabilization of selected flight parameters – the pilot is able to enter flight parameters (e.g. altitude, airspeed, heading) via an autopilot interface panel and the autopilot holds selected values.

The design on the controller structure uses the stability evaluation principles known from classical control theory. Hence, the phase and gain margins may be estimated based on the tools available for linear, time invariant systems. Other criteria, known as settling time, control anticipation parameter etc., have been used for the controller tuning and optimization [10].

Simulations

Complete flight control algorithms, as well as navigation and flight management systems have been implemented in a real-time rapid prototyping environment or, depending on the implementation level of the autopilot's embedded units, also in a handwritten code compiled on the target hardware platform. Two principal flight control configurations have been emulated depending on the selected autopilot mode. First, software configuration mimicked the manually operated mechanical flight control system, whereas the second configuration virtualized the autopilot commanded electromechanical system. An integral part of the autopilot flight control system prototyping and HIL simulations with the embedded peripherals was the verification of the functional integrity within the scope of its implementation. The overall design integration and the suitability of the autopilot modes have been verified through the compatibility on the communication network level. Hardware elements whose functionality has been primarily investigated throughout the simulations included the primary flight display and a set of digitally controlled electromechanical actuators.

Quantities provided by the aircraft state, navigation and system sensors were for the purpose of HIL simulations virtualized and replaced by a state description from respective simulation sub-models. Engine quantities used for a macroscopic description of the propulsion state definition have been derived from the engine's mathematical model. The AutoTrim unit found its virtual replacement in a software block integrated into the autopilot's control system. Virtualized elements of the autopilot whose physical integration would have required increased simulation framework complexity included the Digital Navigation Platform, AutoTrim and the Propulsion Monitoring Unit.

Laboratory Testing

Laboratory level HIL simulation focused on the evaluation of automatic flight modes with autopilot's peripherals connected to the simulation network via CANaerospace protocol. Included peripherals featured the flight display and a set of electromechanical actuators. One of the actuators attached to a laboratory grade loading mechanism simulating the control surface loading is shown in Figure 9.

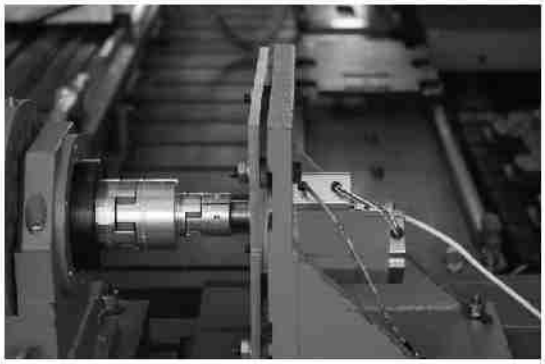

Figure 9. Electromechnical Actuator Testing

Simulated flight experiments were executed from the SimStar lab operator's console. Selection of the autopilot modes (FMS, direct stabilization of flight parameters) initiated automated flight sequences. The operator was given the choice of altering IAS, ALT, VS, TRK, HDG. By activating the mode selection, the commanded values appeared on the console. In order to account for the safety aspects, the IAS value needed to be selected under all flight conditions when controlled by an automatic flight control system. For this reason, canceling the

IAS setting while in an automatic flight was not possible. Preprocessed waypoints were allowed to be uploaded from the mission-planning interface.

A series of simulated flights have been performed using the laboratory level prototyping framework. The mission profiles of the flights were selected to demonstrate the controllers' stability and the ability of a complex trajectory definition. The simulation's commanding and monitoring parts were executed using the Matlab/Simulink modeling environment. An important aspect of the simulation was the definition of characteristic atmospheric conditions for the specific flights.

Aircraft Ground Testing

After a successful laboratory level simulation in SimStar lab, the simulation process proceeded towards experimental implementation of the primary flight display and parallel installation of electromechanical actuators onboard of the Evektor SportStar aircraft shown in Figure 10. The aim of simulated navigation flight was to verify operational suitability of investigated autopilot components for the performance and installation compatibility.

Figure 10. Aircraft for Ground Simulation

Therefore, the research aircraft's flight program was temporarily put on hold and the aircraft has been modified to be used as "iron bird" for ground simulations of the autopilot program. The actual instrumentation and installation of new avionics was extended by a ground command and monitoring station. This installation is depicted in Figure 11. Attitude, force, navigation and system quantities were obtained from numerical flight simulation and considered as inputs replacing hardware elements of the autopilot installation. The inclusion of external loading mechanisms mimicking the effects of flight loads on the control surfaces hasn't been considered due to substantial increase in complexity of the simulation loop and a considerable increase of simulation cost. Considering the mentioned limitations, the simulation loop has been supplemented with a software substitution of loading mechanism dynamics.

Figure 11. Command and Monitoring Station

For the ground verification of the prototyped autopilot, a navigation task has been programmed into the flight management unit. The aim of the simulation was also to demonstrate the coordination of individual elements of the control algorithms and the controller stability in a reaction to external disturbances introduced via an external signal. The test operator has artificially injected the externalities into the system. An overall picture of the simulation setup is shown in Figure 12. Controller's response to externally introduced signal is shown in Figure 13.

Figure 12. Overall Picture of the Simulation Setup

Figure 13. Response of Digitally Controlled Aileron to External Disturbance

Simulated navigation flights are shown in Figure 14. The aircraft took off in a manual regime from Syracuse airport (SYR) and after activating the autopilot continued in an automatic flight regime.

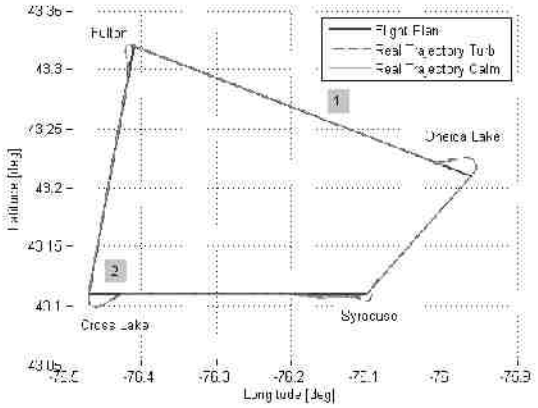

Figure 14. Automatic Flights with Manual Take-Off and Landing

The route included SYR followed by the Oneida Lake, Fulton, and Cross Lake back to the point of take off. Part of the simulation included selection of flight conditions – calm and turbulent air. After the manually flown take-off, the aircraft was guided to climb to 3000 ft MSL. The second part of the flight required a descent to ALT 2500 ft MSL while holding 100 kts IAS, followed by an automatic climb to 4000 ft in the third phase and a subsequent descent to 2000 ft MSL in the final phase. The flight was concluded through a manual approach and landing on SYR. Altitude and airspeed profiles are shown in Figure 15 and Figure 16. Figures 14-16 show two parts of the flight trajectory which have been marked as a specific flight regime: steady state flight (1) and steady banked turn (2). These trajectory elements have been used for the evaluation of the FCS stability according to SAE AS94900. Drawing from SAE requirements, the pitch angle shall be maintained in smooth air conditions with static accuracy of ±0,5 degree (wings level) with respect to the initial reference.

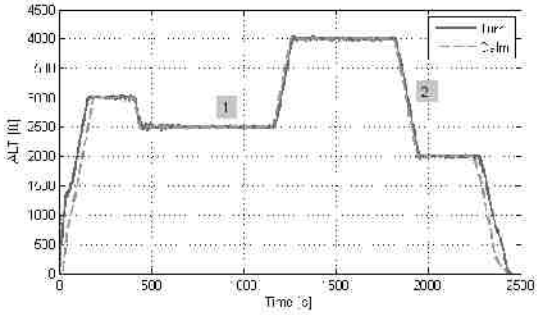

Figure 15. Vertical Profile of Automatic Flights from Figure 13 Referenced to MSL

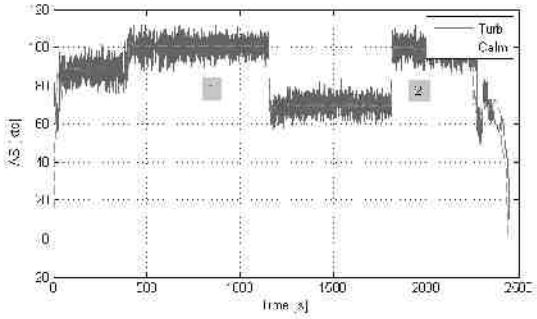

Figure 16. Indicated Airspeed Graph for Automatic Flights from Figure 13

Furthermore, the RMS attitude deviations shall not exceed 5 degrees in pitch angle [11]. For the coordination in steady banked turns, the sideslip angle shall not be greater than 2 degrees in smooth air. Figures 17 and 18 show the recorded flight quantities and related criteria in the abovementioned trajectory elements, which demonstrate the compliance with the FCS design requirements. Both

figures present computed responses under calm and turbulent air. In the steady state horizontal flight example from Figure 17, the pitch angle deviation in a calm air was practically negligible and similarly did not violate the 4 degree threshold from RMS initial value under turbulent air.

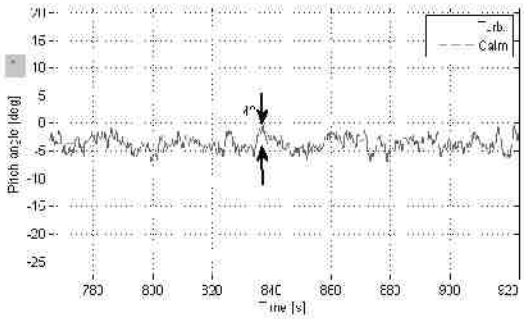

Figure 17. Pitch Angle during Steady State Flight

For the steady banked turn shown in Figure 18, the controller was able to hold the FCS angle of sideslip below 5 degree for the turbulent air conditions. The deviations of angle of sideslip in calm air were practically negligible.

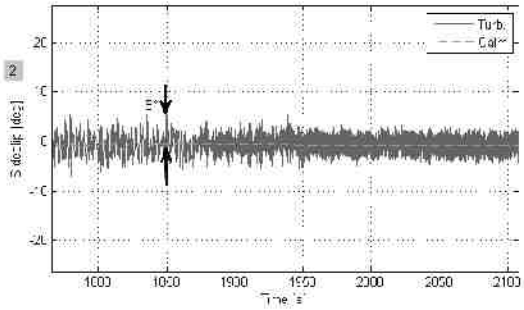

Figure 18. Angle of Sideslip during Coordinated Steady Banked Turn

Conclusion

A digital flight control system (autopilot) has been designed using the presented prototyping framework. Its peripheral units have been subjected to simulations in the light aircraft flight simulator laboratory SimStar and were tested under the conditions of hardware implementation on the Evektor SportStar aircraft. The primary flight display unit and electromechanical actuators were under both scenarios connected to the network using the CANaerospace protocol. Laboratory level simulations allowed testing of prototyped system features in real-time simulation environment before the actual installation onboard of the experimental aircraft. A similar approach has been applied to the software and simulation elements from the laboratory testing level as these could have been customized and re-implemented for the flight control system ground simulations on the test aircraft. Simulations with the prototyped aircraft installation demonstrated the expected performance and the compliance to the defined qualitative objectives. HIL simulations provided a deep insight into the developed flight control system performance prior to its experimental flight-testing.

References

[1] Chudy, P., Rzucidlo, P., Zemcik, P., "Affordable Light Aircraft Flight Simulators," Meeting Papers on Disc, Vol. 15, No. 9, AIAA, Renton, 2010.

[2] Chudy, P., Rzucidlo, P., Tomczyk, A., "Safety enhanced digital flight control system," Aircraft Engineering and Aerospace Technology, Vol. 81, Issue 5, 2009, pp. 416-423.

[3] Stock, M., CAN Aerospace, Stock Flight Systems, Revision 1.7, Berg, Germany, 2006.

[4] Dittrich, P., Chudy, P. "HIL simulation of a light aircraft flight control system", DASC, Williamsburg, VA, 2012

[5] Stevens, B. L., Lewis, L. L., Aircraft Control and Simulation, 2nd ed., John Wiley & Sons, New York, 2003.

[6] McCormick, B. W., Aerodynamics, Aeronautics, and Flight Mechanics, 2nd ed., John Wiley & Sons, New York, 1995.

[7] Etkin, B., and Reid, L. D., Dynamics of Flight – Stability and Control, John Wiley & Sons, New York, 1996.

[8] Bociek, S., Gruszecki, J., "Aircraft Control Systems," Rzeszow University of Technology Press, Rzeszow, 1999.

[9] Michalew, I., Okojemow, B., Czikulajew, M., Automatic Aircraft Control, Maszynostrojenije, Moscow, 1987.

[10] Hodgkinson, J., Aircraft Handling Qualities, Reston, AIAA Education Series, AIAA, VA, 1999.

[11] SAE Aerospace, AS94900, Flight Control Systems – Design, Installation and Test of Piloted Military Aircraft, General Specification For, SAE International, Warrendale, PA, 2007

Acknowledgements

This work has been supported by the by the Technology Agency of the Czech Republic research project "Smart Autopilot" TACR TA01010678.

3 Automatic flight control system

The AFCS is a complex automatic flight control system with a touch operated user interface designed to meet the light aviation industry requirements. The AFCS contains a touch controlled Primary Flight Display (PFD) built around an asymmetric multicore computer platform, which supports deterministic execution of flight control tasks. The PFD is connected to the onboard CAN network to provide commands and to read feedback data from digitally controlled Electromechanical Actuators (EMA) used for the automatic control of thrust, for commanding the deflections of control surfaces and Autotrim. The aircraft avionics network also contains data from onboard systems, attitude, and navigation sensors. The only two implemented hardware buttons are the push-buttons on the control stick grip and the instrument panel installed *Home* button.

The AFCS executes automatic flight in pilot selected modes of operation using computer processed digital data for a 4-axis aircraft control. The AFCS control concept includes an automatic regulation of Indicated Airspeed. This feature alone represents a beyond state-of-the-art system design used on light aircraft, see Figure 1. The PFD's asymmetric multicore computer platform is a distributed system designed for an efficient implementation of flight control and flight data visualization. The flight control task can therefore be continuously supported even in the unlikely event of a visualization system malfunction.

The AFCS allows for pilot workload reduction and an intuitive redistribution of attention towards execution of navigation tasks and avionics control. The ergonomic aspects or limitations imposed by the state-of-the-art solutions are resolved through the pilot/automation interaction modes using a touch controlled user interface. These modes account for the pilot's physiological limits and cockpit environment restrictions including the vibration effects and maneuver or turbulence-induced abrupt Load Factor changes. This requires an uninterrupted accessibility of touch controlled elements using a palm–stabilized position. The AFCS' user interface was designed to be conveniently operated by an unrestrained or stabilized hand. The user interface design introduces activation and direct control of commanded flight quantities within the visual representation of individual flight instruments. User confusion and irritation is avoided through careful location of touch sensitive areas over the PFD/MFD visual area.

Figure 1: Light Sport Aircraft

An important aspect of the AFCS is the ability to support flight along defined trajectories, while managing the flying system's total energy, reducing the environmental footprint and related acoustic emissions. The AFCS supports continuous system health monitoring. Due to the utilization of CANaerospace protocol, serving as a communication standard for data exchange within the onboard networks, the AFCS has a wide implementation and configuration potential. The AFCS units included in the installation are listed in Table 1 [1], [2].

Table 1: AFCS components

Units of the AFCS
Primary Flight Display with integrated Flight Control Computer
Multifunction Display
Digital Navigation Platform (DNP) including ADC[1], AHRS[2] and GPS[3] receiver
Propulsion Monitoring Unit (PMU)
Autotrim
Digitally Controlled EMA
Data Acquisition Unit (DAQ)

Figure 2 displays a general scheme of the AFCS including a schematic diagram of data and power networks. Communication within the AFCS network is done using CAN and CANaerospace communication protocol [2].

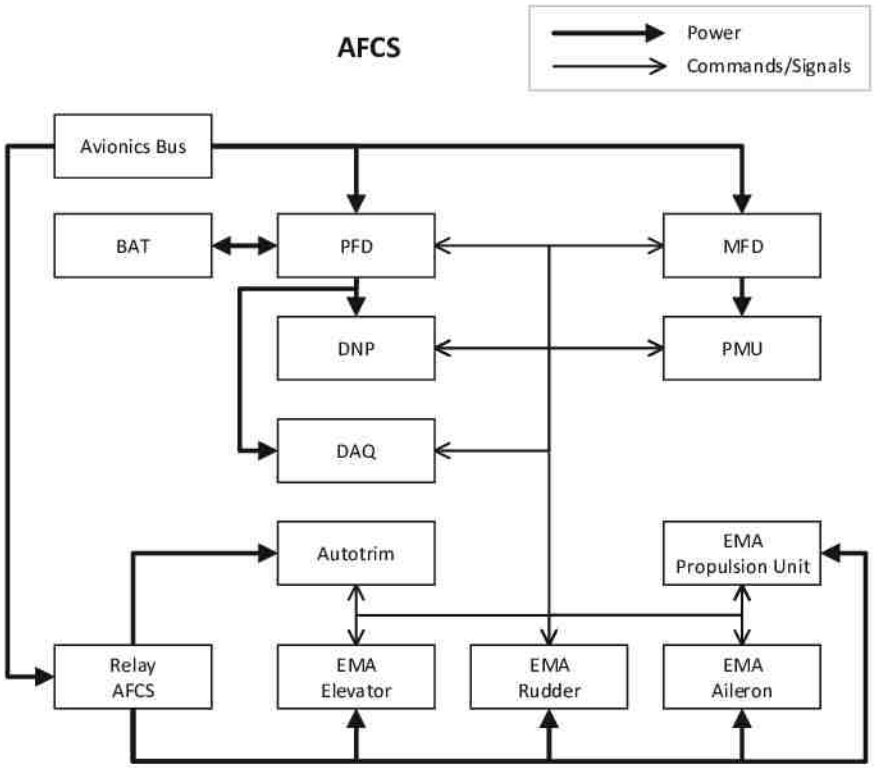

Figure 2: Block scheme of AFCS aircraft installation

The AFCS operational envelope limits are displayed in Table 2. Indicated Airspeed, attitude angles, Pressure Altitude and Load Factor ranges define the cruise regime of a light aircraft [2], [10]. The following description introduces individual phases of the AFCS operation. The AFCS regimes are shown in Table 3 [10]. Figures 3, 4 and 5 display the PFD and MFD interface for regimes A/P ENABLED, A/P ENGAGED and A/P DISCONNECT respectively [2].

[1]ADC – Airdata Computer
[2]AHRS – Attitude and Heading Reference System
[3]GPS – Global Positioning System
[4]AGL – Above Ground Level

Table 2: AFCS operational envelope

Quantity	Description	Unit	Range
IAS	Indicated Airspeed	kts	70 to 100
ALT	Pressure Altitude	ft	>900 AGL[4]
HDG	Heading Angle	deg	0 to 360
ϕ	Roll Angle	deg	-20 to 20
θ	Pitch Angle	deg	-10 to 10
n_z	Load Factor	1	0.5 to 1.5

Table 3: AFCS operation

Regime	Action
Activation	The system is powered on using the *Master* switch. Subsequent activation of the *Avionics* and A/P switches initiates an automatic Built–in Test (BIT) sequence.
A/P ENABLED	Inflight activation of the A/P pushbutton, located on the control stick grip, or activation of a predefined flight plan activates an automatic BIT. Successful completion of BIT will activate system status A/P ENABLED. The main screen of the PFD will display the AFCS graphical user interface. This regime supports the setting of the AFCS' variables.
A/P ENGAGED	The AFCS can be switched over inflight from A/P ENABLED to A/P ENGAGED by pressing the A/P pushbutton on the control stick grip.
A/P DISCONNECT	Pressing on the A/P pushbutton at the control stick grip, any of the trim switches, the *Home* button located at the instrument panel, or turning off the A/P switch will disconnect the AFCS and cause the transition to a manual flying regime. Inflight violation of operational limits will cause an automatic AFCS disconnect indicated by a flashing sign A/P DISCONNECT.
Deactivation	Turning off the A/P switch deactivates the electromechanical actuation units. Deactivation will interrupt powering the rudder, aileron, elevator and propulsion unit's electromechanical actuators. The *Avionics* switch must be turned off for a complete system deactivation.

Figure 3: A/P ENABLED interface on PFD (left) and MFD (right)

Figure 4: A/P ENGAGED interface on PFD (left) and MFD (right)

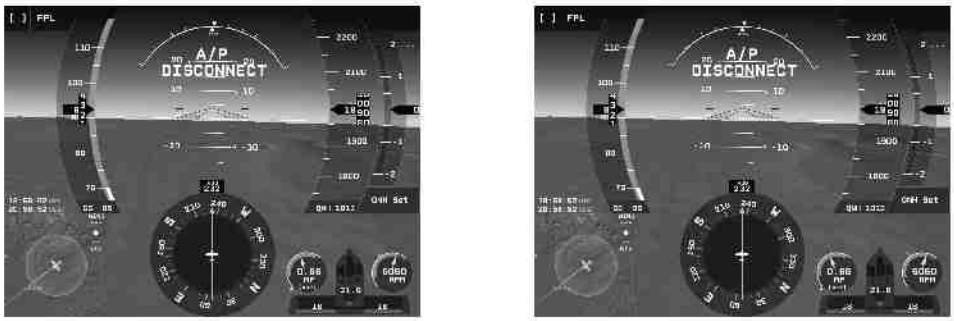

Figure 5: A/P DISCONNECT interface on PFD (left) and MFD (right)

The AFCS operational parameters are set through the PFD's touch interface which supports individual selection of QNH, IAS, ALT and HDG. Table 4 shows the main types and ranges of adjustable control parameters [2].

Table 4: Adjustable AFCS quantities

Quantity	Description	Unit	Increment
QNH	Atmospheric Pressure at Mean Sea Level	hPa	1
IAS	Indicated Airspeed	kts	10
ALT	Pressure Altitude	ft	100 or 1000
HDG	Heading Angle	deg	1 or 10

3.1 Operational trials

An important aspect of the AFCS development process is an inflight evaluation of the designed technology under real world operating conditions. A series of flight tests were organized incrementally form ground testing up to and including the evaluation of fully automatic test flights [4]. The aim of the system's inflight testing was twofold: first, to quantifiably record and evaluate flight parameters and, second, to investigate the intuitiveness of the user interface operational modes. This section is based on [5].

The initial tasks of the testing methodology contain an operational evaluation of Primary Flight Display and Multifunction Display performance, acceptance tests of individual control elements, and inflight evaluation of ergonomic aspects of flight display user interfaces. Figure 6 displays the PFD and MFD visualization modes at the take–off roll on a paved runway. Preflight setting of the PFD/MFD variables for a planned execution of flight is performed before taxiing. Figure 7 displays the pilot activation of the A/P ENABLE mode, which executes a BIT for the evaluation of system's operational status and flight mode readiness.

Figure 8 introduces the pilot's activated transition to A/P ENGAGED regime and the activation of the AFCS. After engaging, the AFCS controls the aircraft into steady level flight. When in automatic flight, the crew is provided with system interaction modes using touch controlled PFD and MFD interfaces to alter commanded values of ALT, IAS and HDG. Figure 9 shows the selection of ALT target values using a touch sensitive area over the PFD's altimeter graphics.

Figure 10 displays active heading control using a touch sensitive interface over the PFD compass for selection of Heading Angle. An option in the flight data visualization is a visual interface mode in which the PFD displays basic flight instruments, 3D synthetic terrain, a moving map, basic engine parameters, and autopilot settings; and, the MFD presents the crew with navigation aids, flight statistics, and an extended engine management display. In the A/P ENGAGED mode, the AFCS automatically commands all 4 available control axes.

Figure 6: AFCS before take-off

Figure 7: A/P ENABLED

Figure 8: A/P ENGADED

Figure 9: A/P ENGAGED – ALT

Figure 11 displays an automatic flight under modified target IAS conditions. The reduction of pilot workload due to automatic flight control system autonomous operation allows the crew to redirect its attention to navigation and management tasks, such as uninterrupted communication with Air Traffic Control (ATC). The return to manual flight mode is shown in Figure 12, where the pilot deactivates the AFCS by pressing the A/P button on the control stick. The disconnected AFCS is indicated by the A/P DISCONNECT icon. Disconnecting the AFCS automatically transits the MFD interface to visualization of primary flight instrument graphics, and clears the AFCS selected target values. An automatic disconnect can also occur when the AFCS' operational envelope limits are exceeded.

Figure 13 shows a cabin view on the landing approach with both of the displays set to PFD visualization mode. This mode introduces basic flight indicators displayed on top of a synthetic 3D terrain background with an integrated virtual aerodrome and related ground infrastructure models. The left bottom part of the PFD and MFD contains a moving map representation with a graphical interpretation of colliding terrain colored in a pseudospectral palette with red indicating dangerous terrain proximity.

Figure 10: A/P ENGAGED – HDG

Figure 11: A/P ENGAGED – IAS

Figure 12: A/P DISCONNECT

Figure 13: AFCS at final approach

Flight crews rated the AFCS user interface positively due to its intuitiveness, precision, clarity of displayed data, and appealing design. This positive recognition can be attributed to the selected touch control strategy, which improved pilots' learning curves when experiencing the new avionics. Perceived correlation between the AFCS displayed synthetic terrain and the cockpit view of the surrounding environment stimulated pilots' confidence in the AFCS' flawless operation.

3.2 Performance evaluation

An important aspect of the automatic flight control system's design is the evaluation of the quantitative control performance indicators under both smooth air and atmospheric turbulence conditions. Actual flight testing was executed according to approved flight test program protocols from [4]. Selected paragraphs of SAE AS94900 [24] were used to establish criteria for the control performance evaluation. Although [24] is not a legally binding document for light civil aircraft, its unified character provides a complex basis for an automatic flight control system design.

Performance characteristics of the AFCS have been investigated for control modes and flight conditions shown in Table 5. Since the AFCS provides an integral 4-axis aircraft control in longitudinal and lateral-directional motion individual control criteria for both smooth and turbulent air conditions were used in the performance evaluation process. The presented combination of modes and respective atmospheric conditions forms a representative sample for the control quality evaluation.

Table 5: AFCS control modes

Mode	Condition
Steady banked turn	Smooth air
Straight and level flight	Smooth air
Attitude hold	Turbulence
Heading hold	Turbulence
Heading select	Turbulence
Altitude hold and altitude select	Smooth air
Airspeed hold	Smooth air

The AFCS supports user selection of visual displays system units. The user has the option to choose between imperial or metric units for visualizing flight instruments. The flight tests used in the evaluation process were performed with the AFCS visual interface set to imperial units. However, due to author's preference, the Pressure Altitude and Indicated Airspeed data shown in graphs supporting the evaluation process have been converted to the metric system. For the evaluation of flights in turbulence, the measured quantities were supplemented with their respective Root Mean Square (RMS) values.

Steady banked turn
Figure 14 shows the flight trajectory of the AFCS controlled aircraft in a steady banked turn in smooth air. The aircraft is commanded to execute a level right turn, changing its Heading Angle from 159° to 200° at Pressure Altitude of 550 m. The figure with flight trajectory displayed over a geodetic grid is supplemented with graphs showing time histories of measured Heading Angle HDG, Pressure Altitude ALT, Incremental Sideslip Angle $\Delta\beta$ and Lateral Acceleration a_y at the aircraft's center of gravity.

The observations made from the graphs shown in Figure 14 are summarized below:

- The measured Heading Angle HDG reached its commanded value of 200° in a steady right level turn with an initial overshoot of 1.3°. The measured maneuver accuracy range remained within the limits $[-0.4°, +0.5°]$.

- The measured Pressure Altitude ALT remained throughout the investigated AFCS controlled coordinated steady level right turn within the range $[542.7\,m, 558.4\,m]$.

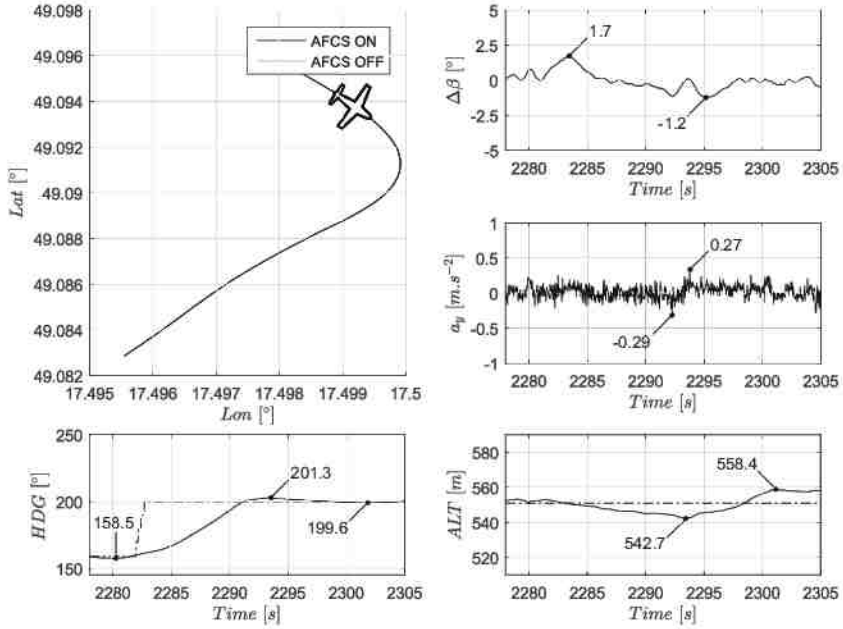

Figure 14: Coordinated steady banked turn

- The measured Incremental Sideslip Angle $\Delta\beta$ at a steady bank angle remained throughout the investigated AFCS controlled steady right turn within the range $[-1.2°, +1.7°]$.
- The Lateral Acceleration a_y at the aircraft's center of gravity remained throughout the AFCS controlled steady level right turn within the range $\left[-0.29\, m.s^{-2}, +0.27\, m.s^{-2}\right]$.

Based on the evaluation of criteria defined in [24], it can be stated that the investigated AFCS performance complies with the requirements pertaining to coordinated steady banked turns introduced in the specified aerospace standard.

Straight and level flight
Figure 15 shows the AFCS controlled aircraft trajectory in straight and level flight in smooth air conditions. Displayed trajectory is complete with graphs showing time histories of measured Heading Angle HDG, Pressure Altitude ALT, Incremental Sideslip Angle $\Delta\beta$ and Lateral Acceleration a_y at the aircraft center of gravity.

The observations made from the graphs shown in Figure 15 are summarized below:

- The measured Heading Angle HDG maintained its reference value of 102° in straight and level flight within an accuracy range $[-0.4°, +0.3°]$.
- The measured Pressure Altitude for the AFCS controlled ALT target of $581\, m$ remained throughout the straight level flight within the range $[572.1\, m, 586.4\, m]$.
- The recorded Incremental Sideslip Angle $\Delta\beta$ remained throughout the AFCS controlled straight and level flight within the range $[-0.90°, +0.85°]$.
- The Lateral Acceleration a_y at the aircraft's center of gravity remained throughout the AFCS controlled straight and level flight within the range $\left[-0.17\, m.s^{-2}, +0.19\, m.s^{-2}\right]$.

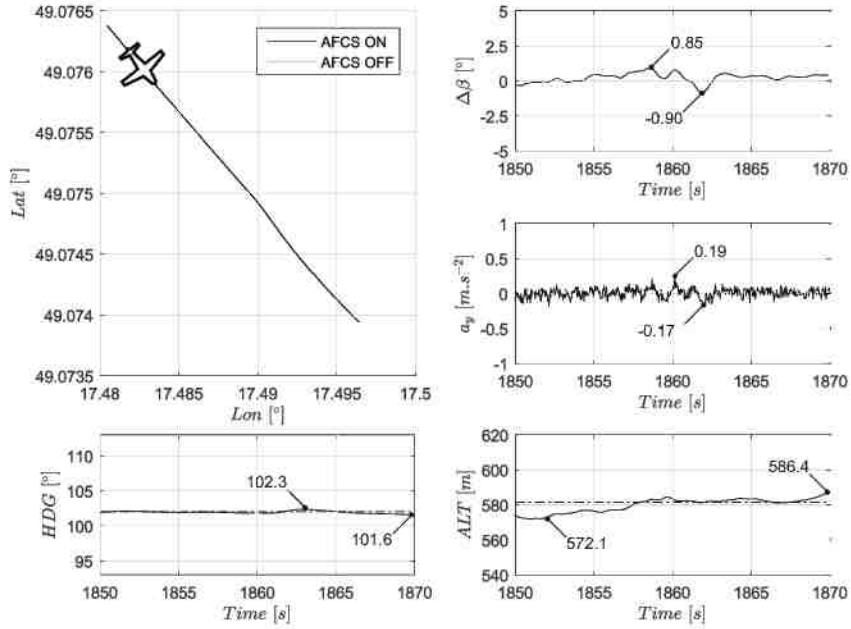

Figure 15: Coordination in straight and level flight

Based on the evaluation of criteria defined in [24], it can be stated that the AFCS performance complies with the requirements for straight level flight introduced in the specified aerospace standard.

Attitude hold

Figure 16 shows the aircraft's trajectory in steady level AFCS controlled flight under atmospheric turbulence conditions as part of the attitude hold evaluation. As the AFCS implemented flight control laws do not directly support general attitude hold commands, the selection of wings level maneuver serves as the evaluation basis. Depicted trajectory is completed by graphs showing time histories of measured Heading Angle HDG, Pressure Altitude ALT, Roll Angle ϕ and Pitch Angle θ.

The observations made from the graphs shown in Figure 16 are summarized below:

- The AFCS maintained after engaging in steady level flight its measured Heading Angle HDG at a value of 160.4° RMS, with deviations ranging from $[158.2°, 162.5°]$. The AFCS target HDG value was set to 160°.
- The AFCS maintained after engaging the measured Pressure Altitude ALT throughout the investigated steady level flight within the range $[544.5\,m, 558.2\,m]$.
- The recorded Roll Angle ϕ remained throughout the investigated AFCS controlled attitude hold flight in atmospheric turbulence within the range $[-6.2°, +7.1°]$, with a RMS value of 3.7°.
- The recorded Pitch Angle θ remained throughout the investigated AFCS controlled attitude hold flight in atmospheric turbulence within the range $[-1.8°, +2.1°]$, with a RMS value of 1.2°.

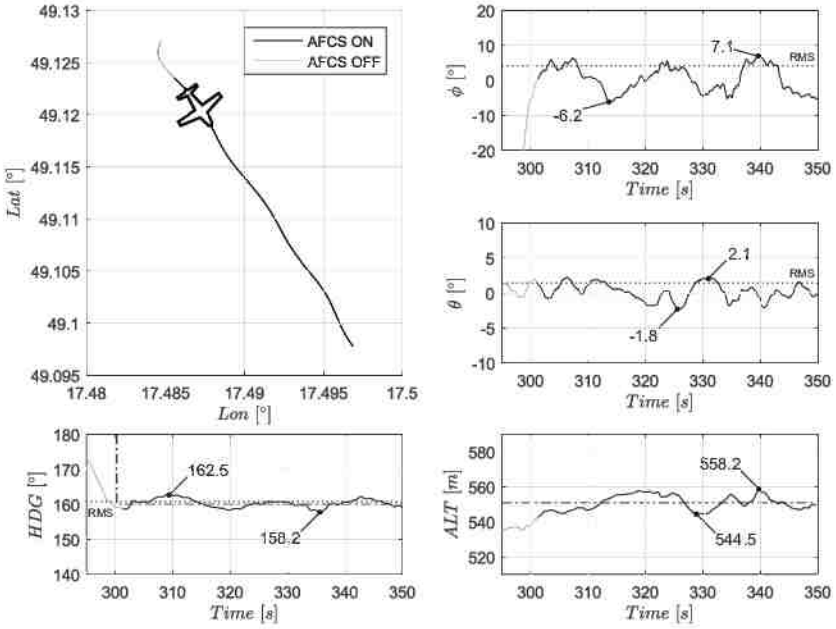

Figure 16: Attitude hold in atmospheric turbulence

Based on the evaluation of criteria defined in [24], it can be stated that the AFCS complies with the attitude hold requirements for a wings level flight introduced in the specified aerospace standard.

Heading hold
Figure 17 shows the aircraft trajectory in steady level AFCS controlled flight in atmospheric turbulence conditions. The displayed trajectory is completed by graphs showing time histories of measured Heading Angle HDG, Pressure Altitude ALT, Roll Angle ϕ and Roll Rate p.

The observations made from the graphs shown in Figure 17 are summarized below:

- The engaged AFCS maintained the desired Heading Angle HDG of 107°. The Heading Angles measured during heading hold mode in atmospheric turbulence remained within the range $[105.6°, 108.5°]$, while the Heading Angle RMS reached a value of 107.2°.
- The measured Pressure Altitude for the AFCS controlled ALT target of $581\,m$ remained throughout the heading hold flight in atmospheric turbulence within the range $[573.1\,m, 587.2\,m]$.
- The recorded Roll Angle ϕ remained throughout the investigated AFCS controlled heading hold flight in atmospheric turbulence within the range $[-2.6°, +3.7°]$, with a RMS value of 1.8°.
- The recorded Roll Rate p remained throughout the AFCS controlled heading hold mode in atmospheric turbulence within the range $\left[-2.7°.s^{-1}, +6.2°.s^{-1}\right]$.

Based on the evaluation of criteria defined in [24], it can be stated that the AFCS complies with the heading hold requirements introduced in the specified aerospace standard.

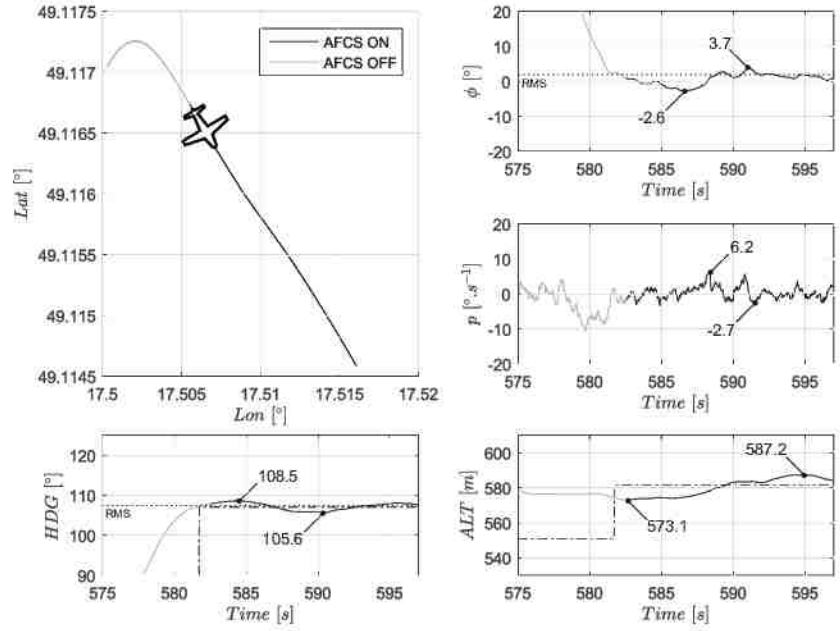

Figure 17: Heading hold in atmospheric turbulence

Heading select
Figure 18 shows the aircraft's trajectory with an AFCS commanded heading change in atmospheric turbulence. The left turn maneuver starts from a steady level flight. Depicted trajectory is reflected in the graphs showing time histories of measured Heading Angle HDG, Pressure Altitude ALT, Roll Angle ϕ and Roll Rate p.

The observations made from the graphs shown in Figure 18 are summarized below:

- The AFCS commanded target Heading Angle HDG of 170° is approached through a left level turn. The measured angles at the target heading remain within the range $[169.1°, 170.4°]$. The RMS Heading Angle in the heading hold mode reached a value of 169°.

- The measured Pressure Altitude for the AFCS controlled ALT target of $642\,m$ remained throughout the investigated level left turn in atmospheric turbulence within the range $[636.6\,m, 649.1\,m]$.

- The recorded aircraft Roll Angle ϕ remained for the wings level sections of the maneuvers within $[-3.2°, 2.9°]$, with a RMS value reaching 1.7°. The max. Roll Angle ϕ measured in the left turn maneuver reached a value of $-15.7°$. The Roll Angle RMS value during the turn reached $-13°$.

- The recorded Roll Rate p remained throughout the AFCS controlled maneuvering in atmospheric turbulence conditions within the range $\left[-8.3°.s^{-1}, +9.4\,°.s^{-1}\right]$.

Based on the evaluation of criteria defined in [24], we can state that the recorded AFCS performance in heading select mode complies with the requirements introduced in the specified aerospace standard.

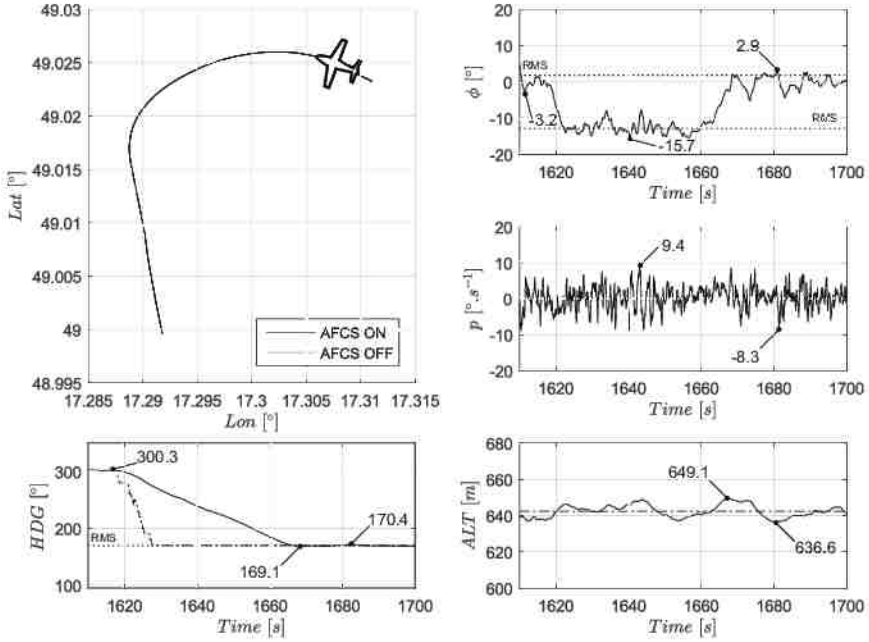

Figure 18: Heading select in atmospheric turbulence

Altitude hold and altitude select
Figure 19 shows an AFCS controlled aircraft's trajectory, flown in smooth air conditions, consisting of an initial altitude hold sequence at $620\,m$ followed by a commanded descent to a target Pressure Altitude of $490\,m$. The altitude descent profile includes two commanded incremental changes in heading. The flight trajectory graph displayed over a geodetic grid is supplemented with time histories of measured Heading Angle HDG, Pressure Altitude ALT, Roll Angle ϕ and Load Factor n_z at the aircraft's center of gravity.

The observations made from the graphs shown in Figure 19 are summarized below:

- The aircraft maintained its Heading Angle HDG of 240° within $[-0.5°, +0.4°]$ after engaging the AFCS in steady level flight. The following set of 20° stepwise Heading Angle increments resulted into a series of right turns.
- The engaged AFCS held the target Pressure Altitude ALT of $620\,m$ within the range $[618.3\,m, 622.3\,m]$ before entering the descending profile to reach the commanded ALT of $490\,m$. The target Pressure Altitude remained within the range $[483.0\,m, 490.2\,m]$.
- The AFCS maintained throughout the descent maneuver an average Vertical Speed VS of $2\,m.s^{-1}$.
- The recorded Roll Angle ϕ remained throughout the initial level flight within the range $[-0.9°, +1.0°]$. The AFCS' commanded changes in HDG resulted in a series of right turn maneuvers with measured Roll Angles up to 14.8°.
- The Load Factor n_z at the aircraft's center of gravity remained throughout the investigated AFCS controlled flight in smooth air conditions within the range $[-0.82, +1.20]$.

Based on the evaluation of criteria defined in [24], it can be stated that the AFCS' performance complies with the requirements on altitude hold and altitude select as introduced in the specified aerospace standard.

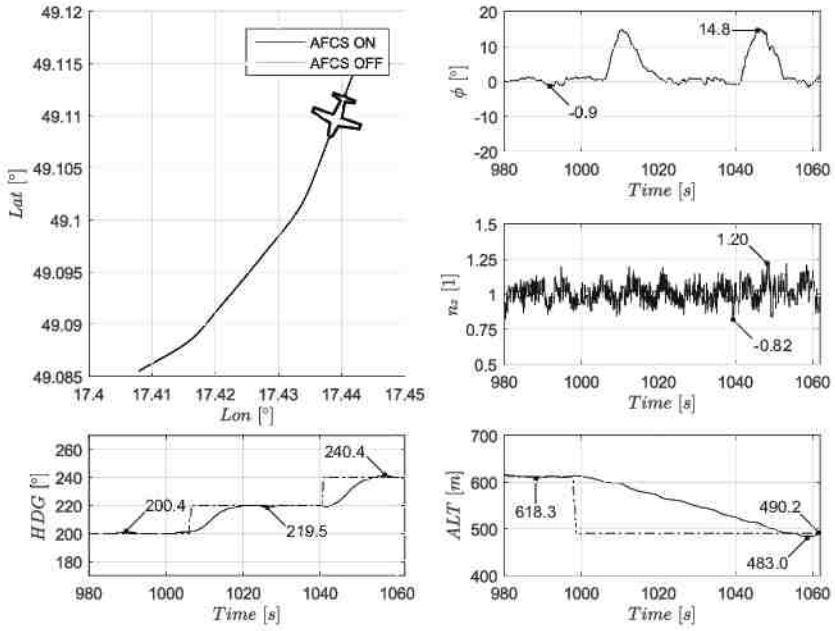

Figure 19: Altitude hold and altitude select

Airspeed hold

Figure 20 shows an AFCS controlled aircraft's trajectory for climb and straight level flight conditions. The aircraft is commanded to reach ALT of $460\,m$, while maintaining its Indicated Airspeed IAS at $41\,m.s^{-1}$ and Heading Angle HDG of 345°. The flight trajectory displayed over a geodetic grid is supplemented with a recorded time history of measured Heading Angle HDG, Pressure Altitude ALT, Indicated Airspeed IAS and Roll Angle ϕ.

The observations made from the graphs shown in Figure 20 are summarized below:

- The AFCS maintained the commanded Heading Angle HDG at 345° within an accuracy range $[-0.3°, +0.5°]$ throughout the climb and level flight.
- The AFCS reached the target Pressure Altitude of $460.0\,m$, having an average Vertical Speed VS of $2\,m.s^{-1}$. The ALT accuracy remained throughout the investigated flight within the range $[-3.7\,m, +2.5\,m]$, with an overshoot of $0.2\,m$.
- The recorded Roll Angle ϕ remained throughout the investigated AFCS controlled flight in smooth air within the range $[-0.80°, +0.95°]$.
- The commanded Indicated Airspeed IAS remained throughout the investigated AFCS controlled flight within the range $\left[40.36\,m.s^{-1}, 41.90\,m.s^{-1}\right]$.

Based on the evaluation of criteria defined in [24], it can be stated that the AFCS complies with the airspeed hold requirements introduced in the specified aerospace standard.

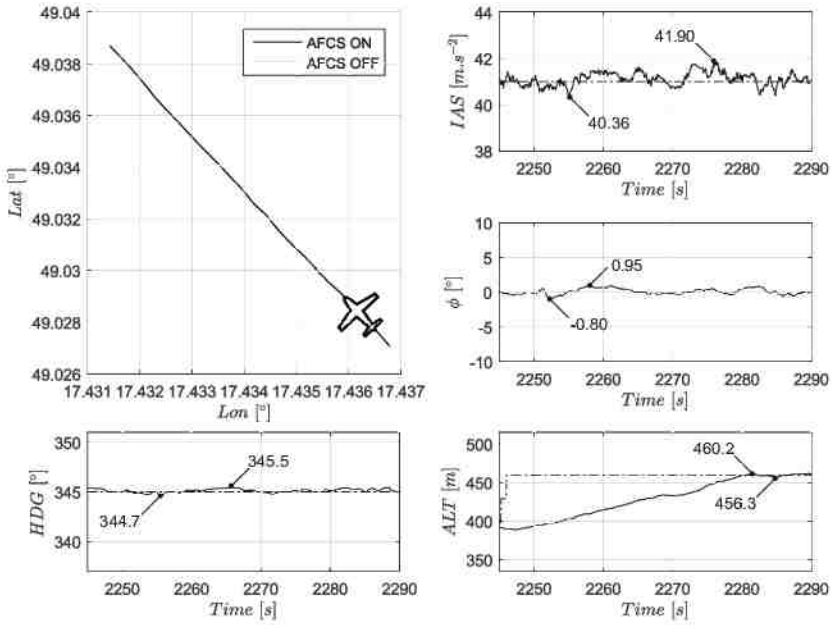

Figure 20: Airspeed hold in smooth air conditions

3.3 Results

The AFCS evaluation included the assessment of the user interface under real flight conditions, a series of operational trials with the flight crews commanding the automatic control system to acquire and maintain desired flight state and, finally, an analytical performance evaluation of the integrated control system. The user interface was found to comply with the design goals and received positive crew ratings for its ergonomic design, intuitive layout, unobstructed clarity of visualized data, and swift responsiveness to touch commands. The control for differences across flight crews and how they might affect results remained beyond the scope of presented work. The operational trials were executed in various atmospheric conditions at different operating points of the aircraft's flight envelope. The flight crew entered commands into the AFCS computer by using the system's touch screen interface. In order to analyze the system's inflight performance, selected flight quantities were recorded and subsequently evaluated against the requirements introduced in [24]. Even though the system provides a coordinated 4-axis control in longitudinal and lateral-directional motion, individual criteria for steady coordinated turn, level flight, attitude hold, heading select and heading hold, altitude select and altitude hold and, finally, airspeed hold of [24] were considered. The evaluations confirmed the AFCS' compliance with performance requirements of [24] in smooth air and atmospheric turbulence.

4 Conclusion

The presented prototyping framework with its individual steps introduced throughout this thesis led to the development of an innovative digital Automatic Flight Control System for light aircraft. The AFCS was designed using industry accepted standards for flight controls and digital avionics in a single line system, with redundancy considerations resolved through a parallel integration of the Electromechanical Actuators to the primary mechanical control system. This approach found support in the digital flight control system's use case scenarios, assuming the support of VFR operations only and including a manual override capability.

The flight control system's prototyping relies, at the laboratory level, to a large extent on rapid prototyping protocols and simulation technologies with the system's fidelity depending on the modeling accuracy of individual simulation blocks. In order to operate with high fidelity data, parameter identification techniques were used at the aircraft and system component levels. The flight parameter estimation required the investigated aircraft to be equipped with a laboratory grade data acquisition system. The recorded data were, after careful post-processing and consistency checks, used in the parameter identification process based on numerical optimization methods. Similar identification techniques were used for the estimation of the system's component models.

Design of the flight control laws strongly benefit from using a rapid prototyping environment with integrated performance evaluation tools. Matlab®/Simulink® was used in the design of the investigated flight control laws based on a number of approaches reflecting both classical and advanced control theory. Presented control strategies featured coordinated SISO, MIMO, and NDI schemes. The software implementation of the AFCS flight control laws considered best practices drawn from [7], [17]–[19]. These control codes were subjected to careful software-in-the-loop simulations prior to their installation on the flight control computer's hardware platform.

Individual AFCS hardware units were developed considering best practices drawn from [15], [16], [20], [23], [24]. The development of the AFCS' dedicated hardware units introduced the option of laboratory level hardware-in-the-loop simulations. These simulations were typically performed within the SimStar flight simulator framework optionally extended with modules to provide desired system interfaces. The SimStar flight simulator was used throughout the design and evaluation of the AFCS' user interface, the investigation of the AFCS' interaction modes, evaluation of the flight dynamics models, pilot-in-the-loop simulations of integrated flight control laws, and laboratory tests of the CAN–based on–board network including the AFCS peripherals. Successfully accomplished laboratory level hardware-in-the-loop simulations were a prerequisite to the aircraft level system integration and testing.

The AFCS' aircraft integration represented another important qualitative step towards the system's testing. The AFCS equipped aircraft was subjected to a series of inspections, calibrations, measurements and ground tests to prove the system's airworthiness [3]. The ground experiments with a fully operational flight control system included the "iron bird" simulations with computer generated state and feedback information. These experiments were of a great value not only to the flight test engineers but, also, to the flight crew itself. Subsequent testing meant leaving the comfort zone of carefully orchestrated laboratory experiments and exposing the AFCS to real world environments, such as low and high speed taxi trials initially.

After clearing the ground–testing phase, an AFCS equipped aircraft took its maiden flight. The flight test series included initial avionics familiarization flights with the AFCS' actuation units temporarily disengaged, followed by a series of successful automatic flight experiments with the full onboard automation active [4]. The flight experiments were performed in

smooth air as well as in turbulent atmospheric conditions to record flight data for post flight analysis and performance evaluation. Based on the evaluations of criteria defined in [24], it can be stated that the developed AFCS complies with the design requirements. The exposure to regular operating environments and routine onboard procedures confirmed compliance with the system's design goals.

As the density of high-traffic flight areas grows, advances in air traffic management will be required. State-of-the-art tactical instructions issued by air traffic controllers will likely be replace with autonomous trajectory–based digital flight control systems such as the one described herein.

References

[1] P. Chudý and P. Dittrich, "Letounová instalace 'chytrého autopilota', Zástavba systému 'chytrého autopilota' do letounu," Vysoké učení technické v Brně, Tech. Rep. AW-EVK 1.2013, Sep. 2013.

[2] P. Chudý and P. Dittrich, "Ovládání systému 'chytrý autopilot' experimental, Podmínky aktivace a popis ovládání experimentálního systému 'chytrého autopilota'," Vysoké učení technické v Brně, Tech. Rep. AWPOM 01.2013, Mar. 2013.

[3] P. Chudý and P. Dittrich, "Pozemní ověření zástavby, Pozemní funkční ověření zástavby prvků 'chytrého autopilota'," Vysoké učení technické v Brně, Tech. Rep. AWTST G1.2013, Jun. 2013.

[4] P. Chudý, P. Dittrich, and J. Vlk, "Ověření systému 'chytrý autopilot' experimental, Popis ověření experimentálního systému 'chytrého autopilota'," Vysoké učení technické v Brně, Tech. Rep. AWTST 01.2013, Mar. 2013.

[5] P. Chudý, P. Dittrich, and J. Vlk, "Ověřovací letové zkoušky, Letové ověření systému 'chytrého autopilota'," Vysoké učení technické v Brně, Tech. Rep. AWEXP 1.2013, Dec. 2013.

[6] P. Chudý and K. Rydlo, "Intuitive flight display for light aircraft," in *AIAA Modeling and Simulation Technologies Conference*, Portland, OR: American Institute of Aeronautics and Astronautics, 2011, pp. 1–10. DOI: 10.2514/6.2011-6348.

[7] P. Chudý and K. Rydlo, "Tvorba a verifikace kódu, Postupy pro tvorbu a verifikaci softwaru leteckých systémů," Vysoké učení technické v Brně, Tech. Rep. AWDVV 01.2012, Dec. 2012.

[8] P. Chudý and P. Rzucidlo, "TECS/THCS based flight control system for general aviation," in *AIAA Modeling and Simulation Technologies Conference*, Chicago, IL: American Institute of Aeronautics and Astronautics, 2009, pp. 1–13. DOI: 10.2514/6.2009-5689.

[9] P. Chudý, A. Tomczyk, and P. Rzucidlo, "Safety enhanced digital flight control system," *Aircraft Engineering and Aerospace Technology*, vol. 81, pp. 416–423, 2009, ISSN: 0002-2667. DOI: 10.1108/00022660910983699.

[10] P. Chudý and J. Vlk, "Systém řízení letu 'chytrého autopilota', Popis implementace automatického řízení pro systém autopilota," Vysoké učení technické v Brně, Tech. Rep. AWFCS 1.2013, May 2013.

[11] P. Chudý, J. Vlk, and P. Dittrich, "Evolution assisted flight control system design," in *32nd Digital Avionics Systems Conference (DASC)*, Syracuse, NY: IEEE, 2013, pp. 1–9, ISBN: 978-1-4799-1536-1. DOI: 10.1109/DASC.2013.6712641.

[12] P. Chudý, J. Vlk, and P. Dittrich, "Prototyping framework for digital flight control systems," in *32nd Digital Avionics Systems Conference (DASC)*, Syracuse, NY: IEEE, 2013, pp. 1–12, ISBN: 978-1-4799-1536-1. DOI: 10.1109/DASC.2013.6712632.

[13] P. Chudý, J. Vlk, M. Leitão, and F. Stroscher, "Evolution driven controller design for aeroservoelastic aircraft," in *AIAA Modeling and Simulation Technologies Conference*, Boston, MA: American Institute of Aeronautics and Astronautics, 2013, pp. 1–17. DOI: 10.2514/6.2013-5153.

[14] P. Chudý, P. Zemčík, and P. Rzucidlo, "Affordable light aircraft flight simulators," in *AIAA Modeling and Simulation Technologies Conference*, Toronto, Ontario Canada: American Institute of Aeronautics and Astronautics, 2010, pp. 1–10. DOI: 10.2514/6.2010-8097.

[15] EUROCAE ED-14F, *Environmental conditions and test procedures for airborne equipment*, Malakoff, France: EUROCAE, Mar. 2008.

[16] F 2245-07, *Standard specification for design and performance of a light sport airplane*, West Conshohocken, PA: ASTM International, Mar. 2007.

[17] IEEE Std 12207-2008, *Systems and software engineering – software life cycle processes*, New York, NY: IEEE, Jan. 2008. DOI: 10.1109/IEEESTD.2008.4475826.

[18] MISRA-C:2004, *Guidelines for the use of the c language in critical systems*, Nuneaton, United Kingdom: MIRA Limited, Oct. 2004.

[19] RTCA/DO-178B, *Software considerations in airborne systems and equipment certification*, Washington, DC: RTCA, Inc., Dec. 1992.

[20] RTCA/DO-254, *Design assurance guidance for airborne electronic hardware*, Washington, DC: RTCA, Inc., Apr. 2000.

[21] K. Rydlo, P. Rzucidlo, and P. Chudý, "Simulation and prototyping of FCS for sport aircraft," *Aircraft Engineering and Aerospace Technology*, vol. 85, pp. 475–486, 2013, ISSN: 1748-8842. DOI: 10.1108/AEAT-10-2012-0186.

[22] SAE ARP4754, *Certification considerations for highly-integrated or complex aircraft systems*, Warrendale, PA: SAE International, Nov. 1996.

[23] SAE ARP4761, *Guidelines and methods for conducting the safety assesment process on civil airborne systems and equipment*, Warrendale, PA: SAE International, Dec. 1996.

[24] SAE AS94900, *Aerospace - flight control systems - design, installation and test of piloted military aircraft, general specification for*, Warrendale, PA: SAE International, Jul. 2007.

List of Figures

List of Tables

INTENTIONALLY LEFT BLANK

Acknowledgment

This document summarizes the work that has been done between years 2008–2013. I would like to thank my family, my friends and my colleagues at Faculty of Information Technology, Brno University of Technology for their support and valuable comments.

This work has been partially supported by Technology Agency of Czech Republic, project TA01010678 "Smart Autopilot", 2011–2013.